Dynamics of Endovascular Stent Expansion

by

James C. Squire

B.S., United States Military Academy (1989)

M.S., Massachusetts Institute of Technology (1996)

Submitted to the
Department of Electrical Engineering and Computer Science
in partial fulfillment of the requirements for the degree of

DOCTOR OF PHILOSOPHY

at the

MASSACHUSETTS INSTITUTE OF TECHNOLOGY

July 2000

Author _____
Department of Electrical Engineering and Computer Science
July 19, 2000

Certified by _____
Elazer R. Edelman
Thomas D. and Virginia W. Cabot Professor
Thesis Supervisor

Accepted by _____
Arthur C. Smith
Chairman, Committee on Graduate Students
Department of Electrical Engineering and Computer Science

Dynamics of Endovascular Stent Expansion

by James C. Squire

Submitted to the Department of Electrical Engineering and Computer Science on July 19, 2000, in partial fulfillment of the requirements for the degree of Doctor of Philosophy in Electrical Engineering and Computer Science.

Abstract

Advances in prosthetic science and engineering have spurred the rapid development of many new permanent implants such as arterial reinforcement grafts, venous filters, hepatic pressure shunts, vascular embolization coils, myocardial perforation-sealing "clamshells", and stents that strengthen and scaffold the biliary duct, urethra, veins, and arteries. Typically, these devices are attached to a delivery catheter and threaded to the site of interest where they are expanded. The very nature of the remote delivery systems make the mechanical details of implantation difficult to ascertain, yet this is important to quantify since there may be a link between how the devices are emplaced and the body's acute and chronic response. **This thesis examines the hypothesis that the responses to implants are influenced by the manner in which the implants are placed within the body.** Endovascular stents provide an ideal medium to examine this hypothesis as they 1) provoke a well-documented but incompletely-understood acute and chronic response (thrombosis and neointimal hyperplasia, respectively) 2) take issues of strain to extremes, which has been linked with hyperplasia, and 3) employ a regular geometry amenable to modeling.

Thesis supervisor: Elazer R. Edelman
Thomas D. and Virginia W. Cabot Professor of Health Sciences and Technology

Acknowledgments

It's only appropriate that acknowledgements traditionally are placed at the physical beginning of the work, yet written at the temporal end. The most important support, advice, and encouragement is that given at the beginning when the future is uncertain and can only be appreciated in hindsight. Mom, Dad: thanks for giving me your unconditional love and support no matter what fool idea I follow, whether it leads to a career as an Army officer, high school teacher, or engineering professor: I'd have given up long ago if I thought the difference really mattered.

Acknowledgments by their very nature tend to engender some suspicion…were the people really *that* good? I've worked with many people over several careers, and can assure the reader, yes, these men and women are exceptional, even by MIT's standards.

To Elazer: thank you for demonstrating the same qualities of integrity, faith, fascination, and perseverance that frequently blur the line between your roles as advisor, scientist, and teacher. You have a more positive influence on people than you realize. Steve Burns: You are an ideal teacher of teachers; you have taught me that a blend of faith in the student, genuine interest in the material, and compassion are far more important than board technique. Campbell: your élan and grace under fire is inspiring. If my diet doesn't improve I'm keeping your business card in my wallet. Martha: you have guided my graduate career from start to finish. Thanks for your advice and encouragement over the years, and for knowing when to dispense each. And Prof. Senturia I am indebted to your farsighted advice, both concerning this research and my career.

I would like to thank my fellow students and post-docs in Elazer's lab for the fellowship that comes not just with the Friday after work happy hours but also with the late-night-and-the-computer's-bluescreened-and-the-staining-didn't-take-*again* unhappy hours as well. Dave Ettenson and Dave Wu, two of the nicest guys I know, have helped me to no end. Yoram, who isn't at all hurt by not being named the nicest guy I know, is the lab's only hope for someone whom can regularly beat Elazer at squash—I tried.. I firmly believe one day I'll see the comedy and music of Cooper as host of the Tonight Show, and expect he will probably *still* be poking fun at the Canadians. My running partners Henry and Adam, and squash partner Yi have worked hard with me to the grad-student gut at bay, while equally-regular buffets

with Gowri, Tim, Elizabeth, and Vishal threatened to put it back on. My old office was next to Tim's, and had I not moved I'd probably still be solving his paradox puzzles.

Frank: Buddy, our frequent talks and short-notice but much-needed vacations kept me mostly sane throughout. If nothing else works out, Virginia could use a few Starbucks franchises. To my "other" Mom and Dad: thanks for your valiant efforts to keep me appropriately dressed throughout my graduate student days. The fashion police tickets I've accumulated only reflect the need for the folks who make Dockers and Geranimals to talk.

Most of all my thanks and love to Laura, who intimately knows both the joys and sacrifices that have accompanied this path. We pushed/pulled each other through this, and this thesis is a product of both our dreams. I thank the Lord we both know this is a journey, because were it an end I would have no way to repay all those who invested in me their time, money, and selves.

This thesis is dedicated to the memory of my father, James Lewis Squire, Jr.

Patents

Work on this thesis has yielded two prototypes of improved stent-delivery balloon catheters, and their descriptions were filed in two preliminary patents with the U.S. Patent Office on May 12, 1998. These patents have been reviewed and have been assigned provisional patent numbers 60,985,098 and 60,085,097. These are available for licensure through the M.I.T. Technology Licensing Office, Room NE25-230, Cambridge MA 02139. Two additional disclosures have been submitted describing improved methods for stent/balloon placement prior to crimping, and a stent geometry that minimizes acute arterial injury imparted during expansion.

Table of Contents

Table of Figures

CHAPTER 4: Intrastrut Expansion Characteristics

CHAPTER 1 Introduction

1.1 Aims of research

Advances in prosthetic science and engineering have spurred the rapid development of many new permanent implants such as arterial reinforcement grafts, venous filters, hepatic pressure shunts, vascular embolization coils, myocardial septal defect closure devices, and hollow cylindrical stents that strengthen and scaffold the biliary duct, urethra, veins, and arteries against collapse and closure. Typically, these stents are attached to a delivery catheter and threaded to the site of interest where they are expanded. The very nature of the remote delivery systems make the mechanical details of implantation difficult to ascertain, yet this is important to quantify since there may be a link between how the devices are placed and the body's acute and chronic response.

This thesis examines the hypothesis that the acute and chronic responses to implants are influenced by the manner in which the implants are placed within the body. Endovascular stents provide an ideal medium to examine this hypothesis as they 1) provoke a well-documented but incompletely-understood acute and chronic response (thrombosis and neointimal hyperplasia, respectively) 2) impart extreme deformations to the arterial wall, which has been linked with hyperplasia [1,2,3,4,5], and 3) employ a regular geometry amenable to modeling.

This work has three specific aims:

1. Characterize the manner in which endovascular implants expand in arteries by quantifying the strain tensor they impose on the arterial surface as a function of both location and time
2. Determine whether different types of expansion cause different types of vascular injury
3. Determine whether one can modify stents and their expansion characteristics to reduce vascular injuries

1.2 What are endovascular stents?

Ischemic heart disease, the end result of reduced flow through narrowed atherosclerotic coronary arteries (Figure 1.1), is the leading cause of mortality in the world; it affects more than 58 million Americans and is responsible for 41.5% of all deaths in the United States [6]. Currently, the two most common procedures for patients that do not respond adequately to purely pharmacologic therapy are percutaneous transluminal coronary balloon angioplasty (PCTA) and coronary artery bypass grafting (CABG). The frequent lack of long-term efficacy of these techniques and the physical toll associated with major coronary surgery have prompted the search for new technologies, including laser angioplasty, atherectomy, and implanted endovascular scaffolding devices called stents. Of these, stents are rapidly gaining the lion's share of the vascular intervention market because of their high initial success rate, minimally invasive nature, and improved long term effectiveness. In 1995 approximately 100,000 patients in the United States received stents [7]; by the end of 2000 the annual number of stenting procedures is expected to exceed the number of angioplasty procedures (currently 900,000 worldwide) [8].

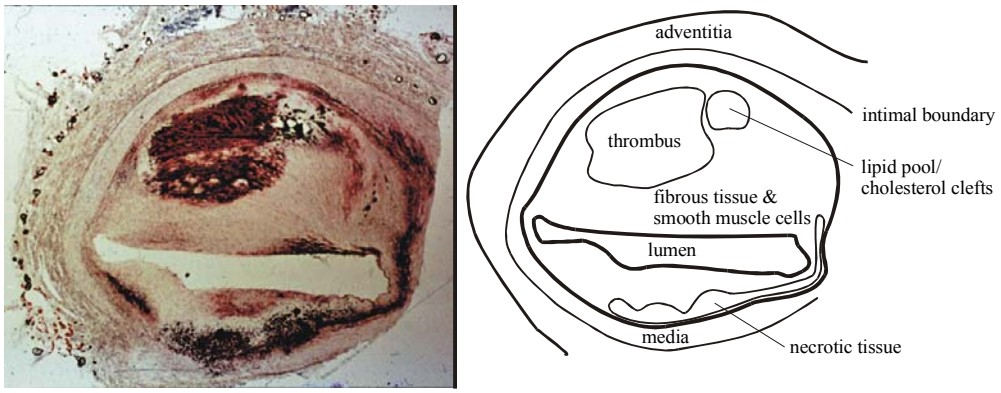

Figure 1.1: A diseased human coronary artery with an advanced complicated atheroma. The lightly stained collar of concentric elastic lamella that forms the media is clearly visible at this 100x magnification. In a healthy artery these cells regulate local vessel tone and blood flow by contracting or relaxing leading to constriction or dilation of the artery, however now they have undergone phenotypic transformation from a contractile state to a synthetic or proliferative state. In place of tone regulation they now grow and stimulate further growth. Before the onset of atherosclerosis, the media was lined with a thin intima that bounded the lumen. In this artery the intima is occupied by a hyperplastic mass of smooth muscle cells, necrotic debris, a lipid pool, cholesterol clefts, and organized thrombus that has reduced the luminal area by 85%.

Endovascular stents are expandable tubes 6 mm to 60 mm in length and 2 mm to 10 mm in diameter most commonly made from stainless steel and the nickel-titanium alloy nitinol, although tantalum [9], platinum [9], plastic [10], and biodegradable materials [11, 12] have also been used. In a compressed state the stent is mounted on a catheter and threaded through the vascular tree to a site of narrowing. The stent is next enlarged in diameter approximately 50%, either by a spring-like recoil into their naturally expanded shape (nitinol) or by plastic deformation under the influence of a cylindrical balloon inflated within the stent to 8-20 atmospheres (atm) of pressure. Once the catheter is withdrawn the stent is left as a permanent implant within the artery (Figure 1.2).

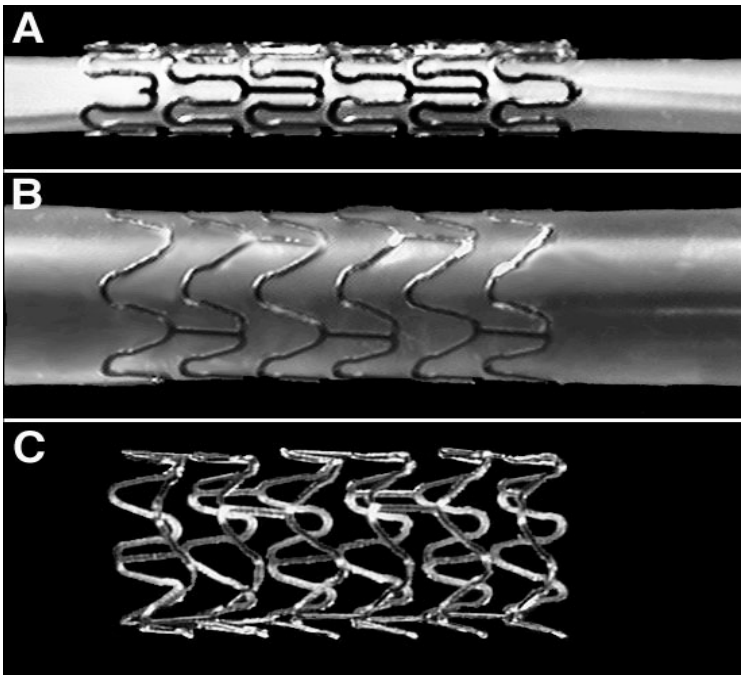

Figure 1.2: A stainless steel stent mounted upon a balloon catheter (A) before and (B) after balloon inflation, and (C) after balloon withdrawal.

1.3 Complications: why 30% of interventions fail

Despite many recent advances in stent designs and delivery systems, failure to achieve adequate vessel perfusion at three months is still not achieved in approximately one-third of patients [13]. There are four

distinct periods during which failure may occur, each with its own characteristic pathology: procedural, acute (0-several hours), subacute (1-14 days), and chronic (3+ weeks).

Procedural complications arise from the failure to place the stent correctly. The endovascular stent is delivered through more than one meter of tortuous vasculature using a series of coaxial guidewires, catheters, and guide catheters, and often must be emplaced with 1 mm accuracy. Early stenting procedures were hampered by problems such as slippage of the stent during delivery and imprecise positioning, however improvements in delivery systems have made these failures rare.

Acute failures occur immediately postoperatively, and are caused by either disorganized thrombus or more commonly delamination of the plaque lining the vascular wall next to the stent [14]. Blood is driven between the plaque and the wall, causing further dissection, and possible obstruction of the lumen. Such dissections may be tacked up against the vessel wall with a second stent while the patient is still in the catheterization laboratory.

Subacute failures are caused by an accumulation of organized thrombus in the vicinity of the stent from 1 to 14 days postoperatively, and in the early 1990's were a leading cause of stent failure occurring in 5-12% of cases. Although the clotting cascade in response to vascular injury has been extensively studied, it is not clear what the precise nature of the stent-imposed injury is. Endothelial denudation [15], tearing of the elastic lamina [4], tensile strain [16], and changes in the blood shear force caused by turbulence [17,18] have all been observed to occur post-stenting; their roles in initiating thrombosis is the target of current research efforts [for an overview, 19]. Despite these uncertainties, improvements in both pharmacologic treatment and clinical techniques have reduced subacute thrombosis rates six-fold to less than 1% [20,21], making this also a minor contribution to overall stent failure.

The primary failure mode of stenting occurs several weeks after implantation. The permanent addition of a stent to the arterial wall frequently induces a persistent and aggressive vascular response causing nearly 1/3 of stented patients to require further intervention within six months [13] to restore patency after thrombosis, fibrosis, and rapidly proliferating smooth muscle cells progressively occlude the lumen (neointimal hyperplasia) (Figure 1.3). Unlike acute complications, this reaction has not been greatly reduced by refinements to the implantation procedure. The biological underpinnings of vascular response to injury are complex and include platelet aggregation, monocyte infiltration, and change in smooth muscle cell phenotype [5] (Figure 1.4). Despite continued investigation into the biological causes and remedies, restenosis from the combined effects of neointimal hyperplasia, medial degeneration, and vascular remodeling remains an unsolved problem in modern interventional cardiology.

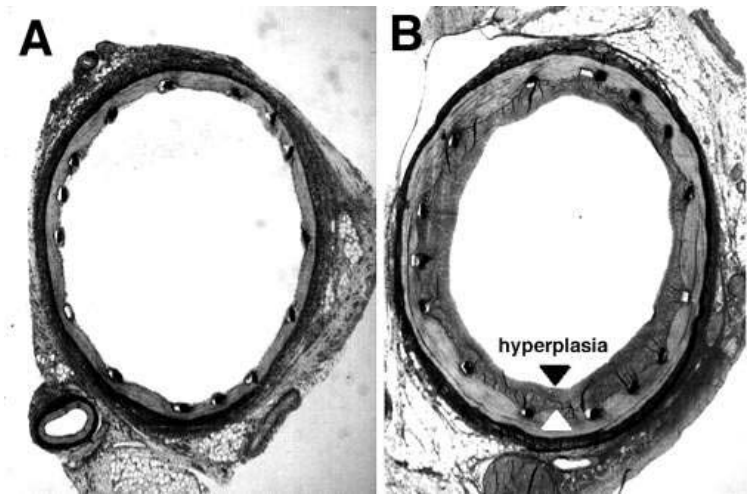

Figure 1.3: Pig coronary artery 3 days (A) and (B) 28 days after stenting. Smooth muscle cells have begun to migrate and proliferate in response to stent placement. The decrease in luminal area from intimal hyperplasia is highlighted. This hyperplasia often progresses, restenosing the stented vessel.

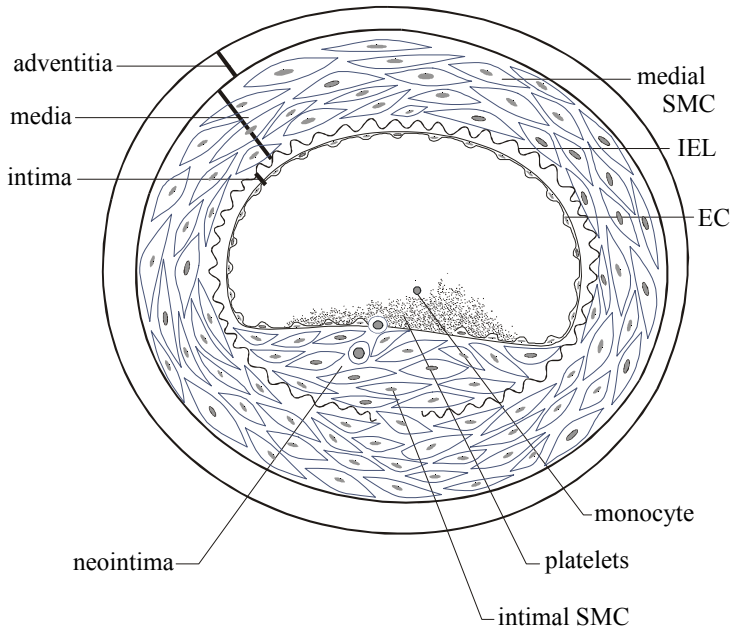

Figure 1.4: The upper portion of this figure shows a cross-section of a healthy artery. The endothelial cell (EC) monolayer rests upon basement membrane covering the internal elastic lamina (IEL). The media is composed of smooth muscle cells (SMC). After EC injury (bottom), platelets are adhering to the exposed thrombogenic surface of the vessel wall and are attracting monocytes, and SMC have begun to proliferate and migrate through the IEL to form a neointima.

In summary, a typical advanced human coronary artery lesion, such as shown in Figure 1.1, is comprised of a heterogeneous mass of calcified plaque, fatty atheroma, lipid pools, and necrotic debris that has developed over the course of many decades. An endovascular stent implanted into such a lesion may provide excellent acute postoperative results as shown in the angiography of a left anterior descending coronary artery (Panel A, Figure 1.5). However the vascular response to the stent reduces the initial gain in luminal area, as shown in Panel B taken three months later. In both angiograms the stented region is boxed. The stainless steel stent itself cannot be seen as it is not sufficiently radio-opaque. A postmortem cross section of a stented human coronary with extensive hyperplasia is shown in Figure 1.6.

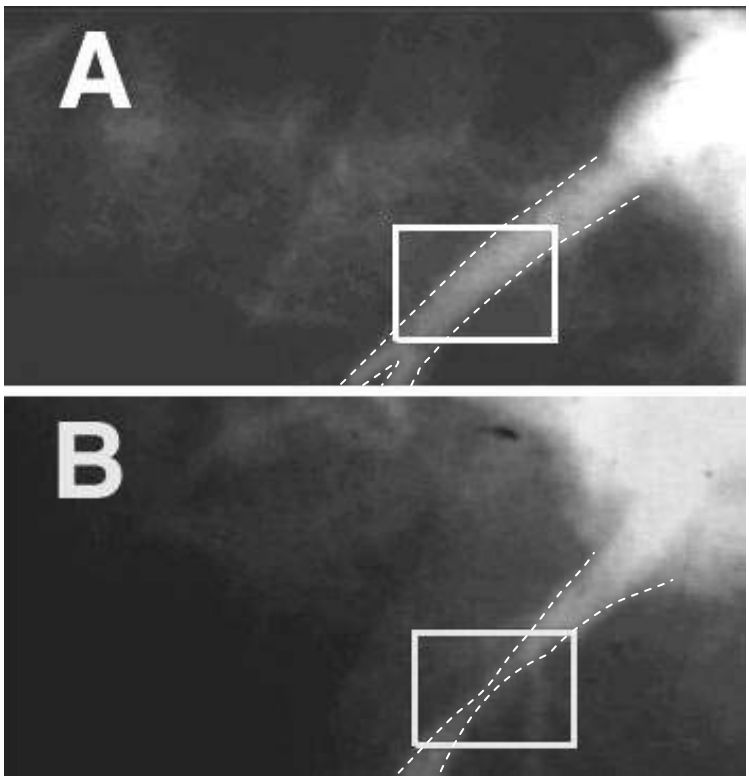

Figure 1.5: Angiograms showing the progression of restenosis in a porcine left anterior descending (LAD) coronary artery immediately after stenting (A) and 3 months post-operatively (B). Radio-opaque contrast dye has been injected into the coronary and appears as white or light gray. The artery is outlined in white and its narrowing is visible in the boxed area of B.

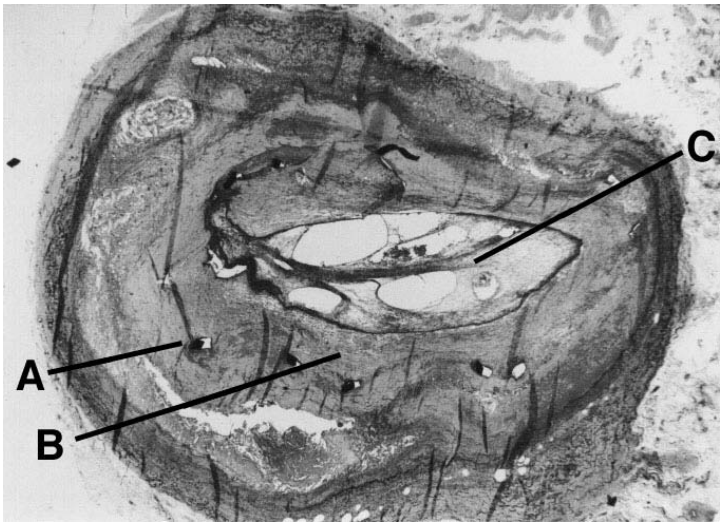

Figure 1.6: Human saphenous vein graft after stenting with strut legs (A), neointima (B), and lumen (C) partially occluded with postmortem thrombus. The prestenting lumen of this diseased vessel is marked by the light grey collar surrounded by the struts. The struts are deeply embedded in a matrix of intimal smooth muscle cells formed after the stent deployment.

1.4 Mechanical basis of arterial injury

1.4.1 Why investigate the *mechanical* basis for arterial injury?

The desire to understand and limit the most common mode of stenting failure—chronic restenosis—must include an understanding of the mechanical basis of arterial injury. A purely biological approach is inadequate because the cellular signal transduction mechanisms that regulate the response to injury are not fully understood, and it is difficult to find an adequate animal model of human restenosis in which to perform experiments. Although many mammalian vessels do respond to injury with neointimal proliferation, only primates develop calcified atherosclerotic plaque, and require years to approach the complex heterogeneity characteristic of advanced human coronary lesions. To underscore this difference, *all* pharmacologic treatments have failed when tested in clinical trials even when they proved highly effective in animals trials [22].

The cellular signaling mechanisms that result in platelet deposition, thrombus formation, and smooth muscle cell proliferation begin in response to specific external stimuli. Gross mechanical deformation seems the most likely candidate for this stimulation; studies have documented that the extracellular matrix [23], smooth muscle cells [23, 24,25], and endothelial cells [26] all release smooth muscle cell mitogens when exposed to mechanical strain. Preliminary data has shown that the magnitude of restenosis is dependent on the stent geometry [16], lending added support for this hypothesis.

1.4.2 Mechanical arterial injury: during stent insertion

Mechanically-based arterial injury may occur during any of three stages of stent implantation: during insertion, during expansion, and chronic.

Prior to stent expansion, the stent/catheter system must be inserted into the stenosed arterial lumen. The lumen is usually first predilated with a balloon catheter placed over a guidewire to create sufficient room for the unexpanded stent. If the artery is severely occluded, the guidewire may leave the lumen and create a false lumen. If the false lumen is formed within the atherosclerotic lesion, strips of plaque may delaminate and occlude blood flow. As previously discussed, this may be treated with the placement of a second stent and is unlikely to directly injure the vessel. If however the false lumen is created deeper in the vessel wall, there will be tearing of the media and possible arterial puncturing. This type of injury is rarely reported clinically, and is unlikely to be the cause of the post-stenting neointima observed in animal models that develop only a soft atheroma.

1.4.3 Mechanical arterial injury: during stent expansion

Several different modes of vascular damage may occur during the short time period of stent expansion. The stent may not expand in an even manner, but instead transiently adopt shapes asymmetric with respect to either its longitudinal axis (e.g. a funnel), its circumferential angle (e.g. an ovoid cylinder) or both. These asymmetries may in turn either directly injure the artery by causing the stent struts to scrape or lacerate, may allow the delivery device to abrade the vessel wall, or may initiate a normal or shear strain-sensitive cellular signaling mechanism. The endothelium provides a natural marker for this type of injury; it is an exquisitely delicate structure that can completely be removed by even the gentle rubbing of a nylon monofilament loop. Recent data from this laboratory reveal that characteristic patterns of post-stenting endothelial denudation are likely caused during stent expansion (vs. chronic injury) since they can be first observed minutes after stent emplacement [15].

Arterial deformation may be completely characterized by a nine component strain tensor. Gross device expansion characteristics as described above can be quantified by characterizing only the external surface of the stent, which requires a four component strain tensor, of which three components are independent. As defined in cylindrical coordinates (Figure 1.7) these are: circumferential $\varepsilon_{\theta\theta}$ which will tend to make the stent increase in diameter, torsional $\varepsilon_{\theta z}$ which will tend to make the stent twist around its axis, and longitudinal ε_{zz} which will tend to make the device lengthen or shorten. In general, this tensor varies as a function of location along the stent, and changes with time as the stent is expanded.

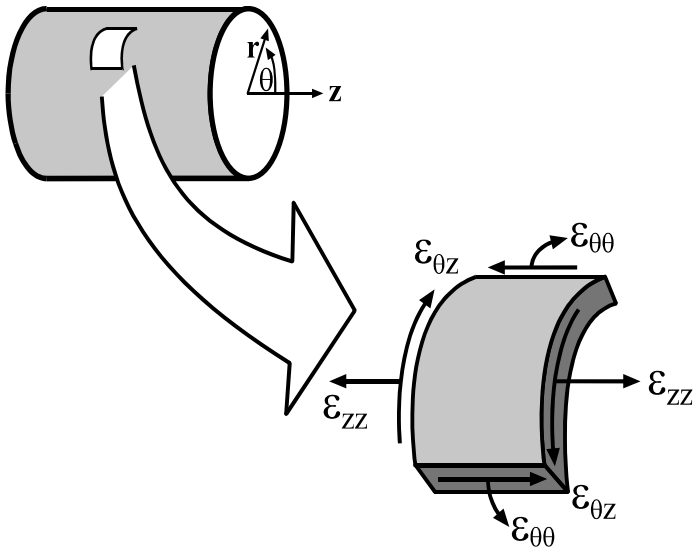

Figure 1.7: The two-dimensional strain field of a tubular surface shown in cylindrical coordinates. The components $\varepsilon_{\theta\theta}$, ε_{zz}, and $\varepsilon_{\theta z}$ are referred to in this thesis as circumferential, longitudinal, and torsional strains, respectively.

1.4.4 Mechanical arterial injury: chronic

The permanent nature of stents introduces chronic changes that may also influence the vascular response. The stent itself may elicit a material response from the artery, even when constructed from materials usually considered to be biocompatible [27, 28]. As earlier discussed, large strains such as those imposed by implants on the endothelium and media have been directly linked to production of smooth muscle cell growth factors [23-26]. Another possible initiator of the vascular repose to stenting arises from remodeling of the vascular wall to relieve chronic stress.. Fung has shown that rat pulmonary arteries subjected to hypoxic hypertension (which induces less than 20% of the strain induced by stenting) begin to change their zero-stress state in as little as 72 hours [29]. This permanent remodeling changes both the geometry of the

arteries and the material properties of the tissue [30]. Vascular implants also alter the blood flow hemodynamics by introducing regions of turbulence, stagnation, flow separation, and altered wall shear [31]. This may explain why remodeling has been shown to depend at least in part on stent geometry [32]. Recent studies show that the endothelial lining is sensitive to spatial changes in shear force, and also that step dislocations of the wall shear such as imposed by stent struts cause endothelial cells' morphology to change over short distances on the order of 1 mm [17,33].

1.5 Arterial injury caused during device emplacement

Of the preceding modes of implant-caused vascular injury, I have chosen to examine the hypothesis that the acute and chronic tissue responses are influenced by the manner in which the implants are placed within the body. I have chosen this because:

1. It has been shown that deep injury to the media occurs during stent expansion, and this damage is linearly related to chronic levels of restenosis [4], and further

2. superficial injury to the endothelium also occurs during stent expansion [34],

3. yet there has been comparatively little research to understand the precise nature of the transitory mechanical phenomena that initiate these biological sequelae.

1.6 Thesis objective and organization

Thesis objective: Model and understand the interaction between the dynamic manner of implant expansion and the tissue response as a function of the device geometry, the tissue characteristics, and the qualities of the exerted forces.

Specifically Chapter 2 will describe experimental quantification of stent expansion through measurement of the temporally and spatially-varying surface strain tensor developed on the arterial surface.

Chapter 3 uses this method to compare expansion characteristics of different stent geometries in different arteries using different expansion systems. Differences between the expansion characteristics of the stent systems are examined and the relationships between the manner of expansion and the superficial and deep injuries produced are analyzed. Minor modifications to existing stent designs are proposed that reduce these injuries, and the results of these modifications will be experimentally compared to unmodified designs.

As Chapter 3 examines stent expansion from a macroscopic viewpoint, Chapter 4 investigates the manner in which injury within each repetitive strut element may arise. One set of simulations were designed to both quantify the distribution of intrastrut in-plane strain that develops across each stent strut. A second set of simulations determine the relative positions of the balloon and luminal arterial surface to establish whether any normal forces are exerted by the balloon into the artery during stent expansion. The results of these simulations will be compared with histological evidence taken from animals stented with several stent geometries, and general rules for minimizing this mode of injury will be examined.

CHAPTER 2 Measuring Arterial Strain

2.1 Introduction

Stent implantation imparts extreme vascular strains and focal mechanical injury to the vessel wall, ranging from denudation of the endothelial cell monolayer that covers the interior of the lumen, to progressive laceration of deeper vascular structures [4,35]. The amount of injury inflicted by the stent is not only a function of the final vessel enlargement ratio but also of the stent geometry [36] which dictates whether the stent axially contracts or twists as it circumferentially expands. This suggests that a more complete characterization of the form and extent of strain imparted by stents may deepen understanding of the vascular response to strain, and may also lead to improved endovascular implant designs that minimize injury.

To fully characterize the deformation of the arterial surface by the expanding stent, the circumferential, axial, and torsional components of the strain tensor must be determined. In general, these components vary as a function of location along the stent, and change with time as the stent is expanded. The ability to measure these *in vivo* is constrained by two factors not addressed by techniques presently in use. First, although it is necessary to track the three-dimensional locations of arterial markers over the curved arterial surface, the surgical incision required to expose the artery for imaging without altering its orientation and environment is deep and narrow, making a multiple-camera approach impractical. Second, as the strain field tensor varies along the length of the stent, it must be determined locally as a function of position along the artery. This chapter describes a method using a single camera to measure the dynamic, local strain tensor developed along the surface of a cylindrical wall as it deforms in an axisymmetric manner. Testing was performed *in vitro* on excised bovine arteries deformed by stenting to determine the method's suitability to measure stent-induced arterial strain. Accuracy was determined using a large-scale inflatable latex phantom. The feasibility of using this system to measure arterial strain *in vivo* was assessed on a rabbit undergoing stenting in both femoral arteries.

2.2 Methods

2.2.1 Experimental

A system was developed to imprint the surface of the artery with a fine grid of high-contrast ink marks by mounting an ink-jet printer cartridge (Cannon CJ-3A) in a handheld stylus and driving it with a low-impedance squarewave (Figure 2.1). Benchtop testing showed the cartridge formed regular 50 μm to 250 μm marks when driven by a 24 V pulse train using a pulse-on duration from 1 to 20 μs. A 10 Hz train of 5 μs pulses was used to produce 150 μm arterial markings.

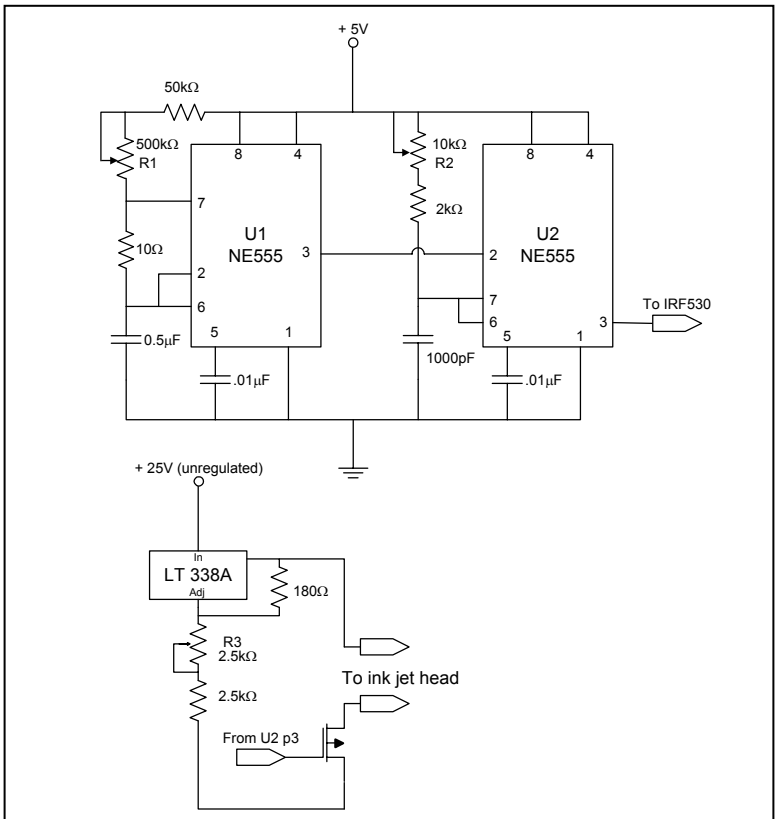

Figure 2.1: Schematic diagram of driver for ink jet printer cartridge head. By altering pulse width and height by R2 and R3 respectively, the operator can control the quality of the marks (over and underdriving produces overspray) and the size of the marks from 50 μm to 250 μm. The operator controls the rate of mark production with R1. Not shown are the 5V, 100 mA and 25V, 1A switching power supplies, a momentary on/off switch mounted on the marking stylus, and a rotary selector switch to choose one of the nine ink jet ports available on the Cannon CJ-3A cartridge.

Experimental data were recorded using an imaging system (Figure 2.2) consisting of a deep-field zoom lens (Computar 18-108 mm, f2.5) with attached polarizing lens mounted on a CCD camera with 640x480 pixel resolution (Hitachi VC-C370). The camera's NTSC signal was recorded on an S-VHS system, channeled to a frame grabber (Raster-Ops 24XLTV) via S-video cable, and digitized to 640x400 pixel resolution. The strain measuring system was first tested using excised bovine coronary arteries deformed by a stainless steel endovascular stent (Advanced Cardiovascular Systems/Guidant) mounted on a 3 mm polyethylene balloon catheter (Advanced Cardiovascular Systems/Guidant). The arterial surface was marked using the ink-jet system and imaged as the catheter was inflated to a maximum pressure of 8 atm in 2 atm steps. To determine the accuracy of the strain measurements, a large-scale latex phantom artery was imaged as it underwent deformation using the same setup shown in Figure 2.2. We hand-marked a grid upon the phantom, and recorded data as the tube was inflated in step increments from an average diameter of 46 cm to 175 cm. After each step the tube was allowed to stabilize for 1 minute to reduce creep or other viscoelastic effects that might confound manual measurements. The distances between 60 pairs of markers were hand-measured, yielding the circumferential, axial, and torsional strain components at 20 locations on the phantom's surface. The image was concomitantly digitized with a comparable field-of-view to the bovine coronary experiment, and the digitized data were processed with the strain measuring system for comparison.

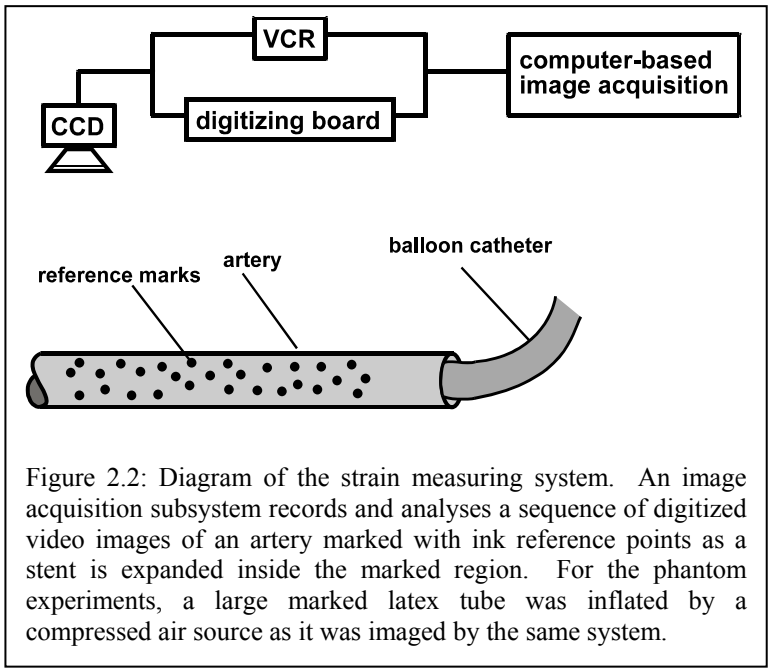

Figure 2.2: Diagram of the strain measuring system. An image acquisition subsystem records and analyses a sequence of digitized video images of an artery marked with ink reference points as a stent is expanded inside the marked region. For the phantom experiments, a large marked latex tube was inflated by a compressed air source as it was imaged by the same system.

In vivo feasibility was demonstrated by measuring the arterial strain in a rabbit undergoing stent implantation in both femoral arteries. A 3.4 kg New Zealand rabbit was anaesthetized with ketamine (35 mg/kg IM) and sodium pentobarbital (Nembutal, 4 mg/kg IM), and a length of each femoral artery was exposed and cleaned of fascia in preparation for the arteriotomy (Figure 2.3). The length of artery isolated was approximately 5 cm longer than required for the arteriotomy, and after the incision was performed a hemicylindrical black plastic cradle was placed behind the excess length to improve contrast of the arterial envelope. The artery was marked in a gridded fashion using the inkjet stylus and a corrugated-ring stainless steel stent (Advanced Cardiovascular Systems/Guidant multilink 3 mm x 12 mm) mounted on a 3mm compliant balloon angioplasty catheter was advanced to the marked section. The balloon catheter was slowly pressurized to 8 atm, expanding the stent while the artery was imaged with the same apparatus used for the *in vitro* experiments.

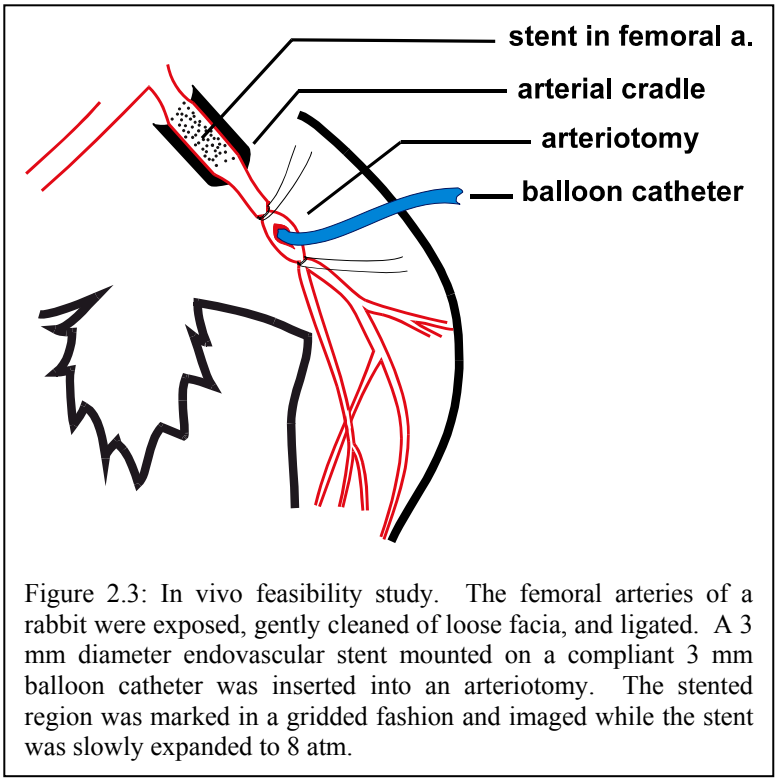

Figure 2.3: In vivo feasibility study. The femoral arteries of a rabbit were exposed, gently cleaned of loose facia, and ligated. A 3 mm diameter endovascular stent mounted on a compliant 3 mm balloon catheter was inserted into an arteriotomy. The stented region was marked in a gridded fashion and imaged while the stent was slowly expanded to 8 atm.

2.2.2 Analytical

Strain data were extracted from the digitized images through several intermediate processing steps (code in Appendix A). To determine three-dimensional locations of the markers from each two-dimensional frame, the artery was assumed to be axisymmetric; i.e. in $\{r, \theta, z\}$ cylindrical co-ordinates of equation $r = f(z)$. The outer envelope of the vessel was digitized and a general two-dimensional quadratic equation fit to the envelope. The general quadratic equation, of the form $A r^2 + B r z + C z^2 + D r + E z = 1$ was chosen to model the vessel's envelope because of its flexibility; with few coefficients it can model two line segments that are parallel, converging (a section cut from an ellipse), or diverging (a hyperbola of two sheets). The coefficients were determined using the Nelder-Meade non-linear least-squares algorithm [37] implemented in the Matlab programming language. Once the two-dimensional equations describing the stent envelope were determined, their paths were swept around their longitudinal axis to create a three-dimensional axially-symmetric quadratic surface model. The locations of the reference marks from each two-dimensional frame were back-projected onto this three-dimensional model and the three-dimensional locations stored for strain analysis.

The surface strain components $\{\varepsilon_{\theta\theta}, \varepsilon_{zz}, \varepsilon_{\theta z}\}$ can be determined within a uniformly-strained triangular region if the change in distance between the vertex points are known [38]. Triads of reference points were automatically grouped by computer under the assumption that the strain, although highly non-uniform over the 12mm length of the stent, varied in space sufficiently gradually between neighboring markers so that a good local approximation could be found using adjacent markers located 0.5-1.0 mm apart. The algorithm that grouped the reference points assigned a weighted score to each potential triad. A positive weight was associated with triads including points separated by an empirically-determined optimal distance. Points separated too widely average-out the locally varying tensor field, reducing the spatial resolution of the system. Points grouped too closely together suffer from a high error-to-measurement ratio caused by additive uncertainties in position. A negative score was associated with triads constraining points progressively closer to the edge of the artery model as they generate exaggerated position measurement error because of the sensitivity of the back-projection. In a typical artery, approximately 40 reference marks were formed, providing nearly 60,000 possible triads. Of these, 50 possibly overlapping triads were chosen as optimal based upon this weighted score. Once chosen, the strain tensor within each reference-point triad was determined and associated with the corresponding area on the arterial surface. Areas of the arterial surface that lacked suitable reference point triads were associated with the strain tensor from the nearest reference point triad. If the earlier assumption of axial symmetry was valid each axial slice should have the same strain tensor, independent of θ. The strain tensor for all segments within each axial slice was therefore replaced with the average tensor for the entire slice, and an alert was generated if any of the values varied from the average by more than 10%.

2.3 Results

2.3.1 *In vitro* artery segment

The system was able to accurately measure large strains in a 2mm diameter excised bovine coronary artery expanded by a 3mm balloon-expandable stent. At 2 atm of pressure (Figure 2.4) the stent had not yet expanded sufficiently to contact the arterial wall. There was so little circumferential expansion at this point that both proximal and distal ends appear slightly bowed inwards, although this is likely measurement error since the system's measurements have a standard deviation of approximately 10%. As the balloon catheter pressure was increased to 4 atm the proximal (left in Figure 2.5) end of the stent began to inflate first, with relatively small gain in luminal area compared to the initial diameter. At 6 atm both proximal (left in Figure 2.6) and distal sides enlarged, leaving the center of the stent less expanded. Torsional strain components remained near zero, while the axial strain became clearly negative, reflecting arterial shortening during circumferential expansion. As the pressure increased to 8 atm the balloon/stent unit expanded to fully contact the arterial wall along its length and the arterial surface regained a cylindrical appearance (Figure 2.7). The proximal end relaxed inwards, becoming slightly less open than the distal region. The small torsional component of strain indicates that twisting around the longitudinal axis remained nearly zero throughout the expansion, although the negative axial component indicates the artery contracted 10% to 20% in length.

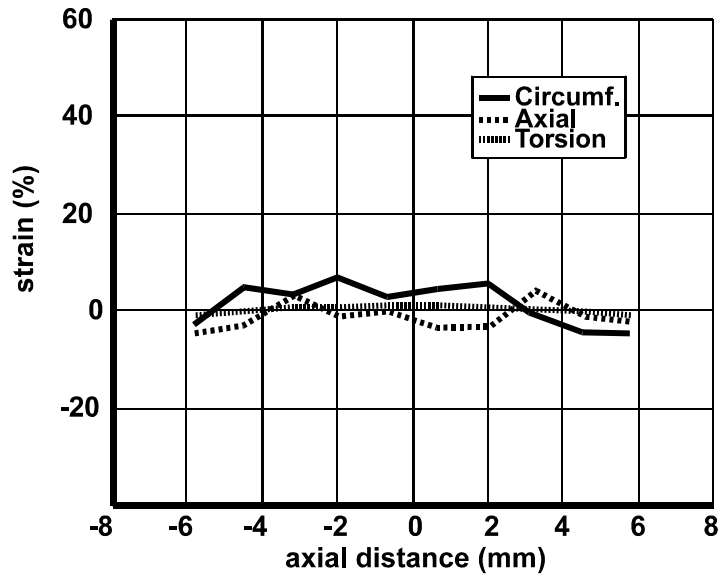

Figure 2.4: Arterial surface strain tensor components after in vitro stent expansion to 2 atm. The horizontal axis represents distance along the length of the artery.

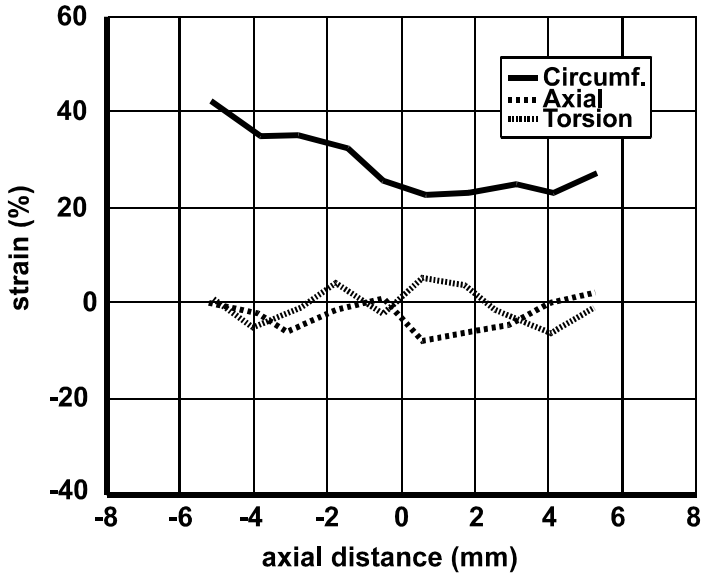

Figure 2.5: Arterial surface strain tensor components after in vitro stent expansion to 4 atm. The stent has begun to expand proximal end first.

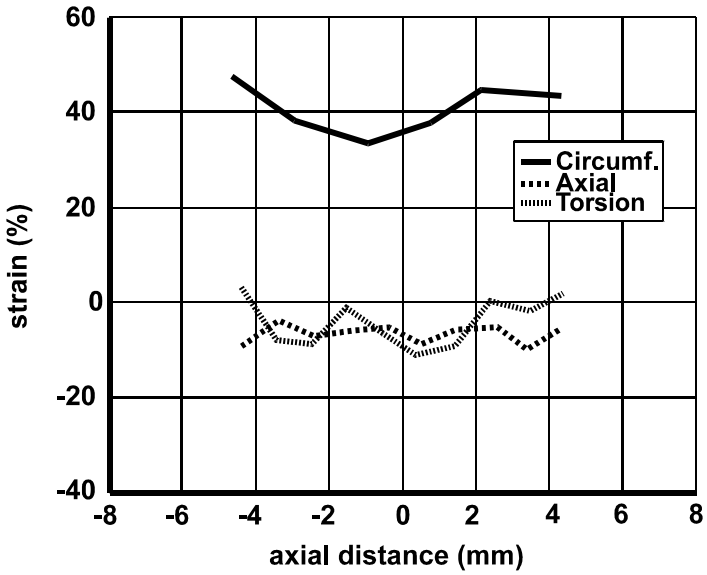

Figure 2.6: Arterial surface strain tensor components after in vitro stent expansion to 6 atm. Both stent ends have deployed leaving the center of the artery unsupported.

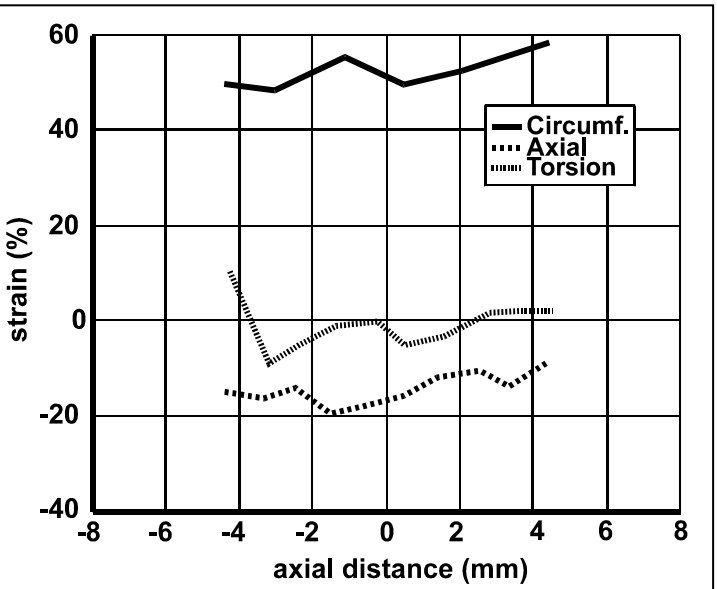

Figure 2.7: Arterial surface strain tensor components after in vitro stent expansion to 8 atm. The stent's middle region has expanded and circumferential strain is now evenly distributed along the length of the stent. Notice the degree of axial contraction that has occurred as the center expanded.

2.3.2 Latex phantom

To examine the errors inherent in the strain measuring system, a large scale cylindrical latex phantom was inflated, and strain was measured both by the imaging system and directly using calipers. Measuring inter-mark distances by hand eliminated errors from the limited resolution of the imaging system and the modeling assumptions inherent in backprojection. Six sets of measurements were taken at incremental stages of increasing balloon radius. The system error was defined as the difference between the computed strain tensor and the true strain tensor as determined by direct hand-measurement. The error is zero mean ($p<0.03$) and is plotted in Figure 2.8.

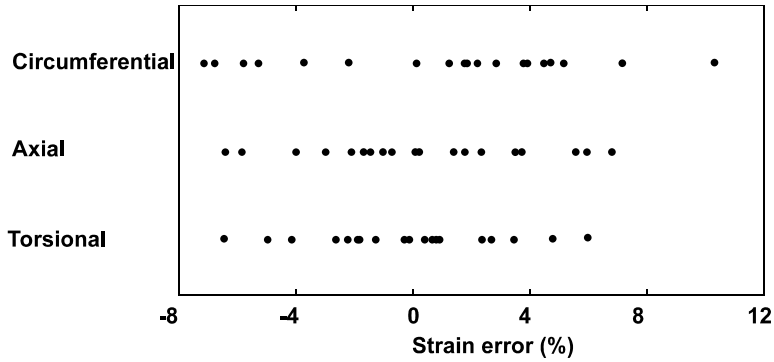

Figure 2.8: The accuracy of the strain measuring system was demonstrated by comparing the magnitude of the strain tensor it calculated on the oversize latex phantom with a hand-measured reference. The difference it between these values are plotted above for each component of the strain tensor. The root-mean-square measurement error of the system is 4.1%.

The assumption that the artery is axisymmetric and has a quadratic surface of revolution was also examined. Table 2.1 shows the standard deviation σ_e of the measured arterial/phantom radii r_i around the least-squares fit quadratic surface $r(x_i)$ as a percentage of the average radius. The standard deviation was calculated as

$$\sigma_e = \left(\frac{1}{N-1} \sum_i \left(r_i - r(x_i) \right)^2 \right)^{1/2}$$

for N = 10 equispaced points along the sample's length. The standard deviation of the error is a small fraction of the average radius, indicating that the arterial/phantom surfaces are nearly quadratic.

Table 2.1: Determining the validity of the assumption that the artery and phantom are axisymmetric and have a quadratic surface. The standard deviation of the error is shown as a percentage of the mean radius. Values tending toward zero indicate close agreement of the quadratic envelope to the measured envelope.

Phantom		Bovine coronary		Rabbit femoral	
Step number	$\frac{\sigma_e}{\bar{r}}$	Pressure (atm)	$\frac{\sigma_e}{\bar{r}}$	Pressure (atm)	$\frac{\sigma_e}{\bar{r}}$
0	0.023	0	0.016	0	0.032
1	0.12	2	0.018	2	0.042
2	0.10	4	0.090	4	0.091
3	0.044	6	0.048	6	0.081
4	0.032	8	0.061	8	0.052

2.3.3 *In vivo* artery

The feasibility of using this system *in vivo* was demonstrated by deployment of an endovascular stent within both femoral arteries of a rabbit. The results of arterial marking are shown in Figure 2.9. The moisture on the arterial surface did not impede marking, and there was negligible mark spread due to diffusion. There was a notable circumferential mark spread post-expansion proportional caused by circumferential strain. An example of the calculated arterial strain tensor is shown in Figure 2.10 for a balloon expansion pressure of 6 atm. This pressure corresponded to the maximum end-first expansion timepoint for both arteries, and both can be seen opening proximal (left) side first, in a similar manner to the *in vitro* experiments. The limited field of view imposed by the surgical environment did not impair the ability of the system to measure the strain tensor, although glare caused by the surgical lamps did require installation of a polarizing lens on the camera.

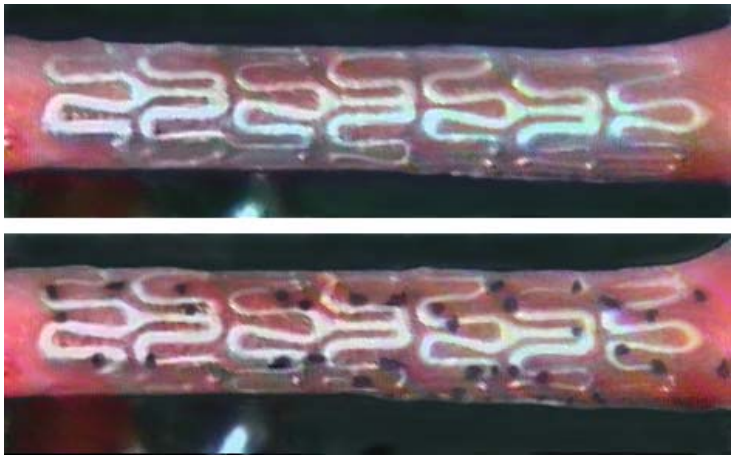

Figure 2.9: The ink-jet marking method was tested in an in vivo environment. An exposed rabbit femoral artery is shown here proximal to the site of arteriotomy before and after marking with 150μm dots. The artery is translucent in a live animal showing the underlying corrugated ring stent.

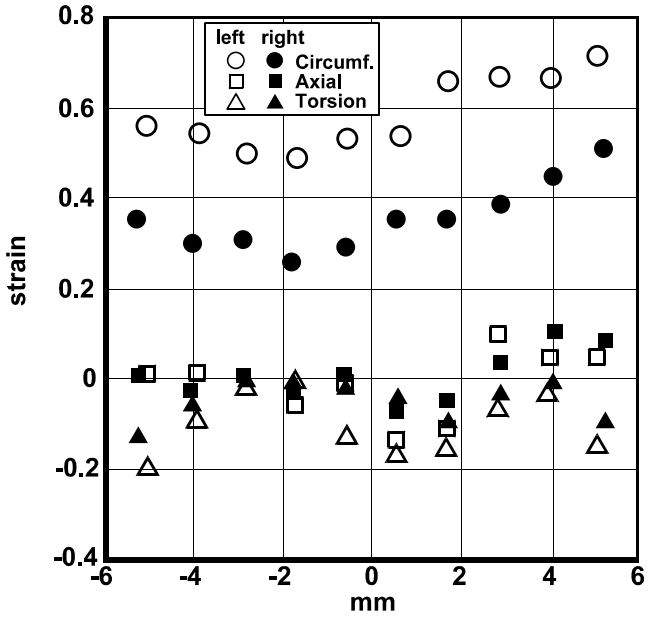

Figure 2.10: The system can measure strains in an in vivo environment. Here strains are shown generated in two rabbit femoral arteries by 3 mm stents mounted on balloon catheters pressurized to 4 atm. The end-first opening characteristic can be clearly seen, accompanied by slight axial shortening and relatively minor torsion, similar to that seen *in vitro* at similar pressures.

2.4 Discussion

We sought to measure the strain imparted to arteries by endovascular stents, as this may be an important determinant of the biological response to these implants. We chose to use the Green tensor formulation [39]as have several other investigators of biologic strains [40,41,42,43].

Of the nine components of triaxial, or solid strain that exist, four can be measured using surface marks alone, and of these biaxial or surface strains, three components are independent. As defined in cylindrical co-ordinates $\{r, \theta, z\}$ these are: circumferential $\varepsilon_{\theta\theta}$ which will tend to make the cylinder increase in diameter, torsional $\varepsilon_{\theta z}$ which will tend to make the artery twist around its axis, and longitudinal ε_{zz} which will tend to make the artery lengthen.

2.4.1 Approaches to measuring strain in biologic materials

The determination of surface strains in low-modulus biological materials such as arteries is not a new problem, and recent advances in imaging and computation systems have made several new measurement methods possible. The large deformations experienced by compliant tissues favor the use of non-contact systems that image tissue-bound markers using a variety of media, including: light ([38,41,42], and others), ultrasound [44], x-rays [43,45], and phase-contrast magnetic-resonance [46]. The most common method used to measure strain in compliant tissues involves marking the specimen before optically imaging the displacement. Ink has been applied to specimens both directly [47] and by sprinkling using the bristles of a toothbrush [48]. Others have used inert particles such as vanilla-bean pieces pressed into the specimen surface [49] or fluorescently-labeled microspheres [50] to achieve the high-contrast needed to identify the markers amidst the visual noise of ambient glare and the irregular surface of moist tissue. Displacement over curved surfaces has been measured using multiple cameras [51,43] to gain three-dimensional displacement information.

Our characterization of the locally-varying strain field imparted by an expanding stent to an intact artery has two unique requirements not addressed by the above techniques. First, although it is necessary to track the three-dimensional locations of arterial markers over the curved arterial surface *in vivo*, the surgical incision required to expose the artery for imaging is deep and narrow, making a multiple-camera approach impractical. Second, the strain field tensor varies along the length of the stent, and so it must be determined locally as a function of position along the artery.

As shown in Figures 2.4 - 2.7 the strain measuring system described in this article satisfies these criteria, and was used to quantify patterns of stent-induced arterial deformation in both *in vitro* and *in vivo* environments. Consistent with behavior in clinical settings, the test stent

opened from its extreme distal and proximal ends inwards which created a slightly dogbone shaped surface as the balloon catheter was inflated to 6 atm. The center region deployed once the balloon pressure increased to 8 atm, which created a more uniform cylindrical envelope. The expansion of the center region from 6-8 atm was accompanied by the first significant levels of observed axial shortening. The nonuniform strain along the length of the stented artery and the presence of negative axial strains separate stent expansion from the expected uniform behavior of balloon-alone expansion.

The system's ability to measure arterial strains in a surgical environment was demonstrated by the *in vivo* experiments, which showed more extreme examples of end-first opening than occurred *in vitro*. The primary factor complicating measurements was glare from the surgical lamps that interfered with the camera. The addition of a polarizing filter reduced but did not eliminate glare. Slight translations and rotations of the artery caused by cardiac and respiratory cycles did not affect measurement accuracy, since the strain tensor is calculated by noting the change in the distance between mark positions, not the change of the mark positions themselves [50].

2.4.2 Error analysis

The three primary contributors of error in the computed strain tensor, henceforth called calculated strain, are lack of arterial axial symmetry, poor fit of the longitudinal envelope to a quadratic model, and measurement inaccuracies from limited resolution of the digitized image. The magnitudes of these errors are difficult to measure directly on the 2 mm diameter artery, and the highly non-linear method of marker association into triads does not lend itself to theoretical methods of error analysis. For these reasons we constructed a large-scale latex phantom which allowed us to hand-measure the distance between markers.

The assumptions that the artery is axisymmetric and fits the quadratic envelope of a cylinder, elliptic section, or hyperboloid is surprisingly small for the *in vitro*, *in vivo*, and phantom samples we investigated (Table 2.1) and contributes less than 10% of the total error. This would not be the case for tortuous arteries such as the human coronary that display little symmetry; backprojection of marker locations in this type of vessel would require a more generalized model of arterial shape. The primary source of error in our investigations arises from the limited resolution of the camera and has two components: spatial quantization that is a function of the finite number of CCD elements within the camera, and the limited line resolution of the S-video standard used to encode the analog video signal. These sources are hardware-dependent and difficult to reduce. Although increasing the magnification to make the stented region completely fill the field of view of the camera would decrease this error, it would be hard to do so *in vivo* because of motion

between the camera and stent from natural cardiac and respiratory cycles, and movements of the catheter during inflation.

The standard deviation of the strain tensor error components is calculated as

$$\sigma_{\varepsilon} = \left(\frac{1}{N} \sum \left(\varepsilon_{actual} - \varepsilon_{calculated} \right)^2 \right)^{1/2}$$

and is shown in Figure 2.8. These data show that the system measures all three components of the strain tensor accurately to a standard deviation of approximately 4%. Since the error is primarily derived from camera quantization error which is not a function of strain, we expect similar measurement errors in an *in vivo* environment.

The strain tensor computed as a function of three specific markers represents the average strain experienced within that marker triad. The system's spatial resolution, or ability to localize changes in strain, is therefore limited to the average distance between these markers. We chose to examine marker triads separated by 0.75 -1 mm which struck a reasonable balance between spatial resolution and the effect of digitization error on strain measurement accuracy. This spatial resolution allows us to examine macroscopically how vascular implants expand and move, although it does make the system insensitive to large changes in strain over a short distance such as might occur in the immediate vicinity of a 0.25 mm strut. Spatial resolution may be improved through the use of higher magnification at the expense of limiting the field of view.

2.5 Conclusions

As use of medical implants grow more common it has become increasingly important to understand how these devices mechanically interact with tissue in their native *in vivo* environment. Endovascular stents, for example, engender a tissue response that is likely a function of the extreme levels of strain they impose, yet these have not been rigorously measured *in vivo*.

The technique described in this chapter is an important step towards this goal. This method can determine the complete surface strain tensor developed along any straight and observable axisymmetric surface undergoing large-scale deformations, and can describe how the tensor changes in space and time. It can do so in an *in vivo* environment using a single camera. Further, the development of a system that can create marks as small as 50 μm permits this method to be used with fine structures such as vessels of several millimeters diameter.

CHAPTER 3 Transient Macroscopic Expansion: Characterization and Control

3.1 Introduction

The techniques developed to measure arterial strain *in vivo* that were described in the previous chapter were used to determine the manner in which stents dynamically deform the arterial wall during expansion. We sought to use this information to answer the following questions: Are there particular modes of expansion that cause acute vascular injury, such as transient endflare, or a transient torsioning moment imparted by the balloon catheter? Can this injurious manner of expansion be controlled? What aspects of stent geometry and balloon length affect this manner of expansion? As permanently implantable devices become increasingly common and mechanically diverse, do the answers to these stent-related questions provide insight to general implant design rules to lessen tissue injury?

The unique pattern of endothelial cell denudation seen in Figure 3.1 provides the motivation behind many of these questions. A corrugated ring stent (Advanced Cardiovascular Systems/Guidant Multilink 3mm x 12mm) was expanded within a rabbit femoral artery, and the arterial surface stained with a solution of silver nitrate [34]. The silver nitrate binds to cellular surface membranes and intercellular junctions, enabling identification of arterial regions with intact endothelium (in light gray, such as in region D), and regions with denuded endothelium exposing the deeper smooth muscle cells of the medial layer (in dark gray, region A). The stent shields vascular wall from the stain and appears as a white shadow (E). Immediately after staining the vessel was excised and incised longitudinally. The stent was removed and the artery unrolled for *en face* mounting. Three distinct regions were immediately apparent: a region of primarily intact endothelium on the inside of the stent (C), a region of nearly entirely denuded endothelium just outside (distal in this image) to the stent (A), and a region near the edge of the stent that appears scraped (B). The first two regions were expected; the largely intact endothelial region is the byproduct of a well-designed stent, and the region of entirely denuded endothelium (A) was caused by direct balloon contact with the endothelium in a similar fashion to that observed during the well-studied procedure of balloon angioplasty [52]. The scraped region, however, was not expected, and its observation

spurred the search for both its cause and its chronic vascular effects. It can be reasoned that stent-induced injury must occur either during stent placement or expansion since its effects can be seen minutes after the device implantation.

Further insight was gained by examining the manner that the stents typically deployed during *ex vivo* benchtop experiments. Slow motion

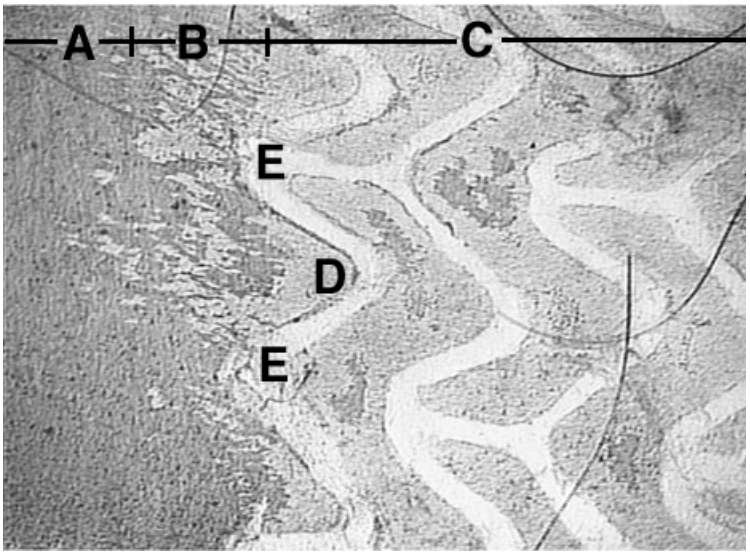

Figure 3.1: Arterial injury immediately post-stenting as evidenced by regions of frank endothelial denudation (region A) and scraped trails of endothelium (B) at the distal end of the stented region (stent outline shown in E). Silver nitrate strained interior section of *en face* mounted rabbit iliac.

replay of unconstrained stent expansion (i.e. stents mounted upon a balloon but not inserted into a vessel) reveal stents typically display a marked tendency to expand end-first. The stent centers expanded a few hundred milliseconds later and the final symmetric cylindrical shape belied the transient flare, and looked remarkably similar to *in vivo* post-stenting angiograms. These data helped form the following hypotheses:

1) Non-uniform stent expansion *in vivo* is responsible for the type of acute vascular injury observed surrounding the edges of the stent.

2) Minor modifications to the stent design can alter expansion dynamics and correspondingly reduce vascular injury.

3.1.1 Chapter organization

Two different series of experiments were performed. The first answered the questions: how do stents expand, and are there specific mechanisms of expansion that cause maladaptive chronic vascular responses? The answer—that a particular mode of end-first expansion does cause acute injury that results in a maladaptive chronic response prompted a second series of experiments. The second set was designed to discover if slight changes in the stent and/or balloon geometry could significantly reduce the degree of transient endflare, and therefore reduce the degree of acute vascular injury. The remaining sections of this chapter are organized around each of these two sets of experiments, named *Stent Expansion Characteristics* and *Control of Expansion* respectively, each with its own sets of materials and methods, results, and discussion.

3.2 Stent expansion characteristics – Materials and methods

3.2.1 Overview of experiments

Experiments were performed to quantify both the manner of stent expansion and the causal acute and chronic response this engenders. Data measuring the arterial surface strain tensor and acute injury were taken using eight stents implanted in four rabbits. Components of strain both on the stent and external surface of the artery were measured and analyzed as the stent deformed, and a theory explaining how transient expansion characteristics caused vascular injury was proposed based upon this evidence. The chronic response was then measured with eight similar stents implanted in four rabbits. After 28 days the stented arteries were harvested and analyzed at proximal, mid, and distal ends for the degree of neointimal hyperplasia.

3.2.2 Strain determination

Four New Zealand white rabbits (3-4 kg, Millbrook Farm Breeding Laboratories, Amherst, MA) were anesthetized with ketamine (35mg/kg IM) and sodium pentobarbital (Nembutal, 4mg/kg IM), and the femoral arteries of each hind leg were exposed and cleaned of fascia in preparation for marking (Figure 2.3). Each of the eight arteries had a length isolated approximately 5 cm longer proximally than required for the arteriotomy to permit observation of the stent. Approximately 0.2cc of 1% lidocaine was topically applied to the distal region and an arteriotomy was performed in that segment. A hemicylindrical black plastic cradle was placed behind the artery to improve contrast of the arterial envelope. The arteries were lightly blotted of excess moisture and bare stainless steel stents (3 mm diameter x 12 mm length slotted tube design, ACS) mounted on a 3 mm diameter by 12 mm length noncompliant balloon angioplasty catheters (ACS) were advanced to the marked region. A grid of 100 μm ink marks were applied to the exterior artery under the stent (Chapter Two). A video camera (Hitachi VC-C370) with a macroscopic lens (Computar 18-108 mm, f2.5) recorded a series of frames over the marked region as the stent was expanded by a balloon catheter pressurized to 8 atmospheres (atm) over a 30 second time period. The time between the blotting and start of stent expansion was less than 60 seconds to minimize changes in arterial characteristics caused by tissue dehydration.

The method used to compute the strain tensor from the relative displacement of the marks is fully described in Chapter Two. Briefly, a three dimensional model of the artery was generated by revolving the two dimensional arterial image around its axis, back projecting each frame's ink marks onto this three dimensional model to extract $\{x, y, z\}$

coordinate information, marks were automatically grouped into triads, and axial and circumferential strains were computed by noting the relative change in distance between the vertices of each triad. The full strain tensor of the external surface of the arterial wall was determined using the sprayed ink dots as registration marks, and the axial component of the strain tensor of the stent using the strut-strut intersections visible through the thin arterial wall as registration marks. Torsional strains were not computed as they were zero to within the accuracy of system measurement for both benchtop and *in vivo* sources.

3.2.3 Chronic response

Eight stents of the same design were placed in a second group of four rabbits and retrieved 28 days later. Although the chronic response of rabbit arteries to injury differs in several respects from the human response, it has become a common and accepted model for many types of human vascular response to injury [53]. Other models, including canine and porcine arterial beds are also common; a full discussion can be found in [54]. To measure the chronic response to stent implantation, animals were anesthetized, as in 3.2.2, and through a 3 cm incision the femoral arteries were isolated in each hind leg, and bare stainless steel stents of the same type as used in the above experiments were deployed using a maximum pressure of 8 atm and an inflation time of approximately 30 seconds. The arteries were not predilated. After 28 days the arteries were fixed *in-situ* with 4% paraformaldehyde and elastic Van Gieson-stained to reveal neointimal formation. The artery segments were embedded in methyl methacrylate and cross-sectioned specimens were taken from proximal, middle, and distal regions. Computer-based morphometric analysis of the neointimal, medial and luminal areas defined the degree and extent of injury as described in [4].

Data are reported as mean ± standard error, unless stated otherwise.

3.3 Stent expansion characteristics – Results

The strain tensor in the exterior surface of the artery was calculated as a function of distance along the stented region, and a typical pattern is shown in Figures 3.2-3.5, each representing a moment in the expansion sequence. Chapter Two determined the standard error of these *in vivo* strain measurements is 4%.

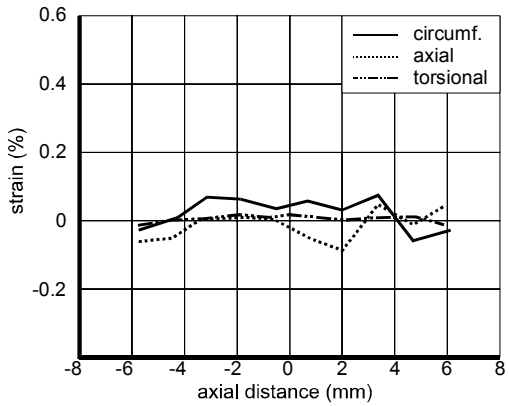

Figure 3.2: The spatially varying arterial surface strain tensor at a balloon pressure of 2 atm. The horizontal axis represents distance along the longitudinal axis of the stent, and the vertical axis represents the magnitude of the circumferential, axial, or torsional component of the strain tensor.

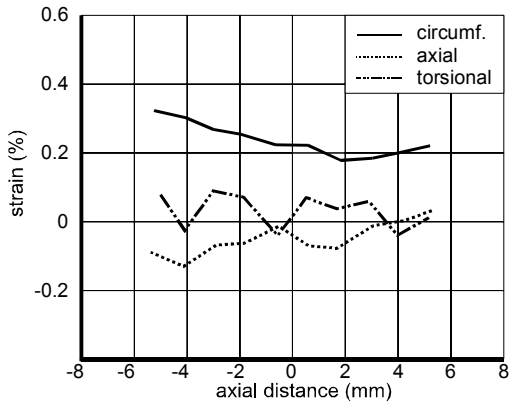

Figure 3.3: The spatially varying arterial surface strain tensor at a balloon pressure of 4 atm. The proximal end has begun to expand.

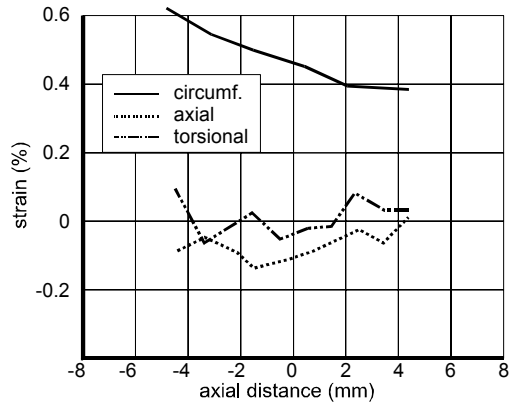

Figure 3.4: The spatially varying arterial surface strain tensor at a balloon pressure of 6 atm. A high degree of circumferential asymmetry is evident.

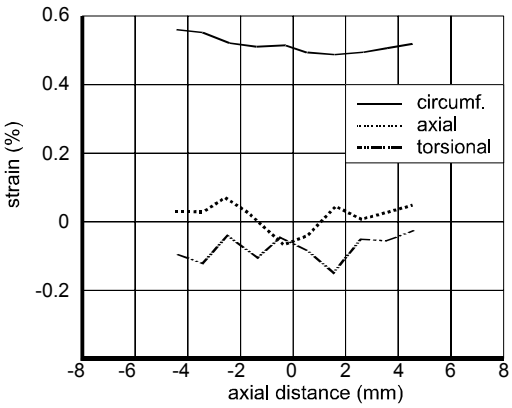

Figure 3.5: The spatially varying arterial surface strain tensor at a balloon pressure of 8 atm. The artery is substantially uniformly expanded circumferentially. Negligible torsion is present.

One remarkable event in this particular experiment is the high degree of uneven circumferential arterial strain that was observed to occur early in the stent expansion cycle; the data show the stent's distal end was expanded 63% more than its center region when the balloon was pressurized to 6 atm. This event was also associated with significant (11% average) axial shortening of the artery. Further balloon pressurization caused the center of the stent, and hence the artery, to circumferentially expand reducing the degree of uneven expansion to 22% while undergoing minimal further axial shortening to an average total axial length reduction of 13%.

The average degree of axial shortening is listed in Table 3.1, calculated for both the artery, and for the stent, visible through the translucent artery. Three timepoints are used: the first early, taken at a balloon

pressure of 2.0 atm, an intermediate timepoint taken when uneven stent expansion is greatest (which occurred at a mean balloon pressure of 5.5atm), and the third at the final expansion timepoint with a balloon pressure of 8.0 atm.

Table 3.1: Axial strain of the stent, artery surface, and difference, averaged over length. The reported standard error is the standard error of each experiment's average axial strain component, not the standard error of the axial strain measurements across the length of each experiment.

timepoint	$\varepsilon_{axial}^{stent}$	$\varepsilon_{axial}^{artery}$	$\varepsilon_{axial}^{stent} - \varepsilon_{axial}^{arteryt}$
early (2 atm)	- 1 ± 1%	0 ± 1%	- 1 ± 1%
maximum endflare (5.5 atm)	- 13 ± 2%	- 8 ± 2%	- 5 ± 3%
late (8 atm)	- 18 ± 1%	- 11 ± 2%	- 7 ± 2%

The steady increase in axial strain differential between the stent and artery, the *excess axial strain*, is accompanied by a non-uniform degree of circumferential expansion. This is graphically depicted in Figure 3.6 which compares the degree of nonlinearity of arterial circumferential expansion, termed *endflare %*, with the axial strain differential as the stent is deployed. The dogbone statistic is defined as the percentage difference between the largest arterial end diameter and smallest middle diameter of the artery over the region covering the expanding stent.

Separate data were obtained from similar rabbits stented in a conventional manner, without arterial marking and strain measurement. Neointimal areas in the proximal, middle, and distal regions are reported in Figure 3.7, and show excellent correlation between sites of endothelial denudation and chronic restenosis.

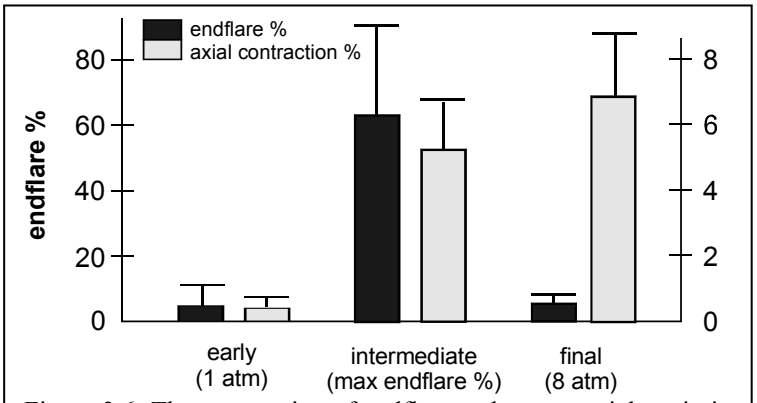

Figure 3.6: The progression of endflare and excess axial strain in the circumferentially expanding stent. The dogbone-like shape introduced by end-first expansion is a transient effect, however axial contraction of the stent monotonically increases with increasing expansion pressure. *Excess axial strain* refers to the difference between stent and arterial axial strain.

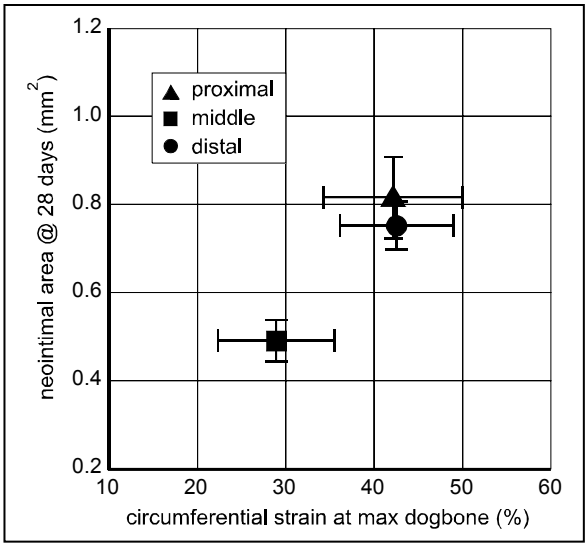
1.2
1.0
0.8
0.6
0.4
0.2
neointimal area @ 28 days (mm2)
proximal
middle
distal
10
20
30
40
50
60
circumferential strain at max dogbone (%)

3.4 Stent expansion characteristics – Discussion

3.4.1 Sequence of events during stent expansion

In vivo data (e.g. Figures 3.2-3.5) reveal that the stent resists any circumferential expansion until the balloon catheter is inflated to a threshold of at least 2 atm of pressure (represented diagrammatically in Figure 3.8a). As balloon catheter is increased, the stent tends to expand in an end-first manner for at least two reasons. The balloon is typically manufactured longer than the stent to compensate for slight slippage that may occur during placement of the device through the vasculature. The unconstrained balloon ends that extend beyond the stent inflate before the constrained middle section expands, and the resulting dogbone shape is transferred to the overlaying stent. The mechanics of the stent geometry itself also contribute to endflare. Most common stent designs consist of a series of ringed cells that repeat along the axis of the stent. A pressure applied to the interior of a single ring that will tend to make it circumferentially expand will be resisted both by the ring itself and by the influence of the neighboring rings on the proximal and distal sides. A pressure over the entire interior of the stent can be considered as the superposition of the above case, with each ring resisting expansion both by itself and with the aid of its two adjacent rings, with the exception of the end rings that have only one neighboring ring and therefore are the

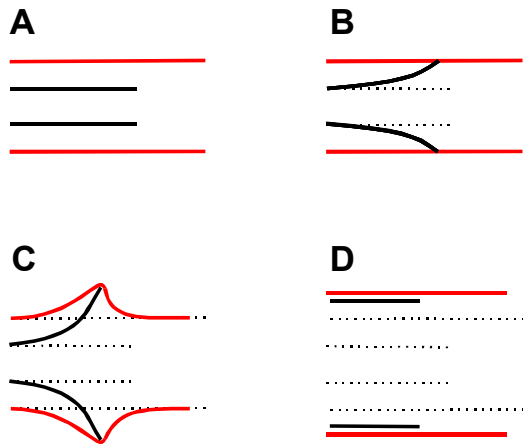

Figure 3.8: Sequence of stent expansion. The device is initially placed within the artery (panel A) and circumferentially expands proximally and distally until the ends are apposed to the vessel wall (B). Further end-first circumferential expansion (C) is accompanied by axial contraction of the stent of about 13%, which at the boundary draws the artery axially inward also by approximately 8%. At the final expansion diameter (D) the stent is evenly apposed to the vessel wall, and there is no evidence of the transient scraping injury.

least able to resist circumferential expansion. (Figure 3.8b). Once the flared edges of the stent contact the artery, further flaring causes a reduction in the stent's tip-to-tip length, in this case of 13 ± 2%, and induces a corresponding axial shortening in the artery, here by 8 ± 2% (Figure 3.8c). As the center of the stent expands, the entire stent further axially contracts because of its change in strut geometry; the combined effects of edge flare and stent contraction are responsible for the characteristic scraped pattern of endothelial cells seen along at least one edge of the artery (Figure 3.1) after the stent is fully deployed (Figure 3.8d). The damaged endothelial cells show surface damage has occurred and also serve as an indicator for deeper arterial injury. This pattern of acute injury may explain the heightened degrees of neointimal hyperplasia that form locally around the far proximal and/or distal edges graphed in Figure 3.7. Two causes of arterial injury are evident from this data: knife-edge focal injury where the flared edges of the stent protruded into the artery wall, and scraping injury caused by the edge-first circumferential expansion followed by axial contraction.

3.4.2 Causes of axial contraction in the stent and artery

Axial contraction of the stent has two causes: endflare and stent cell geometry. Endflare-induced axial shortening is the less-dominant cause, contributing 4.8 of the 13% observed contraction at maximum dogbone, and less than 1% at the final expansion pressure. The diamond-shaped geometry of the stent cell inherently shortens in one dimension as it expands in the other, and this effect is responsible for causing the remaining amount of axial contraction not caused by endflare.

The artery also experiences an axially-contractile force as it circumferentially expands. Poisson's ratio, $\nu_{\theta z,}$ describes the ratio an unconstrained cylinder will axially contract for a given circumferential expansion, and is approximately 0.27 for arterial tissue [55]. Since the artery is tethered into place by both the surrounding *vasa vasorum* and the proximal and distal extensions of the artery itself, a circumferential expansion of approximately 60%, as is typical for expanding stents, will cause less than a 0.60 $\nu_{\theta z}$ = 0.16 axial contraction of the artery. The observed values of approximately 11% post-expansion arterial contraction imply a residual axial stress component remains.

3.4.3 Other observations: symmetry, torsion, placement injury

Stents do not exhibit bilaterally symmetric transient flaring when expanded within an artery, but instead tend to initially expand at either the proximal or distal edge first, distal edge expanding first in 6 of the 8 arteries. Minimal scraping occurred on the edge that flared initially. Once one edge was tethered, flare of the complementary edge was accompanied by endothelial scraping, such as observed in Figure 3.7. Although the animal experiments were done with the stent centered on the catheter, benchtop experiments suggest that the side that opens first can be modulated by the placement of the stent, and that a stent

purposefully mounted 3 mm off-center will always flare first on the opposite end.

The observation that distal scraping was more prevalent than proximal scraping indicates that placement-related injury, i.e. injury occurring prior to balloon expansion, is not the cause of the denudation patterns shown in Figure 3.1.

Torsion experienced on the arterial surface was minimal throughout stent expansion, although in two experiments the stent was observed through the translucent artery to rotate approximately 180° before it was expanded sufficiently to appose the vessel wall. Because torsion was found to be nearly zero, future experiments concerning stent expansion examine only the interplay between circumferential and axial strains.

3.4.4 Designing a less injurious stent

These findings suggest one method to minimize stent-imposed vessel injury is to minimize endflare by designing a system that deploys stents in a center-first manner, thereby eliminating both the possibility of knife-edge focal injury and the existence of two stent/artery contact points separated by a stent region yet to undergo axial contraction. This may be achieved by modifying the stent, the balloon catheter, or the stent/balloon interface. The stent may be manufactured with a increasing strut cross section from the middle region to the ends in either a progressive fashion, i.e. order one or higher, or in a step fashion, e.g. with thicker outermost rings. Medinol manufactures such a device both with and without reinforced end rings in a delta wing geometry. Although marketed as a method to improve tracking during placement, the utility of the end rings to modulate acute injury is examined in Sections 3.5 – 3.7. Conversely, the balloon catheter could be manufactured with a thinner center region. An alternative method (also designed by Medinol to prevent stent/catheter slip during placement) employs sock-like endcaps on the ends of the balloon catheter that restrain the stent ends from initially expanding. As the center region circumferentially expands the edges slip free of the caps.

A different approach to reduce arterial scraping that works independently of the transient stent circumferential shapes is to note the characteristic pattern of artery axial contraction during circumferential expansion, and design a stent that matches these characteristics. This concept is quite different than the thrust of "less-shortening stents are better" design efforts seen in several stent designs [56]. It is important to note that this is not a simple matter of matching final stent axial contraction to final artery axial contraction since any transient differentials would result in scraping, but requires both to develop the same axial component of strain as a function of time. Assuming conventional balloon catheters are used that expand edge-first, only the length-averaged (i.e. end-to-end) axial strains need to be matched until center region deploys.

3.5 Control of stent expansion - Materials and methods

3.5.1 Overview

The first set of experiments analyzed in Sections 3.2 – 3.4 quantified the manner that a slotted-tube design stent expands and proposed a specific mechanism of expansion-induced arterial injury involving endflare followed by axial contraction. It further showed that areas of endothelial denudation matched the spatial distrubution of the chronic vascular response as measured by degree of neointimal hyperplasia at 28 days. While the experiments did prove that several hypothesized mechanisms of injury did not take place, e.g. the vanishingly small degree of torsion measured *in vivo* indicated that stent rotation after apposition with the vessel wall did not occur, because only a single stent/balloon design was used it could not prove that a relationship existed between maximum endflare and arterial injury. Furthermore, it was not clear if the relatively large degree of axial contraction inherent in the diamond-shaped slotted tube design was primarily responsible for the noted scraping injury. Both issues are of import: the first determines if endflare controls arterial injury, and the second determines if devices can, and if so then must be designed to minimize axial contraction as well as endflare.

The set of experiments described in Sections 3.5 – 3.7 that follow were designed to answer these questions. These experiments first established whether it is possible to control the degree of maximum endflare using minor modifications to the stent and/or balloon proposed in 3.4.4, and which modifications were the most effective. The basic stent geometry both in standard and modified designs was chosen to exhibit minimal axial contraction. Once several models of stent/balloon systems nearly identical in all characteristics but maximum endflare were established, it was possible to determine if maximum endflare dictated acute vascular injury, and whether this relationship could be modulated.

A total of 24 stents were deployed in 12 rabbits (Table 3.2). The previous sections determined the strain component $\varepsilon_{\theta z}$ was zero to within the 0.04 RMS error of the measurement system, therefore the code was rewritten (Appendix A) using the assumption of zero torsional strain. Using data from the zero-torsion body experiments (Chapter Two) the new RMS system measurement was reduced to ± 2%. This permitted the reduction of the number of stents needed per experiment from 8 as in the previous chapter (producing a standard error of the mean of $4/\sqrt{8} = 1.4$) to 3 (reducing the standard error to $2/\sqrt{3} = 1.2$). All reported axial strains refer to the net stent axial strain (i.e. the arterial axial strain – stent axial strain).

Table 3.2: Twenty-four stents were deployed in twelve rabbits. Three stents each were tested in a two by two matrix comparing stents of standard and variable (i.e. with reinforced end rings) geometry and balloons of matched (1:1.1 stent/balloon length ratio) and long (1:1.7 length ratio) sizes. Experiments were performed to both measure stent expansion characteristics and determine the degree of acute vascular injury as measured by endothelial denudation.

Number of stents	Stent geometry	Balloon / stent length	Measured characteristic
3	standard	1.1	arterial surface strain
3	standard	1.7	arterial surface strain
3	variable	1.1	arterial surface strain
3	variable	1.7	arterial surface strain
3	standard	1.1	arterial injury
3	standard	1.7	arterial injury
3	variable	1.1	arterial injury
3	variable	1.7	arterial injury

We chose to study the expansion and injury properties of a delta wing stent (NIR, Medinol Corporation) of standard and variable geometry designs. The delta wing design was chosen because it is available in two nearly identical configurations of the same material (bare 316L stainless steel), surface area, and geometry, except that the outermost rings of the variable geometry delta wing stent (3 mm diameter x 9 mm long NIR Conformer, Medinol Corporation) are manufactured with end rings that are 18% thicker and 10% shorter than the standard geometry delta wing stent (3x9 NIR), whose struts are of uniform cross section. The remainder of this chapter will refer to the delta wing conventional geometry and delta wing variable geometry stent designs as simply the *conventional* and *variable geometry* stents.

3.5.2 Quantifying endothelial denudation

Ideally the arteries from the same rabbits used to determine the arterial surface strain would be harvested shortly after stenting, stained to reveal areas of endothelial denudation, and used to reveal the relationship between manner of stent expansion and arterial injury. Unfortunately, to obtain adequate perfusion of the dye to assess endothelial denudation the stents must be deployed superior to the inguinal ligament. The same collateral vasculature that permits adequate dye perfusion destroys the axial symmetry of the vessel and hence prevents accurate measurement of the surface strain tensor of the artery during stent deployment. Therefore a second group of six similar rabbits were stented with 12 stents, one per femoral artery, using stent and balloon catheter combinations as listed in Table 3.2, and arterial injury was quantified as ascertained by acute endothelial denudation.

The animal model and stent insertion techniques were identical to those described in section 3.2.3. Evan's Blue dye was used to quantify endothelial denudation (protocol in Appendix B) rather than the silver nitrate ($AgNO_3$) used in section 3.2.3 because we found the latter method is quite sensitive to the amount of precipitated $AgNO_3$. Changing to Evan's Blue increased our yield of correctly-stained slides from 20% to 85%. Evan's Blue does not bind to intact endothelium but stains the basement membrane where denuded endothelial cells permit albumin penetration. The stents were implanted for a minimum of 30 minutes before the animal was perfused with 5 ml of 5% Evan's Blue dye dissolved in lactated Ringer's solution. The animal was sacrificed 45 minutes after injection of the Evan's Blue, perfused clear with 2 liters of lactated Ringers under pressure, and fixed *in situ* with 4% paraformaldehyde. The arteries were excised, opened longitudinally, and mounted *en face* within 4 hours of harvesting. Percent endothelial denudation was determined using computerized morphometric analysis in the annular region extending 1 mm out from the edge of the stent.

Data are reported as mean ± standard error, unless stated otherwise. p-values reported are one-sided, versus the alternative hypothesis that the stent with the minimum amount of endflare inflicts the least amount of endothelial denudation. ANOVA testing was evaluated using the fixed-effects model, and subsequent t-tests were evaluated using the pooled estimate of the variance computed by the least significant difference method [57].

3.6 Control of stent expansion – Results

The conventional geometry stent was mounted on a 1.1 length ratio balloon and expanded (Figure 3.9 panel A). The stent assumed two distinctly different shapes as it enlarged. It began by flaring its edges by nearly 75% with relatively little axial contraction. The recorded level of endflare indicates the maximum observed dogbone. At maximum inflation the center region of the stent eventually expanded, reducing endflare to 17 ± 5%, and during this circumferential expansion the bulk of stent axial shortening took place. This sequence of events was qualitatively identical to that observed in the slotted tube design (section 3.4). The primary difference was the significantly lower degree of axial shortening of the delta wing stent designs (6-7%) vs. the slotted tube (18%).

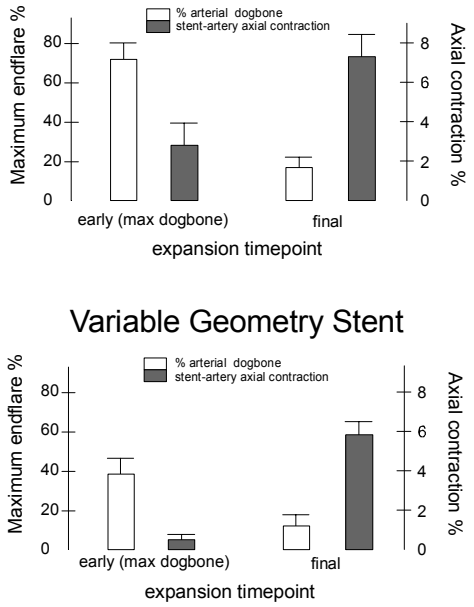

Figure 3.9: Comparison of maximum degrees of endflare (measured on the exterior arterial surface) and net axial contraction (length-averaged stent-artery axial contraction) at mid expansion and post expansion timepoints for the conventional delta wing stent mounted on a matched length balloon (1:1.1 stent:balloon length ratio) (left) and a variable geometry delta wing stent mounted on a matched length balloon (right).

By replacing the far proximal and distal rings of the stents with shorter, thicker struts, originally designed to be more resistant to loosening from the catheter during stent emplacement, it is possible to modulate the degree of endflare during stent expansion. Figure 3.9 panel B shows the degree of maximum dogbone was reduced by nearly 50% from the conventional stent designs ($p<0.01$), a finding made more significant by the marked reduction in pressure required to open (2.0 ± 0 atm vs. 4.7 ± 0.7 atm) and therefore while the flare was a smaller diameter (2.2 ± 0.1 mm vs. 2.7 ± 0.1mm). This suggests that the variable-geometry stent design opens during the bulk of expansion in a far more even manner than the conventional stent, and thus imposes significantly less injury (Figure 3.10). Axial contraction at the moment of maximum endflare was predictably less ($p=0.001$), given the smaller average radius of the variable-geometry stent at that timepoint. The final expansion geometries, axial contraction and percent dogbone, were otherwise indistinguishable from the conventional stent.

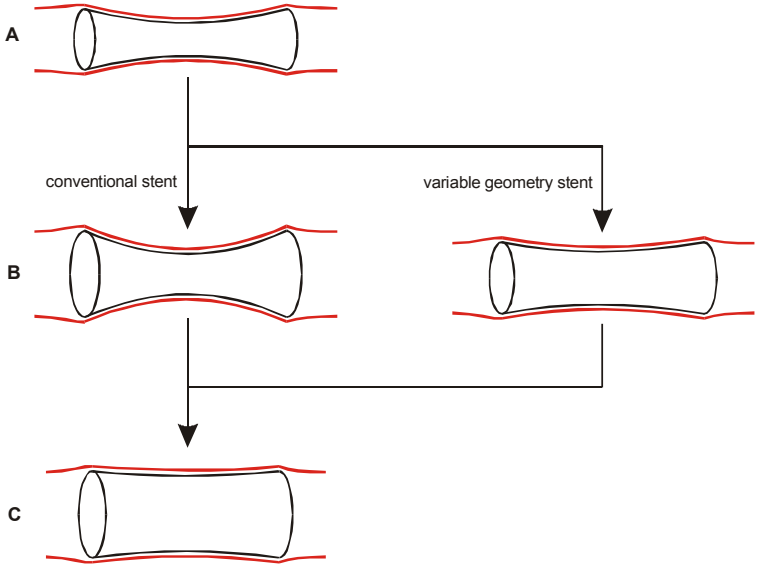

Figure 3.10: Sequence of events occurring during stent expansion for the conventional geometry stent (left) and variable-geometry stent (right), both deployed using matched-length balloon catheters.

Typical patterns of endothelial scraping and denudation that occur at the edges of the stent are illustrated in Figure 3.11. The left panel shows regions of basement membrane (deep blue to left) exposed after the endflare followed by axial contraction of a conventional stent on a matched-length balloon. Scraped white trails of endothelial cell are clearly visible in the center of photomicrograph. The right panel shows a similar region from the variable-geometry stent. The lighter staining to the left reveals much less denudation and an absence of the scraping injury evident in the left panel.

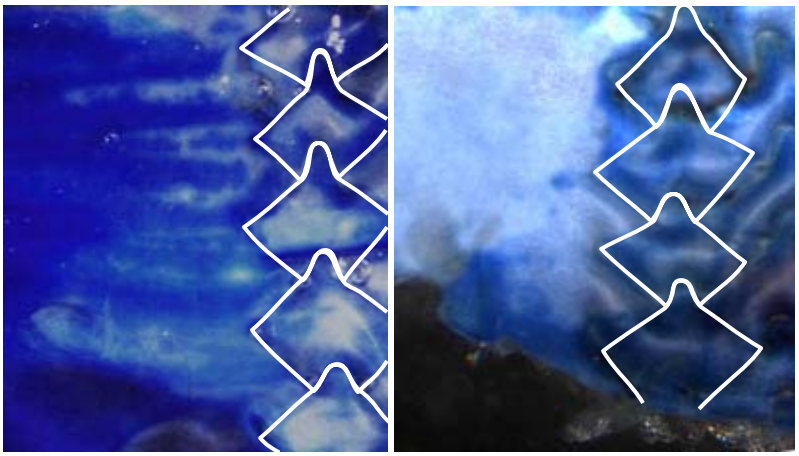

Figure 3.11: *En face* preparation of arterial section stented with conventional stent (left) and variable geometry stent (right) and stained with Evan's Blue. The stent image is highlighted. Light blue regions indicate areas of intact endothelium; dark blue regions such as the expanse to the left of the stent in the left panel show areas where the endothelial layer has been denuded exposing the basement membrane. Marks that appear to have been scraped appear in the left panel.

Data measuring the degree of maximum end-first expansion across all four stent designs are shown in Figure 3.12. Analysis of variance (ANOVA) revealed a significant difference between groups ($p=0.01$), and subsequent t tests show that only the variable-geometry stent mounted upon a matched length (1:1.1) balloon behaved significantly differently ($p=0.001$) than all others.

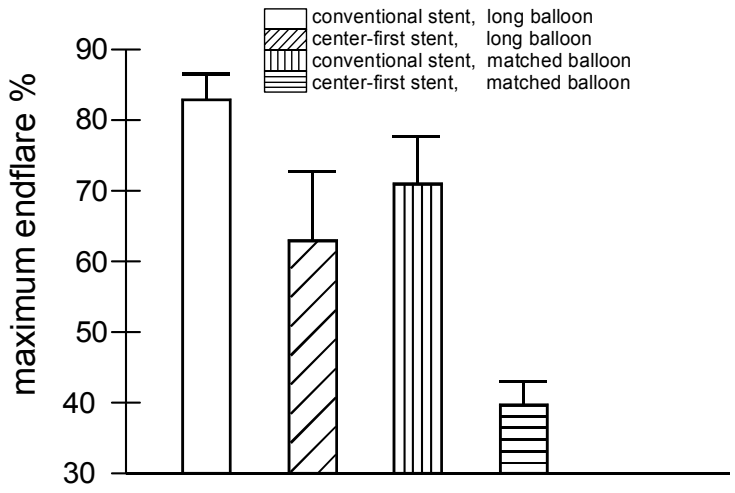

Figure 3.12: Comparison of maximum degrees of endflare across all four tested combinations of stent and balloon designs.

The maximum degree of endflare exhibited by each stent/balloon combination is graphed in Figure 3.13 panel A against the degree of endothelial denudation at the stent edge. Each of the four markers represents one set of experimental data obtained using a distinct stent geometry and balloon length ratio. Unpaired t-tests revealed that although there was significantly less *dogbone* exhibited by the conformer/matched-length balloon combination as reported earlier, this did not translate into significantly reduced levels of *endothelial denudation* when compared individually to other combinations ($p = 0.23$). A statistically significant difference in endothelial denudation is observed, however, when the data is first binned into the two groups of devices that exhibit statistically different manners of expansion. Figure 3.13 panel B graphs the conformer/matched-length balloon data vs. the remaining three groups of devices that exhibited a statistically greater amount of endflare. In this graph the difference in endothelial denudation becomes apparent as the grouping reduces the standard error ($p = 0.05$).

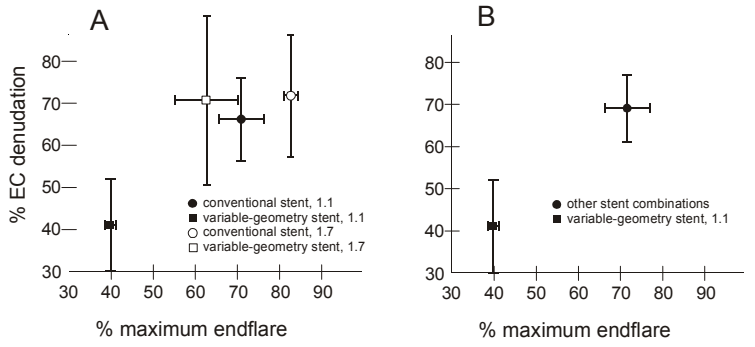

Figure 3.13: Relationship between maximum transient endflare and endothelial denudation. Panel A suggests the variable geometry stent on the matched length balloon (lower left corner) behaves differently than the other combinations, although the high variance in endothelial denudation results in only the maximum degree of enflare achieving a statistically significant difference. Panel B bins the data into the two experimental groups that showed a different manner of expansion, and this approach shows a significant correlation between endflare and endothelial denudation.

3.7 Control of stent expansion - Discussion

3.7.1 Transient endflare can be controlled

The data of Figure 3.9 show two stents of nearly identical properties and pre and post expansion shapes can be coerced to have very different transient expansion properties by slightly reinforcing the outermost rings. The endflare is arrested at 2.0 atm for the variable-geometry designs, but continues to worsen for the conventional-design stents until it peaks at 4.7 atm. These devices can therefore be used to test the hypothesis proposed in Section 3.4 that transient endflare causes acute arterial injury. The measured progression of circumferential and axial strain further support the proposed mechanism by which transient endflare results in acute arterial injury (Figure 3.10).

It was desired to quantify four different stent/balloon models, each grossly similar but exhibiting different degrees of endflare, to test the hypothesis that acute arterial injury is endflare dependent. In addition to varying the thickness of the outer stent struts, an additional degree of freedom was introduced by varying the length ratio of the balloon to stent from matched (1.1 length ratio) to long (1.7 length ratio). Figure 3.12 compares the results of these experiments. Although it was expected that increasing the balloon length would encourage a greater degree of endflare regardless of stent design, it was discovered that all combinations resulted in statistically indistinguishable degrees of maximum endflare except for the variable-geometry stent mounted on the matched-length balloon ($p=0.001$). Later reference to high and low endflare groups refer to these binned data.

3.7.2 Maximum endflare is correlated with acute vascular injury

Although the statistics illustrate not all comparisons of arterial injury between the high and low endflare groups display the marked differences of Figure 3.11, t-tests comparing the levels of endothelial denudation revealed that the low endflare group did have a correspondingly lower percentage of endothelial denudation ($p=0.05$). The data support that this relationship is causal and not merely indicative that *any* change in balloon or stent geometry, regardless of the impact upon maximum endflare, results in differences in endothelial denudation. Specifically, all three groups of stent/balloon geometries that displayed similar levels of maximum endflare also yielded statistically indistinguishable levels of EC denudation ($p=0.67$, 0.50, 0.55 for the conventional/matched, conventional/long, and variable geometry/long, respectively).

ANOVA testing revealed that the large degree of variance in endothelial cell denudation graphed in Figure 3.13 is probably not entirely explained

by changes in the maximum stent endflare (p=0.1). One major cause of this variance is the non-bilaterally symmetric manner in which we observed many stents expand. Often one edge of the stent would expand pronouncedly more than the other introducing transient fish-mouth appearance. This pattern of expansion likely resulted in the first-deployed stent edge to anchor in the artery, causing a single-sided pattern of endothelial cell denudation to occur as only the second end was free to scrape the arterial lining when axial contraction occurred. The presence of one high and one low region of end scraping resulted in the high degree of calculated variance of denudation.

3.7.3 Device optimization

The data shown in Figure 3.12 show that three of the four combinations of the delta wing stent/balloon systems displayed statistically identical degrees of maximum endflare, demonstrating that both stent and balloon design must be simultaneously optimized before improvements in expansion characteristics will be observed. Improvements to the device or deployment system alone will not reduce acute arterial injury.

That comparable patterns and magnitudes of endflare/net axial contraction ($\varepsilon_{stent} - \varepsilon_{artery}$) exists with the conventional delta wing stent design (Figure 3.9) as with the slotted tube geometry (Table 3.1) despite a three fold difference in degrees of stent axial shortening at final expansion suggests that the boundary condition between the edge of the stent and the artery are sensitive to the degree of endflare; a slip condition prevails until the stent attains an endflare of between 40-60%, at which time the sharp boundary of the stent drags the artery inward. Stents that exhibit less axial shortening at final expansion but expand end-first still experience similar degrees of transient axial shortening from endflare, and it is during this transitory time that the injury occurs. Thus, the injury-provoking mechanism is not necessarily reduced by simply reducing the final degree of axial contraction. Reduction of the maximum degree of endflare is critical to reducing acute arterial injury.

3.8 Conclusions

Deployment of permanent implants involve a complex interplay between tissue and device forces that must be considered throughout the expansion process. The device shape and its interaction with surrounding tissue must be characterized and understood as a function of time and not only after emplacement since transitory injurious characteristics can ruin an otherwise optimal device.

For example, despite the uniform cylindrical shape that endovascular stents assume when fully deployed, they rarely expand in a uniform manner. Typically, first the far proximal and distal ends bloom outwards until they contact the intima while the middle region of the stent remains unexpanded. This temporarily stretches the artery over two supporting ring-shaped regions rather than along the length of the stent, focusing stress and causing superficial and possible deep vascular injury. Concomitant axial contraction of the stent relative to the artery pulls these rings inward and is responsible for the characteristic pattern of endothelial cell denudation observed at the edges of stented native vessels (Figure 3.1) and for the corresponding localization of the pernicious chronic vascular response (Figure 3.7).

Other hypothesized mechanisms of this injury, such as torsion of the partially-expanded stent, were ruled out after examining the development of the arterial and stent strain tensor in time (for example, Figures 3.2-3.5).

Endflare can be modulated by relatively minor changes to the device and delivery system such as proposed in 3.4.4, but both must be simultaneously optimal before improvements are observed.

The development of less-shortening stents does not necessarily reduce the degree of acute vascular injury since transient dogboning will be accompanied by transitory shortening, and it is during this period of dogboning/axial contraction that injury occurs. It is important to optimize the device shape throughout its entire expansion process, and not only at its final endpoint.

CHAPTER 4 Intrastrut Expansion Characteristics

4.1 Introduction

The proliferation of vascular implants has been accompanied by the observation of new processes of tissue response to the extreme degrees of strain these devices impose. As discussed in Chapter One, both chronic responses such as the maladaptive formation of neointima and acute responses such as laceration of the internal elastic lamina and endothelial denudation appear tied to events that occur during device implantation. Understanding the precise mechanical initiators of these responses may lead to a new understanding of the processes of vascular adaptation to implants, and possibly to the design and development of less-injurious devices. The previous chapter sought to identify and quantify one such mechanism from a dimensional perspective, more specifically the length of the emplaced device relative to the length of the artery and inflated balloon. This macroscopic view cannot account for all types of observed injuries and a more microscopic perspective is required.

Expandable devices are composed of repeating cellular elements (Figure 4.1, left panels) which impose a different type of vascular damage on their smaller scale. First noted by Rogers and colleagues [34], this response appears universal in varying degrees with all stent geometries, and involves a regular pattern of endothelial denudation. Figure 4.1, right panels shows the areas of superficial acute vascular injury that exist five to fifteen minutes after stenting with three common stent geometries. Each display a border of intact endothelium around the stent struts with regularly-formed regions of destroyed intima and exposed smooth muscle cells. Unless adequate endothelium remains to repopulate the denuded area, thrombogenic and mitogenic factors in the blood will likely initiate a biological cascade resulting in proliferation and luminal migration of the smooth muscle cells [58], restricting blood flow and causing further vascular injury.

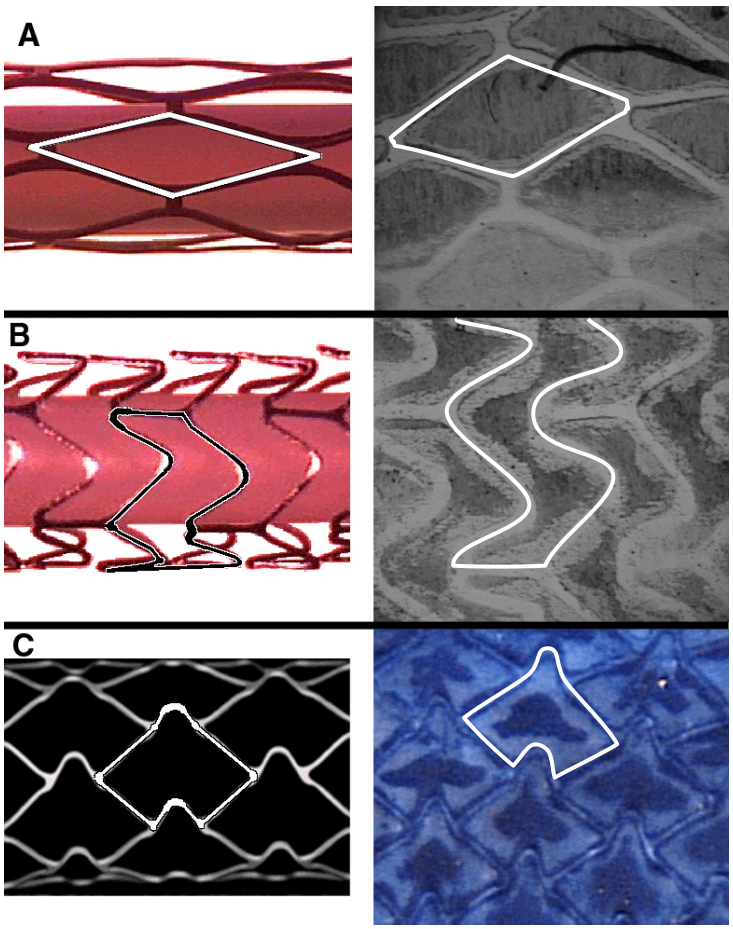

Figure 4.1: The left column illustrates three common stent geometries, the slotted tube (A), corrugated ring (B), and delta wing (C). The repeating element analyzed in this chapter is highlighted. Histological evidence of mid-stent intrastrut acute injury is shown in the right column. (A) and (B) are stained using $AgNO_3$. A border of light gray intact endothelium is visible adjacent to the white stent shadow, slightly wider in the corrugated ring design than the slotted tube. The center region of each cell is completely denuded revealing the dark gray smooth muscle cells. Panel C is stained using Evan's Blue, which binds to the albumin present in the exposed basement membrane in the denuded center regions of each cell. Intact endothelial cells under and adjacent to the struts stain poorly, and appear as light blue.

This chapter investigates the behavior of the artery/stent/balloon system surrounding a singular stent cell such as highlighted in Figure 4.1. The stent cell analyzed is taken from a location in the center region of the stent, away from the localized end-scraping effects discussed in Chapter Two. Most of the analytical and experimental methods will be applied to the simple diamond geometry of the slotted tube cell, and other geometries used to substantiate hypotheses. Two competing hypotheses are examined to explain this pattern of intrastrut vascular injury: strain variance tangential to the artery caused by the stent, and stress normal to the artery caused by the balloon impinging on the intima during expansion. In the course of addressing these hypotheses the following questions will be addressed: how do stent cells expand? What is/are the mechanical initiator(s) of the type of injury shown in the right column of Figure 4.1? Can these initiators be controlled? How do strut thickness and strut shape during deformation affect this injury? Can the design rules that lessen this mode of injury by endovascular stents be generalized to reduce injury imposed by a larger class of expandable implants that employ a repeating geometrical structure?

4.1.1 Chapter organization

Two different series of experiments were performed. The first series sought to determine how the in-plane vascular surface strain imposed over a stent cell varies with position, specifically if it is greatest in the center region where endothelial denudation was found to occur. The second sought to determine whether the complex three-dimensional shape that the artery assumes around the strut cell border results in a transitory normally-oriented impact with the balloon surface. The remaining sections of this chapter are organized around each of these two sets of experiments, named *In-Plane Strain* and *Balloon-Device Interaction* respectively, each with its own subsections describing materials and methods, results, and discussion.

4.2 In-plane strain – Materials and methods

4.2.1 Analytic

The surface strain tensor was computed over a diamond-shape region of artery expanded by a stent cell (modeled from a 3 mm diameter x 12 mm length slotted tube design, Advanced Cardiovascular Systems/Guidant (ACS)) as it expanded from an initial diameter of 1.8 mm to its nominal 3.0 mm diameter. Non-slip boundary conditions were assumed, in accordance with experimental findings determined using the methods in Chapter Two and detailed for mid-stent slotted tube cells (Chapter Three). The artery was modeled as a membrane surface with linear, isotropic in-plane properties, and the simulation used finite difference equations to minimize the total elastic energy absorbed by a 41x41 grid of self-similar regions covering the arterial surface as it was distended by the expanding diamond-shaped strut cell. A sparse matrix solver (Matlab rel. 11.3) was used to compute the solution for the resulting set of 1681 coupled equations which describe the physical borders of the stent cell (code in Appendix C). Preliminary analysis with a two-dimensional model of the stent cell (i.e. a diamond-shaped element deforming in a single plane) was subsequently refined into a bent diamond in three-dimensional space to determine the effects of including the arterial surface curvature.

4.2.2 Experimental

Fluorescent microspheres of 15 μm diameter (FluoSpheres, Molecular Probes) were embedded with gentle pressure into excised bovine coronary arteries. A slotted tube stent of the same variety used in the simulations was mounted on a balloon catheter (3 mm diameter x 12 mm length, ACS), placed in the lumen and expanded while the arterial region over one diamond cell was photomicrographed (Optiphot-2, Nikon) with a charge-coupled device camera (Hitachi VC-C370) under fluorescent illumination at x40 magnification. The resulting images were analyzed using the strain-measuring system (Chapter Two), and circumferential, axial, and torsional components of the surface strain tensor were computed.

4.3 In-plane strain – Results

The simplified planar model of the stent cell calculated the strain tensor shown in Figure 4.2. The homogeneity of the strain distribution indicates that if the pattern of endothelial denudation in Figure 4.1 is caused by an uneven distribution of strain, the two-dimensional planar model is overly simplistic.

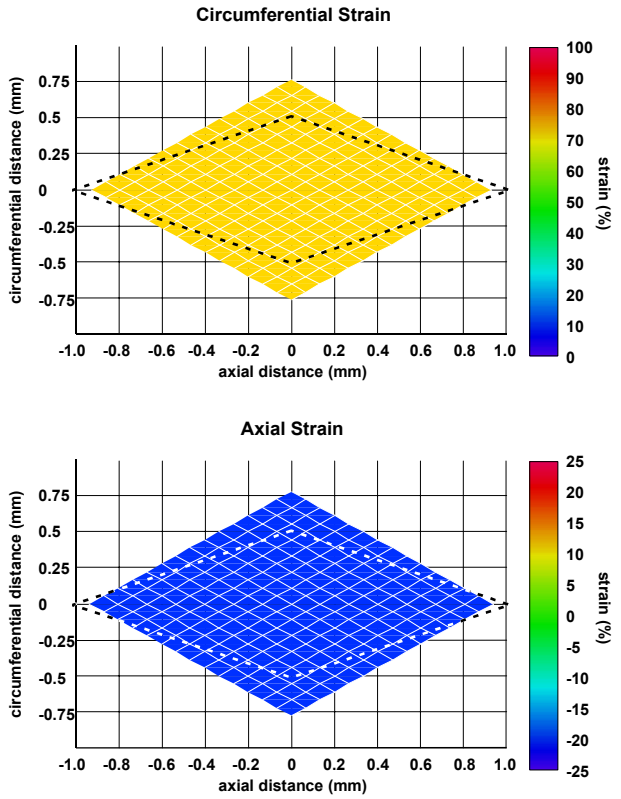

Figure 4.2: Vascular in-plane strain components in the simplified flat model of stent expansion. The stent cell is modeled as a two-dimensional diamond in a plane, expanding by circumferentially elongating and axially contracting. In this graph, the stent is oriented horizontally and the shape of one cell is displayed post-expansion with the degree of strain in each principle axis separately scaled and color-coded. The original shape of the cell is shown in a dashed overlay. The torsional component, not shown, is uniformly zero. The results of the simulation show the arterial strain tensor is constant over the stent cell.

The bounding stent struts are more accurately modeled as a diamond bent along its center vertices (Figure 4.3). The expanding balloon does not force the struts to conform to a cylindrical cross-sectional shape. Instead stress is concentrated at the strut-strut intersections, and plastic deformation at these vertices bend the cell boundary within two planes tangential to the balloon's surface and intersecting above the balloon's longitudinal axis. As the balloon inflates the axial vertices contract and the circumferential vertices expand both radially and circumferentially creating a complex boundary. The artery assumes a surface over this boundary that minimizes its absorbed elastic energy of deformation, with a resulting strain tensor shown in Figure 4.4. The simulation does not perform a finite element analysis of the struts or calculate the forces involved in their expansion; the initial and final strut boundary conditions are determined empirically.

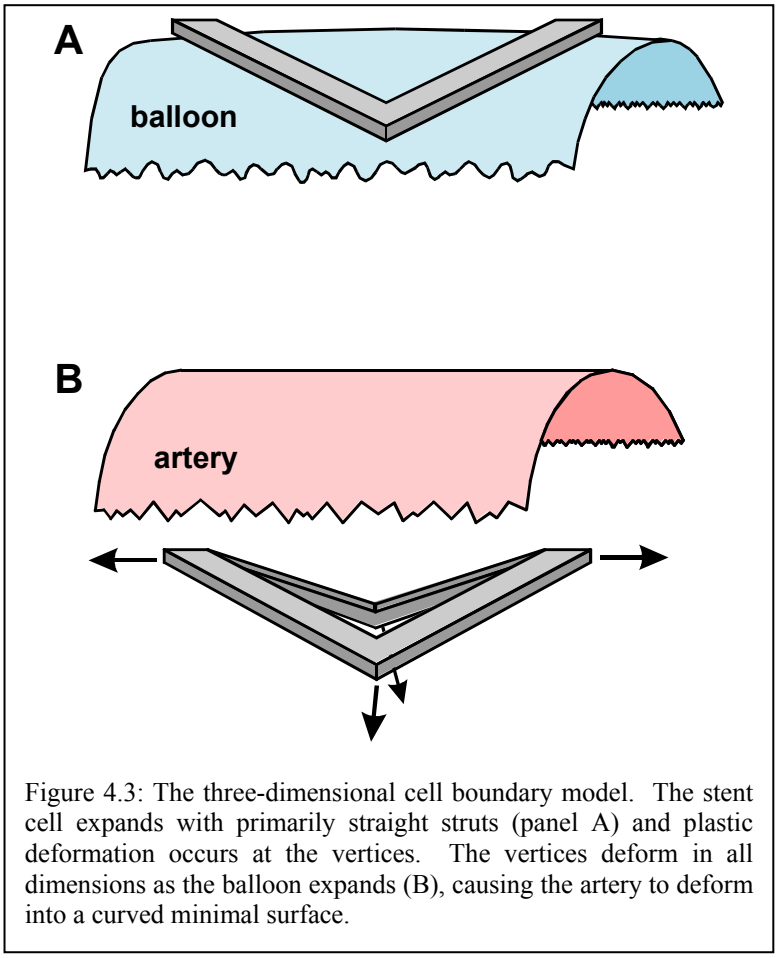

Figure 4.3: The three-dimensional cell boundary model. The stent cell expands with primarily straight struts (panel A) and plastic deformation occurs at the vertices. The vertices deform in all dimensions as the balloon expands (B), causing the artery to deform into a curved minimal surface.

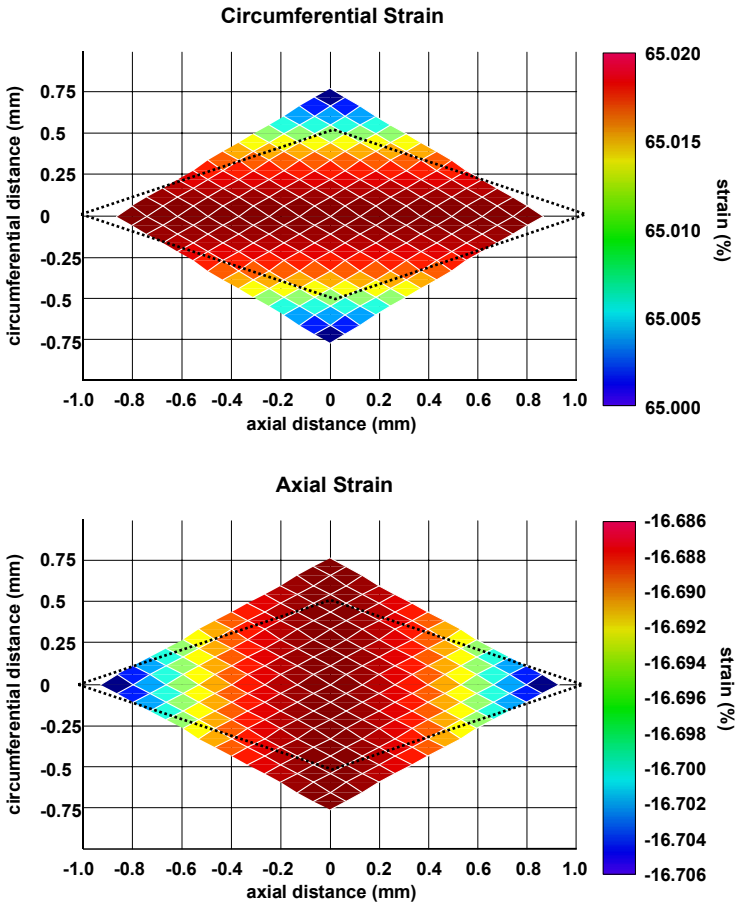

Figure 4.4: Arterial strain tensor components over a three-dimensional model of the bounding stent cell. In contrast to the simpler flat-model of stent expansion, both circumferential components and axial components now exhibit a dependence on position. The highest magnitude of strain is in the region of the artery covering the center of the stent and subject to the greatest degree of curvature in both principle directions. The torsional component, not shown, is uniformly zero.

The results of the more inclusive three dimensional model are grossly similar to those of the two dimensional model except that a slight strain dependence on position is now observed. If the artery can be modeled as a linear elastic membrane, the total elastic energy of deformation absorbed in each region of the artery is proportional to the mean square of each strain tensor component. This scalar field, called the vonMises strain, is calculated in Figure 4.6, and shows the regions of greatest strain magnitude are in the same locations that exhibit post-expansion endothelial denudation. The small variance of strain around the mean prompted a different experiment to characterize the vonMises strain in

an artery expanded to a 1% larger diameter than shown in Figure 4.6. The results (Figure 4.5) show a similar distribution of strain variance with a 2% larger mean.

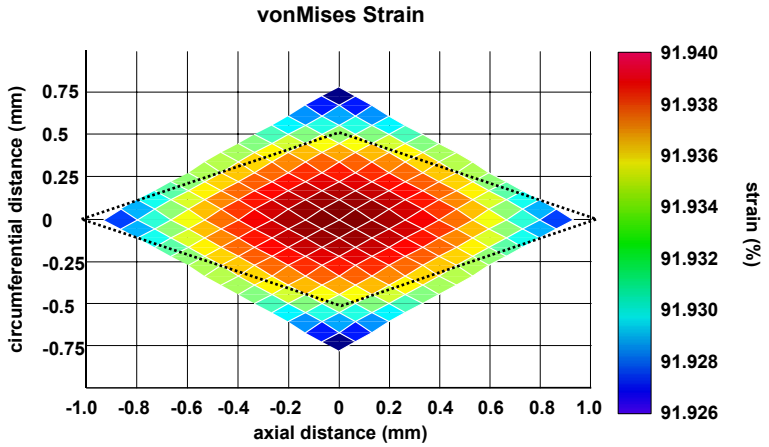

Figure 4.5: The vonMises strain field over an arterial region expanded by a slotted tube stent to its nominal 3.0 mm diameter.

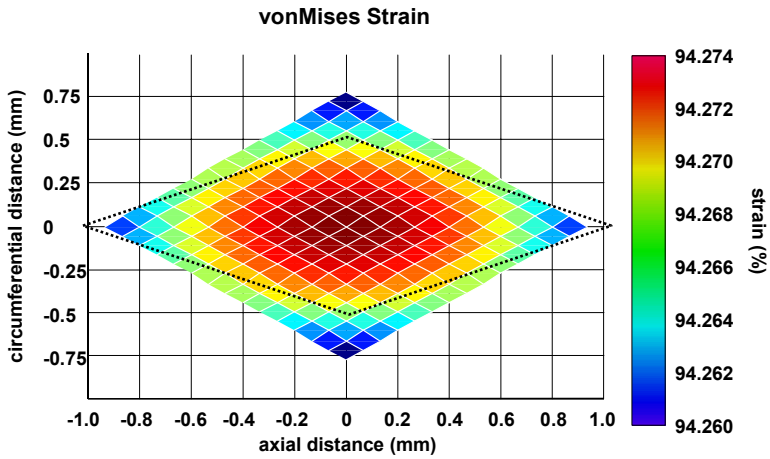

Figure 4.6: The vonMises strain field over an arterial region expanded by a slotted tube stent 1% wider than its nominal 3.0 mm diameter.

Experimental data is shown in Figure 4.7. An excised bovine coronary was embedded with 15 μm fluorescent microspheres and expanded with a slotted tube stent. The images were analyzed using the strain measuring system (Chapter Two), and the resulting experimental surface strain tensor is shown in Figure 4.8. These data show a uniform surface strain field over the intrastrut region, validating the simulations.

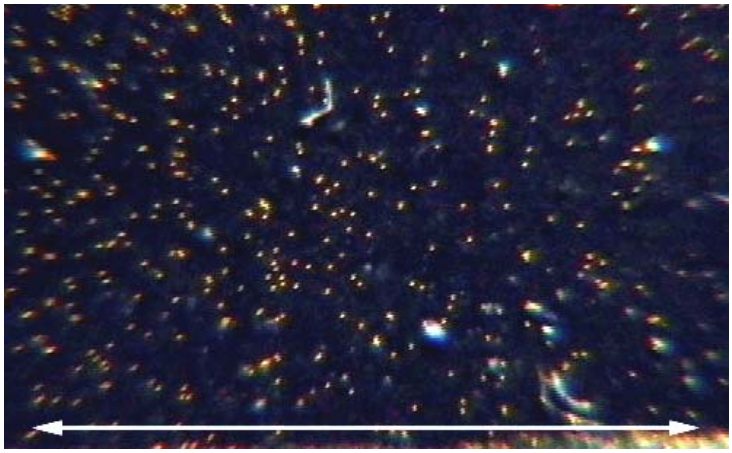

Figure 4.7: Excised bovine coronary embedded with fluorescent microspheres, expanded with a slotted tube stent, and photomicrographed under ultraviolet illumination. The arrow displays the distance between the proximal and distal tips of one stent cell measured along the longitudinal axis, 1.9 mm. The coronary tissue appears black, the beads fluoresce yellow, and the small white circles are holes in the tissue previously occupied by collateral vessels oriented normal to the coronary surface.

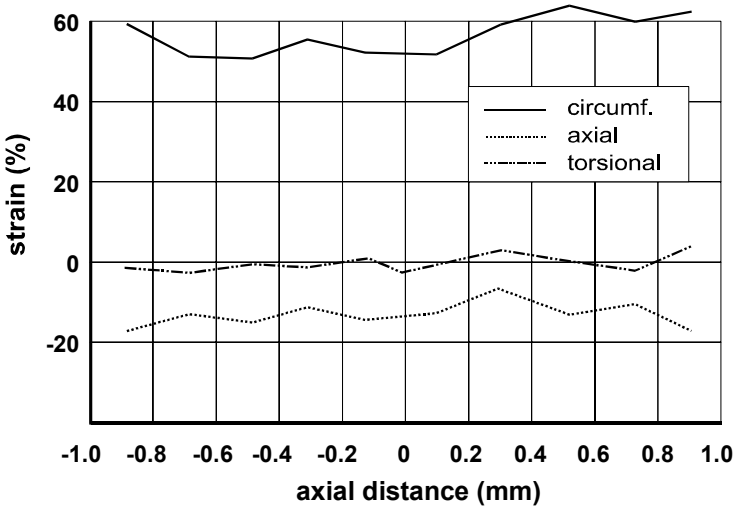

Figure 4.8: The measured surface strain tensor of the excised bovine coronary shown in Figure 4.7. Components are uniform to within ± 8% strain.

4.4 In-plane strain – Discussion

Simulations were constructed that determined the surface strain tensor of the artery covering one intrastrut cell was approximately uniform and not capable of causing the universal pattern of injury observed in Figure 4.1. Experimental evidence corroborates these findings.

4.4.1 Simplified strain model results

The first hypothesis considered was that the pattern of acute arterial injury observed in Figure 4.1 is caused by a variance of in-plane strain imposed by the stent, and that endothelial cells denude after being exposed to a magnitude of strain greater than some threshold. Endothelial cells are known to have different mechanical properties in their longitudinal and circumferential directions when exposed to cyclic stretching [59] and fluid shear [60] and so strain variance in each of the two orthogonal principle axes were analyzed (the geometric symmetry of the stent cell boundary precludes torsion).

Initial simulations used the simplified strain model consisting of an expanding diamond-shaped region in one plane. Results showed the strain tensor did not vary over the arterial surface (Figure 4.2). The uniformity of this strain field can be understood by considering a regular subdivision of that region into self-similar parallelograms. As the stent cell boundary deforms, each subdivision deforms in exactly the same way and therefore the strain field is constant throughout the larger region. This result, although in agreement to within 10% of the experimentally-observed values reported in Chapter 3, fails to explain the position-dependent pattern of endothelial injury and inadequacy of the in-plane model was suspected. A more complex model was therefore constructed that considers membrane strain over a bent diamond shaped region that closely models the true boundary of a stent cell in three dimensional space.

4.4.2 Three dimensional model

The axial and circumferential components of the strain tensor vary with position when considered in the membrane model covering the three-dimensional model of the stent cell boundary Figure 4.4. The position dependence is slight; each component varies by less than 1% over the stent cell region. The manner in which each strain component varies does not match the observed pattern of injury. This leads to the alternate hypothesis that endothelial denudation may be a function of the total energy the cell absorbs during deformation rather than a function of strain along a single axis. A material with a linear stress-strain relationship absorbs a deformation energy proportional to the square of the vonMises strain, defined by

$$\varepsilon_{vonMises} = \sqrt{\varepsilon^2_{circumfernential} + \varepsilon^2_{axial}}$$

for a surface under zero torsion. This scalar strain field is reported in Figure 4.6, and has a positional variance in close agreement with the observed patterns of endothelial denudation. This cannot, however, be the responsible mechanism for causing the denudation, because no suitable energy absorption threshold for endothelial denudation exists. For endothelial cells to denude in the pattern shown in Figure 4.1 there must exist a denudation threshold EC_{thresh} in the range of 91.93 ± 0.01% of vonMises strain. Variations in stent expansion are approximately ± 8% of the nominal diameter, both clinically and in the stented animals used to obtain the photomicrographs of Figure 4.1. Even within a single stent, post-expansion diameter varies by 1% from proximal to distal ends. A simulation of an expansion to 1% greater than nominal post-expansion diameter is shown in Figure 4.5. These data require a denudation threshold in the range of 94.27 ± 0.01% vonMises strain for both regions of intact and denuded endothelium to exist. This would require stent expansion diameters to vary by significantly less than 1% to observe the same characteristic pattern of endothelial injury in different stented arteries, which is not the case. Variances in the arterial surface strain tensor therefore cannot be responsible for the pattern of acute injury seen in Figure 4.1.

4.4.3 Experimental confirmation

The accuracy of these simulations were confirmed by experimental data shown in Figure 4.8 which shows a near-uniform strain distribution over the bovine coronary from a stent cell taken from the center of the stent. In addition to the low strain variance, the length-averaged means of the simulated and measured strains were also in close agreement (Table 4.1).

Table 4.1: Simulated vs. experimentally measured values of arterial strain components averaged over the length of one stent cell.

	Simulated	Experimental
Circumferential	65%	58%
Axial	-16.5%	-15%

The differences between measured and computed values are relatively small, indicating that balloon/artery contact is the primary cause of observed arterial injury. These differences arise from several sources. The primary source of error arises from the fact that simulations calculated strain distribution on a membrane that corresponds to the luminal surface of the artery, but measured values were taken from the exterior surface. If the thickness of the artery remained the same throughout expansion this would introduce no change, but to a first approximation the artery is volume-conserving [61]. The native arteries

were approximately 41 μm thick, and therefore of $\pi T(2r+T) = 0.060\ mm^2$ volume per unit length. Adjusting the simulated results to compute exterior strains would increase the initial and final diameters from 1.8 mm and 3.0 mm to 1.1 mm and 3.11 mm respectively, and decrease the computed circumferential to 66%, in closer agreement with the measured 57% strain. Smaller sources of error are caused by the lack of inclusion of small circumferential tabs in the simulation that link adjacent stent cells together and do not participate in the cell expansion and inaccuracy in the strain measurement system. These errors do not affect the conclusion that intrastrut patterns of endothelial denudation are not caused by variances in the strain tensor. Since these data show that a different mechanism exists and is responsible for the noted patterns of intrastrut injury for the slotted tube geometry stent, it appears highly likely that this is also cause of similar patterns of denudation in the remaining stent geometries.

4.4.4 Validity of model assumptions

Two assumptions were made in the models: nonslip boundary conditions and the arterial behavior mimics that of a stretched membrane. The previous chapter showed that slip conditions at the distal and proximal edges of the stent are responsible for the scraping injury observed in these regions. Slip conditions were not observed in the middle of the stent, nor was scraping-related injury present. The pattern of injury that was noted in the middle cells provides further evidence of non-slip boundary conditions. Figure 4.1 shows intact endothelial cells adjacent to the stent struts, yet these cells are exquisitely sensitive to contact abrasion. A common model of denudation involves touching these cells with a fine 30-gauge nylon loop. Slip in any direction after artery/stent apposition with the struts would cause denudation along at least one axis.

The theory of thin shells shows stresses may be separated into two parts: mean values and deviations from the mean. If transverse shear can be neglected the differential equations governing these mean stresses are exactly the same as the equations describing a membrane coinciding with the midpoint of the artery wall [62]. The membrane approximation for thin-walled vessels such as the rabbit iliac analyzed in this chapter is appropriate (average medial thickness to arterial radius ratio of 2.7 ± 0.4 % and immeasurably small torsional strain components). The membrane model is incapable of modeling the in wall forces that may play an important role in thicker vessels, such as the human coronary.

4.5 Balloon-device interaction – Materials and methods

4.5.1 Analytical

The stent, luminal arterial surface, and balloon were modeled at post-expansion diameters to examine the hypothesis that the curved shape which the artery assumes over the strut borders contacts the balloon in the center of the strut cell, causing endothelial denudation in the manner observed in Figure 4.1.

The strut boundaries established by a single stent cell of each of the three geometries shown in Figure 4.1 were computed in their post-expansion states: the diamond-shaped slotted tube (modeled from a 3 mm diameter x 12 mm length slotted tube design, ACS), a corrugated ring (3 mm diameter by 9 mm length multilink, ACS), and the offset diamond design whose macroscopic opening characteristics were analyzed in Chapter 3 (conventional delta wing design, 3 mm diameter by 9 mm length). In accordance with experimentally observed behavior, the slotted tube was modeled as being composed of straight members that bent at the vertices, giving the six-diamond-ringed stent a dodecagon cross-section. The corrugated ring and delta wing designs were modeled as expanding with circular cross sections. An alternate slotted tube design was also modeled having struts that deformed in circular cross section.

The luminal surface of the artery was modeled as a linear, isotropic membrane capable of sustaining only in-plane stresses. The modeled artery will attempt to minimize its absorbed elastic energy by forming a minimal surface which satisfies [63]:

$$\varepsilon_x \frac{\partial^2 x}{\partial z^2} + \varepsilon_y \frac{\partial^2 y}{\partial z^2} = 0$$

The simulation used finite difference equations to minimize the total elastic energy absorbed by a 41x41 grid of self-similar regions covering the arterial surface as it was distended by the expanding strut cell (Appendix C).

The balloon was modeled as a perfect cylinder.

4.5.2 Experimental

Six rabbits were stented as described in 3.5.2 with a total of 12 stents, 4 each of the slotted tube, corrugated ring, and offset diamond designs. The arteries were harvested 5-15 minutes after stenting, and the slotted tube and corrugated ring design stents were stained *in situ* with silver

nitrate [34]. A desire to improve the yield of successfully-stained arteries led to a change in technique to Evan's Blue (Appendix B) which was used to stain *in situ* the two rabbits receiving the offset diamond stents. The two rabbits were chosen at random from the group of three receiving the conventional design delta wing on the matched length balloon analyzed in Chapter 3. Computerized morphometric analysis was used to determine the average width of the remnant endothelium skirting the strut boundaries.

4.6 Balloon-device interaction – Results

The results of the finite difference simulations to examine the hypothesis that arterial intrusion through the stent struts are responsible for acute post-stenting vascular injury are shown below. Figure 4.9 shows a single cell from the top center of a slotted-tube style stent, modeled with the stretched arterial surface and the coaxial balloon catheter. The simulation estimated a 57% area of denudation, underestimating the 76 ± 3% experimentally measured. As noted by others [32], the slotted tube stent was experimentally observed to deform only at the vertices, i.e. the cross-section of an expanded slotted tube stent with six repeating elements is a regular twelve-sided polygon with an incised circle representing the balloon. The simulations were not designed to calculate arterial stresses, and therefore do not calculate the interaction between the balloon and arterial surfaces. Instead the balloon model is permitted to pass freely through the arterial model, which although unphysiologic does permit calculation of the approximate area of contact between artery and balloon. This approximation is accurate when the distance between the artery and balloon is small, as in these simulations.

The corrugated ring simulation reveals a similar region of endothelial denudation in the center of the stent cell (Figure 4.10). A roughly "W" shaped region of balloon-tissue interaction was calculated to exist leaving a variable-width border of intact endothelium that partitioned the denuded cells into roughly three regions. This distribution is markedly similar to that observed experimentally although the simulations underestimated the degree of denudation area by 42 ± 6%.

The simulations of the delta wing stent cell (Figure 4.11) predict an isosceles triangular-shaped patch of denuded endothelium will exist, with relatively intact endothelium around the upper U-shaped stent strut. As with the previous models, the model underestimated the area of injury by 23 ± 2%.

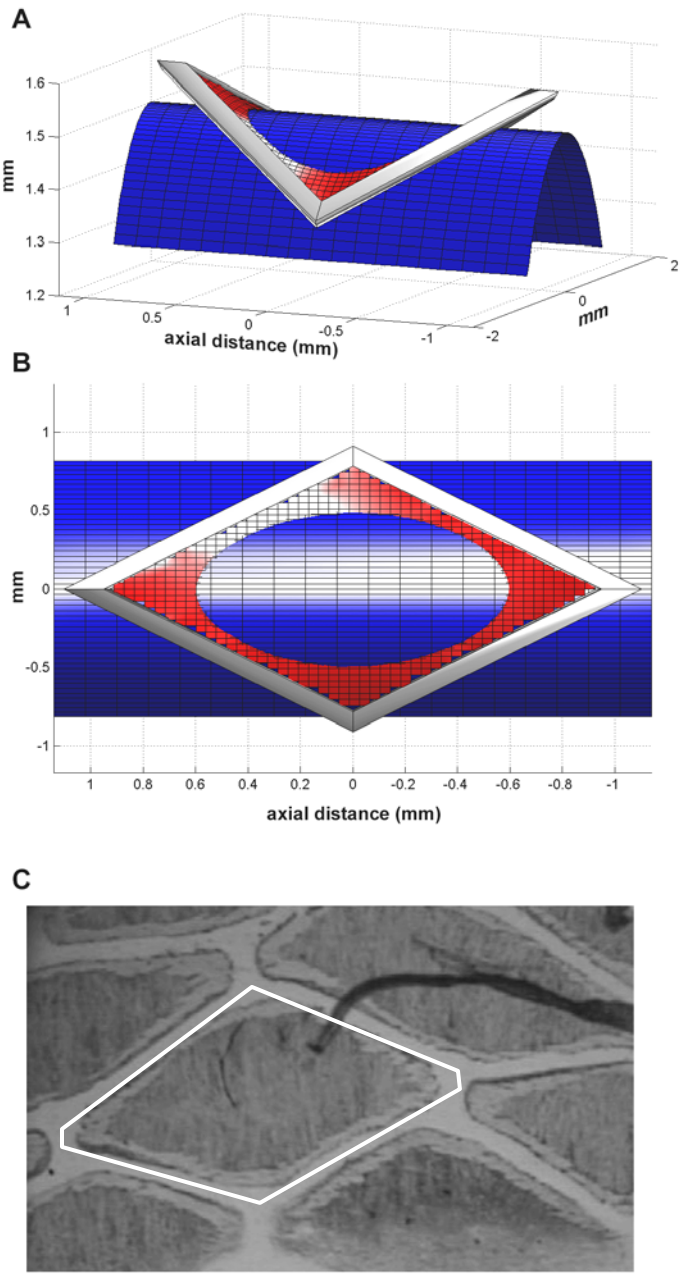

Figure 4.9: Panel A displays a perspective view of the horizontal artery (red), balloon (blue), and struts (gray) of a single stent cell taken from the top center of a slotted-tube design stent. The z axis is scaled to enhance the detail of the region of balloon-tissue interaction, making the balloon cross section appear quadratic and not circular. The model reflects the experimentally-observed fact that the struts deform only at the vertices and contact the balloon at the midpoint between adjacent vertices. Panel B provides a top view of the stent cell. The simulations plot the positions of the balloon and artery independently; regions where the artery disappears beneath the balloon indicate areas of balloon-artery contact hypothesized to result in regions of endothelial denudation shown in panel C.

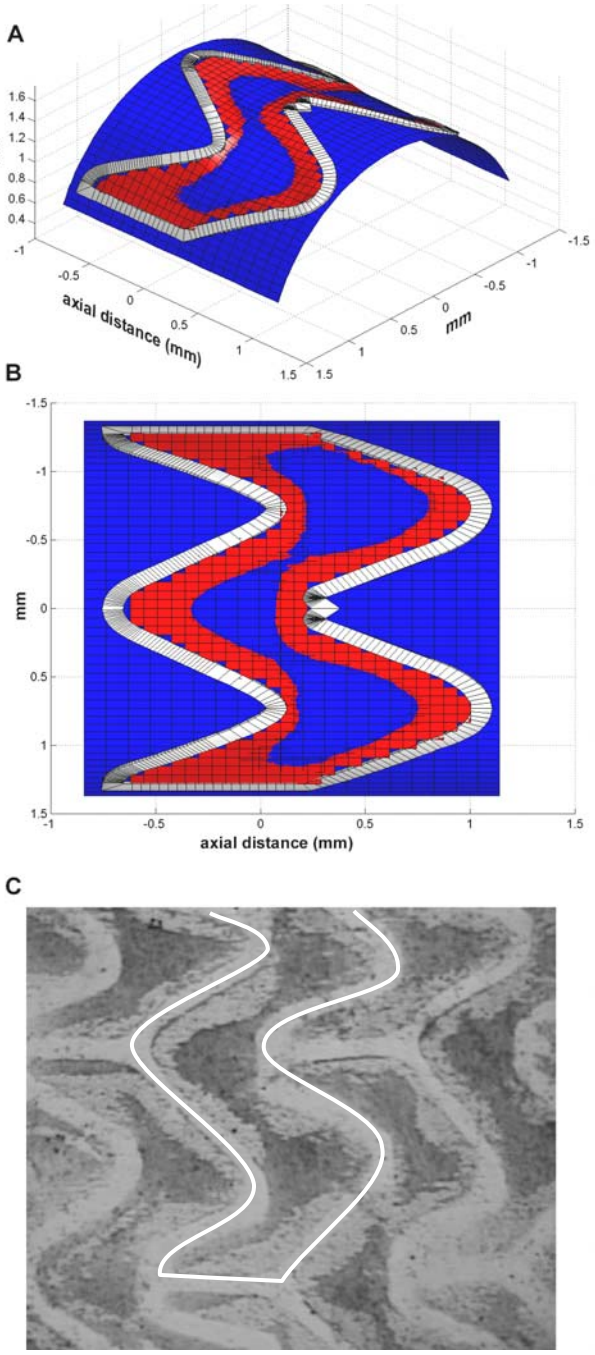

Figure 4.10: Panel A displays a perspective view of the artery (red), balloon (blue), and struts (gray) of a single stent cell taken from the top center of a corrugated ring design stent. Because this geometry uses only three cellular elements to span its circumference the z axis could not be enhanced as in Figure 4.9 without appearing excessively elongated and is therefore drawn using a unity aspect ratio. Panel B provides a top view of the stent cell. The simulations plot the positions of the balloon and artery independently; regions where the artery disappears beneath the balloon indicate areas of balloon-artery contact hypothesized to result in regions of endothelial denudation such as shown in panel C.

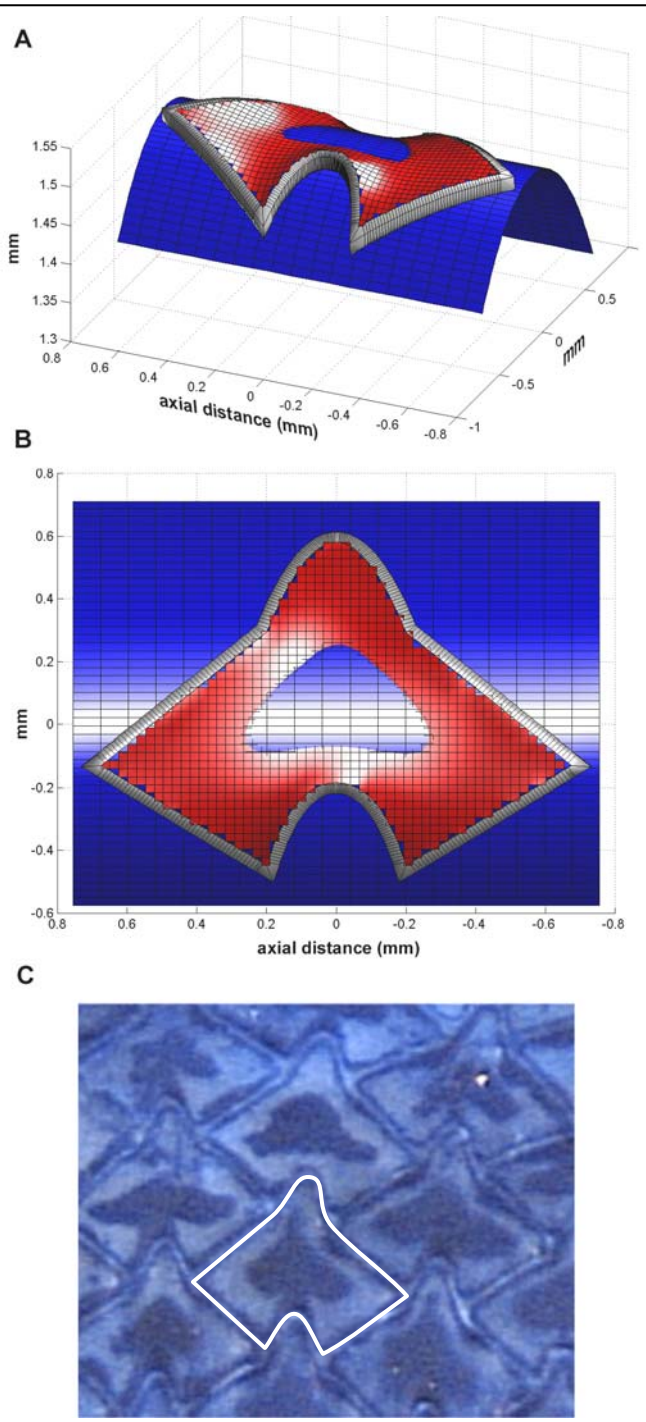

Figure 4.11: Panel A displays a perspective view of the horizontally extending artery (red), balloon (blue), and struts (gray) of a single stent cell taken from the top center of a delta wing design stent. The z axis is scaled to enhance the detail of the region of balloon-tissue interaction. Panel B provides a top view of the stent cell. The simulations plot the positions of the balloon and artery independently; regions where the artery disappears beneath the balloon indicate areas of balloon-artery contact hypothesized to result in regions of endothelial denudation such as shown in panel C.

The simulations were conducted using the parameters of the corresponding physical stent (e.g. strut thickness and width). The strut provides a constant spacing between the artery and balloon, therefore increasing the strut thickness was expected to decrease the degree of arterial injury. This relationship was simulated and plotted in Figure 4.12 for a slotted tube design stent. A zero strut thickness does not cause 100% denudation since the straight struts rise above the balloon at the strut vertices. At a strut thickness of 163 μm the artery is supported entirely away from the balloon and no denudation occurs. In between these two extremes a linear relationship between strut thickness and percent denudation occurs.

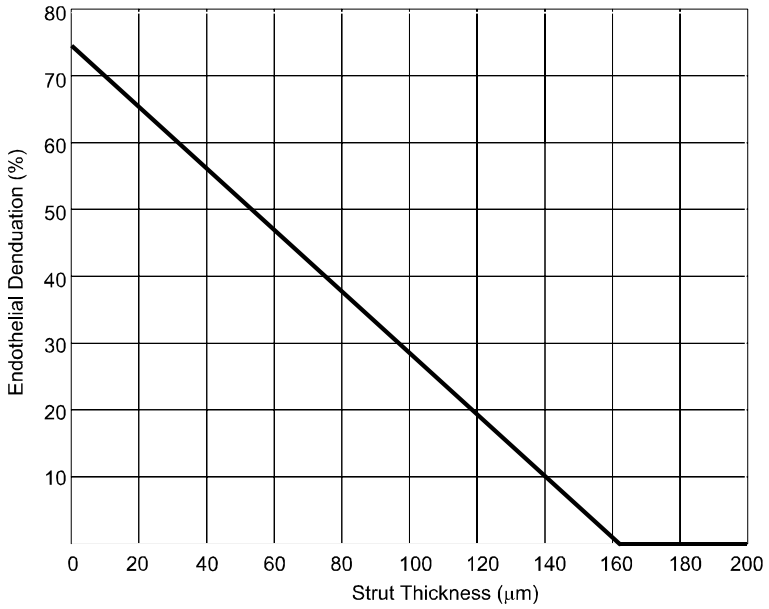

Figure 4.12: A linear relationship exists between radial thickness of the struts in a slotted tube stent and simulated endothelial denudation.

Alternative stent designs can easily be investigated using these techniques. Recent findings [32] propose that one chronic response to stents which impose a polygonal luminal cross-section involves a dysfunctional proliferation of smooth muscle cells in a fashion that restores a circular lumen. This suggests the slotted tube design stent may be improved by manipulating its characteristics to force its conformation to the curved surface of the balloon during expansion, possibly by having non-uniform strut widths, and is visualized in Figure 4.13. If no other parameters are altered, the distance separating the artery and the balloon is everywhere less than or equal to the artery-balloon distance in the original slotted tube design, and therefore the degree of endothelial denudation is greater. To compensate for this, the conforming slotted tube design was modeled with twice the strut thickness of the original non-conforming design. The results are visualized in Figure 4.14. Panels A and B display the cross-section and overhead views of the conventional design slotted tube. The lack of

circularity is apparent; by Garassic's estimate this design will stimulate a 9 % compensatory growth. Altering the design to conforming cross section with thickened struts as shown in Panel C eliminates the mode of chronic injury that Garassic identified as well as reducing the degree of acute injury (Panel D) that has been investigated in this chapter and its chronic sequelae from 57% to 43%.

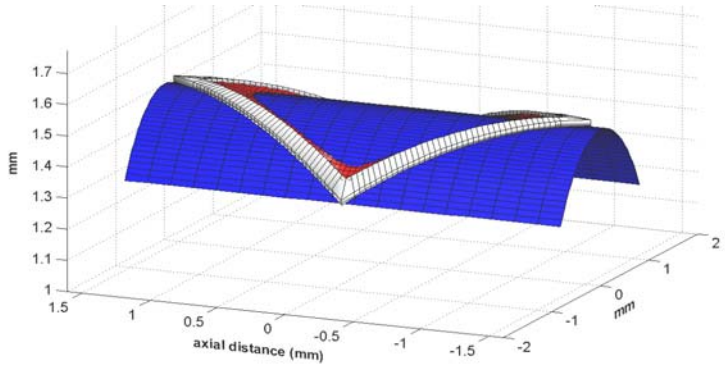

Figure 4.13: Shape of a slotted tube stent cell that conforms to the balloon surface rather than bending only at the vertices.

An alternative explanation of the patterns of observed acute intrastrut vascular injury involves extrusion of the balloon catheter through the stent struts. This mechanism of injury was investigated by experimentally noting the degree of intrastrut balloon protrusion present (Figure 4.15). The stent geometry chosen (3 mm diameter x 9 mm length AVE Micro, AVE) was chosen because its diamond shaped repeating cell element is similar to the slotted tube design, yet it has small interstices that separate adjacent diamonds permitting direct visualization of the balloon profile. No balloon protrusion was found to occur (Panel B); instead the diamond-shaped struts were observed to slightly pinch the balloon inwards, causing a slight (8 μm or 0.3%) degree of intrusion (Panel D).

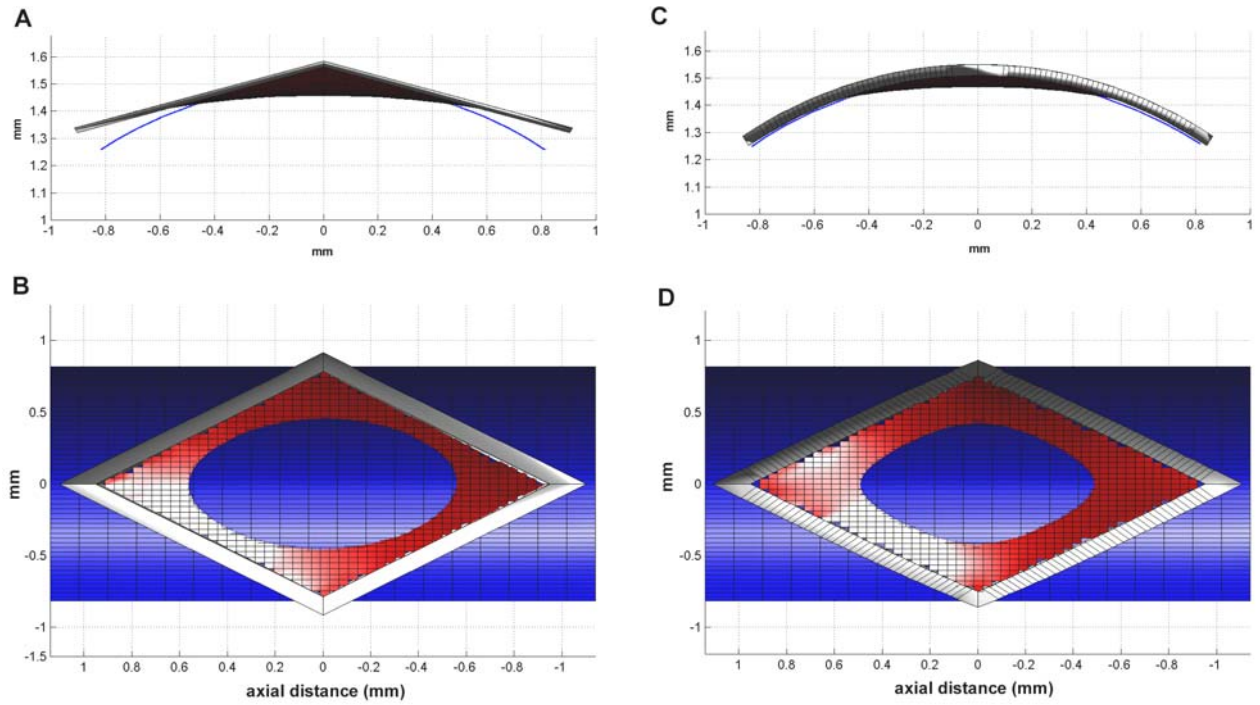

Figure 4.14: Comparison of the standard slotted tube stent (Panels A and B) with a hypothesized conforming slotted tube stent (Panels C and D) whose struts bend along their lengths to create a vascular scaffold with circular cross section. Panels A and C are cross sectional views of the stent, artery, and balloon at their final expansion diameters. All axes are shown using a unity aspect ratio, causing the lines demarking the slight curve in the artery to appear so tightly grouped that from this view the artery appears black. The balloon edge is emphasized in blue. In this simulation the balloon is allowed to pass freely through the artery, which although unphysiologic does permit estimation of the area of acute injury from endothelial denudation. Certain processes of chronic vascular disease have been hypothesized by others to occur in a fashion that restores a circular luminal cross section. The conforming slotted tube eliminates this mode of injury and, by using struts of twice the thickness of the non-conforming design, concomitantly reduces the area of acute vascular injury (Panel D).

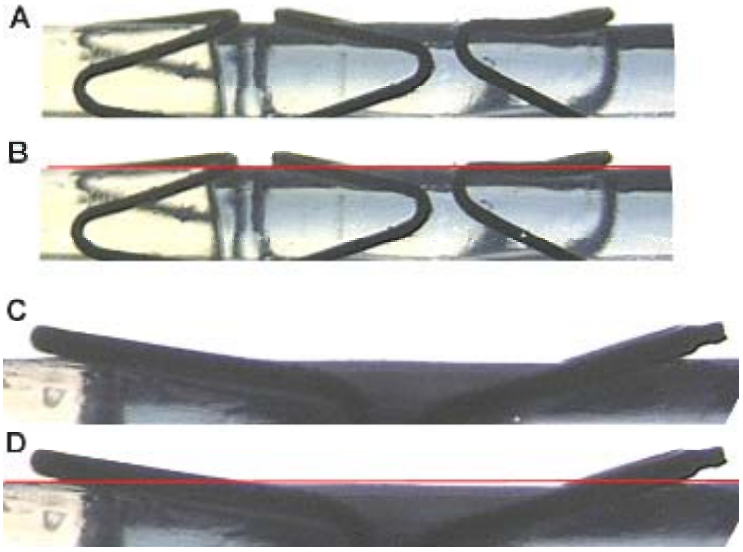

Figure 4.15: Degree of balloon protrusion in the unconstrained stent is minimal or negative. Panel A displays the upper half of a diamond-shaped geometry stent expanded by a balloon catheter at full 10 atmosphere pressure. Balloon protrusion measured relative to balloon height outside the stented region (Panel B includes the reference line) is negligible relative to strut thickness. Closer inspection of a single strut cell (Panel C) reveals the diamond-shaped struts slightly pinch the balloon inwards near the axial strut vertices, causing a small localized balloon intrusion on the order of 8 μm (D).

4.7 Balloon-device interaction – Discussion

4.7.1 Hypothesis

The hypothesis that acute arterial injury is caused by a force exerted normal to the artery surface by the balloon was investigated in this section. Stent cells of three different geometries were simulated with a linear, isotropic membrane model of the artery, and the regions of balloon-tissue interaction were compared to experimentally-observed areas. The comparisons reveal a qualitative agreement in the locations of acute endothelial denudation although the simulation demonstrated a consistent bias to underestimate the area of denudation for each stent design by 21 ± 4%.

4.7.2 Validity of model assumptions

The validity of the rabbit iliac artery modeled as a linear, isotropic thin walled membrane was discussed in 4.4.2. Thicker vessels, such as the human coronary, would respond in a similar but more pronounced manner. Thin vessel can be effectively modeled as a two dimensional mesh of springs in tension, and a thick stented vessel could be modeled as a three dimensional springed latticework, with the radial-pointing springs in compressed by the struts. The focal radial outward force of the struts would embed the struts into the tissue, reducing the effective strut thickness. This effect may have measurable consequences even in the thin-walled vessels studied. The average thickness of the native rabbit vessel wall, i.e. media plus intima, was measured to be 41 ± 4 μm. This validates the use of thin-walled vessel methods to determine strain distribution since the vessel diameter is more than 20 fold greater. This thickness compresses to 30 ± 3 μm underneath the struts (Figure 4.16). This difference of 11 ± 5 μm reduces the effective strut thickness from 33 μm to 22 μm, which by Figure 4.12 increases the calculated denuded area from 57% to 64%, closer to the observed value of 76 ± 3%.

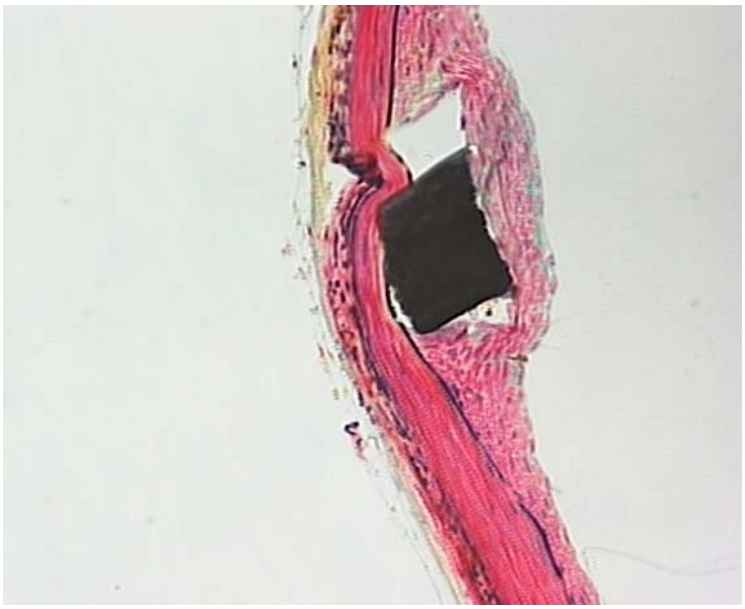

Figure 4.16: The vessel wall in compression under a slotted tube stent strut. The fine black internal elastic lamina is visible dividing the intimal layer to the right from the smooth muscle cells of the media. During transverse sectioning the black stent strut was displaced slightly downwards leaving a vacant hole. This vessel was harvested after 14 days and localized hyperplastic growth of smooth muscle cells covering the luminal surface of the strut is evident. This strut has embedded itself approximately 11 μm into the vessel wall.

4.7.3 Comparison of simulations and experiments

Review of Figure 4.9-11 reveal a similarity in localization of endothelial denudation, summarized in Table 4.2, with a consistent bias of the simulations to underestimate the extent of injury. Certain aspects of each simulation deserve further attention. The slotted tube simulation (Figure 4.10) predicts less denudation in the areas surrounding strut vertices, a finding validated by experiment. These data suggest one method to decrease the degree of stent-induced injury is to design stent cells with regions that lift away from the balloon during expansion, as the vertices of the straight-strut slotted tube do, preserving a border of intact endothelium. Improvements of this fashion incur the cost of inducing a non-circular post-stenting luminal cross section which has been found to be detrimental [32] and in a possibly related manner will also induce abnormalities in blood flow [64].

Table 4.2: Comparison of simulated vs. calculated areas of endothelial denudation in three stent geometries.

Denuded area	Measured	Simulated	% Error
slotted tube	76 ± 3 %	57 %	- 25 %
corrugated ring	42 ± 6 %	35 %	-22 %
delta wing	23 ± 3 %	18 %	-17 %

The sharp angles at the strut vertices shelter the arterial lumen from dual sides and provide a second reason for the localized preservation of endothelium. An alternative design that maintains these in-plane angles while eliminating the out-of-plane angles that detract from the above design involves machining the struts to conform to the balloon during expansion as shown in Figure 4.14. This design reduces both acute injury (43% denuded area vs. 57% in the straight-strut design) and deviation of the struts from a circular luminal cross section (0μm in conforming strut vs. a maximum deviation of 58μm in the straight-strut design) that Garassic [32] has associated with smooth muscle cell hyperplasia. These results may be related; the acute vascular injury investigated in this thesis has been shown to cause hyperplasia of the smooth muscle cells [4]. The findings of this chapter provide a mechanical explanation for Garassic's findings that a stent with four circumferential elements causes a greater hyperplastic response than a stent of identical diameter with 6 smaller-sized circumferential elements.

The corrugated ring simulations (Figure 4.10) show regions of endothelial denudation are partitioned into three self-similar triangular regions centered within the largest openings formed by the struts. This pattern, which is validated by experiment and also seen in the simulations and experiments involving the delta wing stent (Figure 4.11), suggests an intuitive approach to reduce acute vessel injury: minimize large open areas inside the strut cell. A quantitative rule of thumb derived from simulations of the three stent geometries is that the ratio of the largest inscribed circle diameter within a flattened strut cell divided by the strut thickness must be approximately 10 to prevent endothelial denudation (Table 4.3). Although it may not be possible to reduce strut thickness and maintain structural resistance to a compressive radial force, stents could be manufactured with a reduced repeating element size to achieve the same reduction in acute injury.

Table 4.3: Approximate rule of thumb: the maximum inscribed circular diameter (MICD) within the strut cell divided by the strut thickness (ST) must be approximately 10 to avoid transient balloon/tissue interaction and subsequent vascular injury. The strut thickness listed below is the minimum strut thickness for each geometry at which no balloon/tissue contact occurs.

Geometry	MICD	ST	MICD/ST ratio
slotted tube	1.90 mm	0.163 mm	11.7
corrugated ring	0.79 mm	0.112 mm	7.1
delta wing	0.59 mm	0.056 mm	10.5

4.7.4 Alternative hypothesis

An alternative hypothesis explaining the type of observed acute vascular injury is that the fully-expanded balloon catheter may extrude through the stent struts. This hypothesis has been examined by Tseng [65] who has shown that the polyurethane-walled balloon extrudes more than the strut thickness when the stent is constrained from expanding by an external glass tube. These data, although relevant in vessels with extensive lesions of calcified plaque, do not model the acute injury and subsequent chronic disease noted in the stented native iliac vessels investigated in this thesis. These native vessels distend in response to as little as one atmosphere pressure (approximately 7 times physiologic 110 mmHg pressure and 10% of the final expansion pressure) and thus do not prevent the stent, already in its plastic deformation state, from deforming further in response to the 10 atmospheres of balloon pressure. The stent alone clearly offers little or no resistance to the expanded balloon (Figure 4.15) and the stent, by design, offers greater resistance to deformation than the artery. It therefore appears unlikely that balloon extrusion is the primary cause of the noted pattern of intrastrut injury.

4.8 Conclusions

A pattern of intrastrut arterial injury was shown to exist for a variety of stent cell geometries (Figure 4.1). Two hypotheses explaining the source of this injury were investigated: that endothelial cells can tolerate a limited degree of in plane strain and detach when exposed to strain above this threshold, and that the arterial surface experiences a normally-oriented direct contact force from the balloon catheter during expansion.

Using both energy-minimization simulations and *ex-vivo* experiments on the slotted-tube model stent it was determined that neither principle axis of the post-expansion strain tensor matched the pattern of observed endothelial denudation. The pattern did match the distribution of absorbed strain energy, as measured by the vonMises strain field, however the vonMises strain varied by less than 1% over the interior of one stent cell. It was not possible that the strain threshold for endothelial cells lay within this narrow band because the stent-to-stent variability of average strain is considerably larger, yet the same pattern was consistently observed.

Finite difference models of the artery surface over the stent struts revealed that during expansion the balloon contacted the endothelial lining in all stent types examined over a similar region found to be denuded. Several mechanisms contributing to the balloon-artery contact were considered including arterial intrusion, strut embedding, and balloon protrusion; although all may contribute to the injury, arterial intrusion was found to be the predominate cause.

Methods to reduce this mode of injury were considered involving decreasing the size of the repeating cellular element and increasing strut thickness. A rule of thumb was proposed that the mode of intracellular injury investigated in this chapter could be eliminated if the diameter of the largest inscribed circle in a stent cell is less than an order of magnitude larger than the strut thickness.

These data indicate the importance of careful system design of implantable devices. Transient interactions between the deployment system and tissue may impart more tissue damage than the implant itself.

CHAPTER 5 Conclusions

Vascular medical implants are known to invoke a complex and incompletely understood response in tissue that includes a reaction to the presence of foreign materials, changes in the fluid dynamics of blood flow, and a reaction to higher than physiologic levels of chronic stress. This thesis sought to identify, characterize and quantify a fourth mechanism by which implants induce a tissue response: by imposing acute mechanical injury during device expansion.

5.1 Specific findings and summary

Chapter Two described a novel system that can be used to quantify arterial deformation in living animals.

This method was designed to determine the complete surface strain tensor developed along any straight and observable axisymmetric surface undergoing large-scale deformations, and was able to describe how the tensor changes in space and time. It was able to do so in an *in vivo* environment using a single camera. A separate device was designed that could create marks as small as 50 μm which permits this method to be used with fine structures such as vessels of one millimeter or larger diameter. The method was characterized *in vitro* using bovine artery segments and a latex phantom, and tested on rabbits to demonstrate its feasibility *in vivo*. The root mean square error of the strain measurements was experimentally found to be additive (i.e. independent of the true strain) and was determined to be 4%. The system was shown capable of measuring strains of straight, accessible vessels in the presence of respiratory/cardiac motion and visual glare *in vivo*.

This system was used in Chapter Three to determine the manner in which stents dynamically deform the arterial wall during expansion. It was discovered that, despite the uniform cylindrical shape that endovascular stents assume when fully deployed, they rarely expand in a uniform manner. Typically, first the far proximal and distal ends bloom outwards until they contact the intima while the middle region of the stent remains unexpanded. This temporarily stretches the artery over two supporting ring-shaped regions rather than along the length of the

stent, focusing stress and causing superficial and possible deep vascular injury. Concomitant axial contraction of the stent relative to the artery pulls these rings inwards and is responsible for the characteristic pattern of endothelial cell denudation observed at the edges of stented native vessels and for the corresponding localization of the pernicious chronic vascular response. Relatively minor changes to the stent or balloon geometry were proposed to create a center-first opening stent that reduces end scraping. One such design was tested (conforming delta wing) and was found to reduce average scraping from 70% to 42% when compared with its unmodified version, but only when mounted upon a matched-length balloon.

Chapter Four sought to identify and quantify mechanisms of tissue injury that were found to occur during device expansion within the regions of artery covering each of the repeating stent cell elements. Three different stent geometries were investigated and in each case a similar pattern of acute vascular injury, as measured by endothelial denudation, was found to exist. The hypothesis that endovascular cells denude in response to exposure to an in-plane strain field exceeding some preset threshold was examined and discarded. Arterial strain was determined by both simulation and experiment, and found to be nearly uniform, varying by less than 1% over the surface. Further simulations showed that the arterial surface experiences a normally-oriented direct contact force from the balloon catheter during expansion, and the localization of calculated balloon/tissue interaction closely describes the pattern of observed injury. Several methods of liming this mode of injury were described, including reducing the size of the stent cells and increasing the strut thickness.

5.2 General findings and recommendations

Several of the findings of this chapter are relevant to a broader range of permanent medical implants than endovascular stents alone.

1. The manner in which devices are implanted may be a critical determinant of the degree of injury they cause and the chronic tissue response they engender. A device that expands in a manner causing injury may exhibit such a shape only transiently, requiring observation over the entire course of expansion to identify and characterize.

2. Implant design requires attention to not only the implant itself but also to the delivery system. An improperly designed delivery system may injure tissue either directly or by promoting an injurious manner of expansion of the device.

3. Implant and delivery systems must be optimized concomitantly; improved devices may cause no less injury if implanted in a non-optimal fashion.

4. Regulatory agencies, such as the U.S. Food and Drug Administration (FDA) should consider testing and approval of new device and deployment systems as a unit, and not as separate entities.

5.3 Future work

Although the aims of this thesis were to explore all methods of mechanical tissue injury caused during implant expansion, during this investigation several additional forms of injury were identified that have yet to be characterized. Once all acute and chronic candidates for mechanisms of tissue injury derived from implants have been identified, the intriguing problem of identifying the relative importance and relationship between of each of these modes becomes possible. I expect that this will also usher new understanding of the mechanisms of tissue response to stress and strain, and perhaps integrate what was previously thought to be entirely separate modes of injury. For example, at a macroscopic level there appears to be an obvious difference between the response of tissue to extreme levels of strain imposed by a device and frank laceration. On a finer scale, it may be that at some point the cellular disruption from both sources becomes indistinguishable.

I recommend four specific areas for future work in the field of understanding acute tissue injury in response to implant expansion. From most specific to most general these are:

1. Investigate the role of knife-edge injury in stented arteries. The type of injury that was categorized as scraping-induced in Chapter Three may actually be composed of two components: a true scraping and a focal laceration caused by the outward-splayed strut edges pressed against the arterial surface. This latter mode of injury, reminiscent of a knife cut, may cause deep injury since the struts join at acute angles at the stent edges, and may provide both acute and chronic (in stent designs that have substantial post-expansion endflare) injury.

2. Generalizing the above problem, the role of deep tissue injury needs to be examined. This thesis used endothelial cells as a marker of superficial injury since the role of acute superficial injury in causing hyperplasia has been established by Schwartz's experiments [4]. Deep injury may also occur, but lacks an easily-observed marker. A three-dimensional finite element model of the stent, balloon, and artery may enable simulated measurements, which may in turn provide a more rigorous understanding and quantification of the relationships Schwartz has noted.

3. Develop a method to characterize atherosclerotic plaque and vessel tortuosity, and incorporate these effects into the above models. All previous experimental data, simulations, and inferences have involved native, straight vessels. Calcified, heterogeneous plaque and the presence of small-radius bends will almost certainly alter the relationships identified thus far.

4. Once the above modes of acute tissue injury have been identified and quantified, isolate each if possible and examine the type and extent of chronic injury each engenders.

5.4 Final thoughts

There is currently a great deal of interest in the development of permanent medical implants and in the tissue responses they stimulate. Others have investigated mechanical initiators of these responses including changes in fluid dynamics [31], biological inertness and other material properties [20], and effects of remodeling in response to tissue stress [29]. This thesis has identified and characterized several new mechanical stimuli important in determining acute vascular injury that occur during device expansion. It is my hope these findings will lead to improvements in these devices and in the lives of the roughly 500,000 patients expected to receive them each year.

APPENDIX A Macroscopic strain analysis code

The code used to determine the surface strain tensor from a sequence of TIFF image files of an expanding marked artery is presented below. The code is written in Matlab 5 programming language. The code can be divided into two categories: analysis and display.

A.1 Analysis procedures summary

The procedures are listed below in the order in which they are called by the user.

get_dat takes an image map from the frame grabber with a scale factor and returns the encoded matrix rn that describes both the digitized arterial envelope and the two dimensional locations of all the reference points

fit_hypm takes the output matrix from get_dat, completes a non-linear least squares fit of a general quadratic equation to the data, and rotates it to make the axis of symmetry horizontal.

out_dat takes rotates the quadratic envelope determined by fit_hypm to create a data structure describing the three-dimensional arterial surface. It next back-projects the marker locations from get_dat onto this surface, divides the surface into equal patches, and stores all the data in single matrix. The matrix is called dn, where n is replaced by the frame number of the original image.

find_key associates a set of marker triads with every patch location determined by out_dat.

findstr takes the set of marker triads from find_key and their original and displaced locations from out_dat, computes the Green strain tensor, and adds this information to the dn data structure.

A.2 Display procedures summary

show is a wrapper function that draws a graphical user interface and calls show1-show6 as required. It takes a Matlab data file composed of the set of dn matrices produced by outdat and findstr, and can produce still and animated two and three dimensional graphs describing the evolution of strain in time.

A.3 Code

```
function dn = dat_fin(n1,d1,na,da,nn,dn)
% DAT_FIN finds e(x,y,t) and de/dt(x,y,t)
%       dn = dat_fin(n1,d1,na,da,nn,dn)
%
%       See out_dat for description of form of d1
%       See fit_hypm for description of form of n1,na,nn
%
%       James C. Squire   December 1997

% initialize variables

hndl = waitbar(0,'Determining strain...');
nblocks = size(d1,1)-1;
for i = 1:nblocks
  triplet  = findkeyt(i,n1,d1);
  straint  = findstnt(triplet,n1,nn);
  dstraint = findstnt(triplet,na,nn);
  dn(i,12) = straint(3);
  dn(i,15) = dstraint(3);

  ihoriz   = findkeyh(i,n1,d1);
  strainh  = findstnh(ihoriz,n1,nn);
  dstrainh = findstnh(ihoriz,na,nn);
  dn(i,11) = strainh;
  dn(i,14) = dstrainh;

  strainv  = findstnv(i,d1,dn);
  dstrainv = findstnv(i,da,dn);
  dn(i,10) = strainv;
  dn(i,13) = dstrainv;

  waitbar(i/nblocks)
end
close(hndl)
```

```
function khoriz = findkeyh(index,nn,dn)

% FINDKEYH finds key point indicies to determine horizontal strain about a point
%       khoriz = findkey(index,nn,dn)
%
%       khoriz is in the form [index1, index2]
%       index is an index into dn
%       See fit_hypm for description of form of nn.
%       See out_dat for description of form of dn.
%
%       James C. Squire   August 1997

% initialize variables

HORIZTOL = 1;         % Must be at least one patchwidth away from center
DEBUG = 0;          % Set to ~0 for diagnostic printout

nvert  = dn(size(dn,1),2);
nhoriz = dn(size(dn,1),3);
nblocks = nvert*nhoriz;

n3 = nn(1,3);
p2  = nn(3,1);              q  = sqrt(nn(3,2));
```

```
xlist = nn(n3:size(nn,1),2);      ylist = nn(n3:size(nn,1),3);   zlist =
zcalc(xlist,ylist,p2,q,DEBUG);
x1 = dn(index,2);              y1 = dn(index,3);          z1 = zcalc(x1,y1,q,p2,DEBUG);
x2 = dn(index,4);              y2 = dn(index,5);          z2 = zcalc(x2,y2,q,p2,DEBUG);
x3 = dn(index,6);              y3 = dn(index,7);          z3 = zcalc(x3,y3,q,p2,DEBUG);
x4 = dn(index,8);              y4 = dn(index,9);          z4 = zcalc(x4,y4,q,p2,DEBUG);

dyleft = sqrt((y1-y3)^2+(z1-z3)^2);   dyright = sqrt((y2-y4)^2+(z2-z4)^2);
patchheight  = mean([dyleft dyright]);
patchwidth   = x2 - x1;
% the center is the projected value; the intersection of the diagonals
patchxcenter =  -(((x2 - x4)*(x3*y1 - x1*y3) - (x1 - x3)*(x4*y2 - x2*y4))/ ...
     ((x2 - x4)*(-y1 + y3) - (x1 - x3)*(-y2 + y4)));
patchycenter = -((x4*y2 - x2*y4)/(x2 - x4)) + ...
     ((-y2 + y4)*((x2 - x4)*(x3*y1 - x1*y3) - (x1 - x3)*(x4*y2 - x2*y4)))/ ...
     ((x2 - x4)*((x2 - x4)*(-y1 + y3) - (x1 - x3)*(-y2 + y4)));
patchzcenter = zcalc(patchxcenter,patchycenter,p2,q,DEBUG);
distances=sqrt((xlist-patchxcenter).^2+(ylist-patchycenter).^2+(zlist-patchzcenter).^2);

% find horizontal key points
xtol = patchwidth * HORIZTOL;          % must be at lest xtol away from each other
[p1d,p1_index]=min(distances);
p1x = xlist(p1_index); p1y=ylist(p1_index); p1z=zlist(p1_index);
p2d = 999999999;
p2_index = -1;
for i=1:size(xlist,1)
  xt = xlist(i); yt = ylist(i); zt = zlist(i);
  xpatchdist = sqrt((xt-patchxcenter).^2+(yt-patchycenter).^2+(zt-patchzcenter).^2);
  xpointdist = abs(xt - p1x);
  if xpointdist >= xtol & xpatchdist < p2d
    p2d = xpatchdist;
    p2_index = i;
  end
end

khoriz = [p1_index p2_index];
```

function ntriplet = findkeyt(index,nn,dn)

```
% FINDKEYT finds key point indicies to determine strain about a point
%           ntriplet = findkeyt(index,nn,dn)
%
%           ntriplet are in form of [index1, index2, index3]
%           where index is an index into dn
%           See fit_hypm for description of form of nn.
%           See out_dat for description of form of dn.
%
%           James C. Squire   August 1997

% constants
NBEST = 5;            % Examine the closest NBEST points for triplets
NEARCENTERG = .3;     % Narrowness (=relative importance) of near_center grade
[.1,5]
NEARCENTERC = .6;     % Ideal closeness to center is NEARCENTERC*patchwidth
DISTANCEAPARTG = 1;   % Narrowness (=relative importance) of distance_apart grade
[.1,5]
DISTANCEAPARTC = 1.25;   % Ideal distance apart is
DISTANCEAPARTC*patchwidth
EDGEG = 4;            % Relative importance of Edge grade [.1 10]
ANGLEG =3;            % Relative importance of Angle grade [.1 10]
DEBUG = 0;            % Set to ~0 for diagnostic printout

% initialize variables
```

```
nvert  = dn(size(dn,1),2);
nhoriz = dn(size(dn,1),3);
nblocks = nvert*nhoriz;

n3 = nn(1,3);
p2  = nn(3,1);                  q  = sqrt(nn(3,2));
xlist = nn(n3:size(nn,1),2);      ylist = nn(n3:size(nn,1),3);
zlist = zcalc(xlist,ylist,p2,q,DEBUG);
x1 = dn(index,2);               y1 = dn(index,3);
x2 = dn(index,4);               y2 = dn(index,5);
x3 = dn(index,6);               y3 = dn(index,7);
x4 = dn(index,8);               y4 = dn(index,9);

z1 = zcalc(x1,y1,q,p2,DEBUG);
z2 = zcalc(x2,y2,q,p2,DEBUG);
z3 = zcalc(x3,y3,q,p2,DEBUG);
z4 = zcalc(x4,y4,q,p2,DEBUG);
dyleft = sqrt((y1-y3)^2+(z1-z3)^2);   dyright = sqrt((y2-y4)^2+(z2-z4)^2);
patchheight  = mean([dyleft dyright]);
patchwidth   = x2 - x1;
% the center is the projected value; the intersection of the diagonals
patchxcenter =  -(((x2 - x4)*(x3*y1 - x1*y3) - (x1 - x3)*(x4*y2 - x2*y4))/ ...
     ((x2 - x4)*(-y1 + y3) - (x1 - x3)*(-y2 + y4)));
patchycenter = -((x4*y2 - x2*y4)/(x2 - x4)) + ...
     ((-y2 + y4)*((x2 - x4)*(x3*y1 - x1*y3) - (x1 - x3)*(x4*y2 - x2*y4)))/ ...
     ((x2 - x4)*((x2 - x4)*(-y1 + y3) - (x1 - x3)*(-y2 + y4)));
patchzcenter = zcalc(patchxcenter,patchycenter,p2,q,DEBUG);

% Choose the NBEST closest points and arrange in matrix mbest
% mbest = [index1 index2 index3 ...
%         patchdist_score apartdist_score edge_score angle_score total_score]

distances=sqrt((xlist-patchxcenter).^2+(ylist-patchycenter).^2+(zlist-patchzcenter).^2);
[dummy,tindex]=sort(distances);
closeindex=tindex(1:NBEST); % holds indecies to NBEST closest points
ntriplets = (NBEST)*(NBEST-1)*(NBEST-2)/6;  % NBEST choose 3
mbest = zeros(ntriplets,8);
count=1;
for i=1:NBEST-2
  for j=i+1:NBEST-1
    for k=j+1:NBEST
      mbest(count,1:3)=[closeindex(i) closeindex(j) closeindex(k)];
      count=count+1;
    end
  end
end
if DEBUG~=0 & DEBUG<=1
  disp(' '); disp('closest distances are');
  disp('index distance'); disp([closeindex distances(closeindex)]); pause
  disp(' '); disp('mbest = '); disp(mbest);
  disp('Note figure 1')
  n1 = nn(1,1);                    n2 = nn(1,2);
  toplinex    = nn(n1:n2-1,2);       topliney    = nn(n1:n2-1,3);
  bottomlinex = nn(n2:n3-1,2);       bottomliney = nn(n2:n3-1,3);
  keypointsx  = xlist(closeindex);   keypointsy  = ylist(closeindex);
  boxx = [x1 x2 x3 x4 x1];           boxy = [y1 y2 y3 y4 y1];
  figure(1)
  hold on
  for j=1:nblocks
    plot([dn(j,2),dn(j,4),dn(j,6),dn(j,8),dn(j,2)], ...
        [dn(j,3),dn(j,5),dn(j,7),dn(j,9),dn(j,3)],'b-')
  end
  plot(toplinex,topliney,'y-',bottomlinex,bottomliney,'y-', ...
      xlist,ylist,'wo',keypointsx,keypointsy,'rx',boxx,boxy,'g-', ...
      patchxcenter,patchycenter,'g*');
```

```
  hold off
  pause
end

% For each of the triplets determine
%   near_center score from my distribution
%   dist_apart score from distribution
%   edge score from min(cos(theta)) (stay away from edges)
%   angle score from min(sin(theta)) (don't want small angles)

% My distribution: x^a*exp(-b x).  The narrowness is prop to a. Center at a/b
anc = NEARCENTERG;      bnc=anc/(NEARCENTERC*patchwidth);
ada = DISTANCEAPARTG;   bda=ada/(DISTANCEAPARTC*patchwidth);
for i=1:ntriplets
  point1x=xlist(mbest(i,1));   point1y=ylist(mbest(i,1));   point1z=zlist(mbest(i,1));
  point2x=xlist(mbest(i,2));   point2y=ylist(mbest(i,2));   point2z=zlist(mbest(i,2));
  point3x=xlist(mbest(i,3));   point3y=ylist(mbest(i,3));   point3z=zlist(mbest(i,3));

  distc1=norm([point1x-patchxcenter point1y-patchycenter point1z-patchzcenter]);
  distc2=norm([point2x-patchxcenter point2y-patchycenter point2z-patchzcenter]);
  distc3=norm([point3x-patchxcenter point3y-patchycenter point3z-patchzcenter]);
  tin = [distc1 distc2 distc3];
  tv=[distc1^anc * exp(-bnc*distc1) distc2^anc * exp(-bnc*distc2) distc3^anc * exp(-
bnc*distc3)];
  [tf,ti] = min(tv);
  mbest(i,4) = tf;     % near_center grade
  distnc = tin(ti);


  dist12=sqrt((point2x-point1x)^2 + (point2y-point1y)^2 + (point2z-point1z)^2);
  dist23=sqrt((point3x-point2x)^2 + (point3y-point2y)^2 + (point3z-point2z)^2);
  dist13=sqrt((point3x-point1x)^2 + (point3y-point1y)^2 + (point3z-point1z)^2);

  tin = [dist12 dist23 dist13];
  tv = [dist12^ada*exp(-bda*dist12) dist23^ada*exp(-bda*dist23) dist13^ada*exp(-
bda*dist13)];
  [tf,ti] = min(tv);
  mbest(i,5) = tf;    % dist_apart grade
  distda = tin(ti);
  point1r=sqrt(q^2*(1+point1x^2/p2));
  point1a=sqrt(point1r^2-point1y^2)/point1r;
  if imag(point1a), point1a=0; end          % point falls outside modelled surface
  point2r=sqrt(q^2*(1+point2x^2/p2));
  point2a=sqrt(point2r^2-point2y^2)/point2r;
  if imag(point2a), point2a=0; end
  point3r=sqrt(q^2*(1+point3x^2/p2));
  point3a=sqrt(point3r^2-point3y^2)/point3r;
  if imag(point3a), point3a=0; end
  ftedge=min([point1a point2a point3a]); % always from 0 to 1, 1 best
  mbest(i,6)=ftedge^EDGEG;

  r12=[point2x-point1x point2y-point1y point2z-point1z];
  r23=[point3x-point2x point3y-point2y point3z-point2z];
  r31=[point1x-point3x point1y-point3y point1z-point3z];
  angle123=acos((-r12*r23')/(norm(r12)*norm(r23)))*180/pi;
  angle231=acos((-r23*r31')/(norm(r23)*norm(r31)))*180/pi;
  angle312=acos((-r31*r12')/(norm(r31)*norm(r12)))*180/pi;
  ftangle = min([angle123 angle231 angle312])/60;
  % 60 would be equilateral triangle,  tf from 0 to 1, 1 best
  mbest(i,7) = ftangle^ANGLEG;

  mbest(i,8) = prod(mbest(i,4:7))*10000;

  if DEBUG~=0 & DEBUG<=2

    % draw the overall stent picture with current points
```

```
    n1 = nn(1,1);                       n2 = nn(1,2);
    toplinex    = nn(n1:n2-1,2);        topliney    = nn(n1:n2-1,3);
    bottomlinex = nn(n2:n3-1,2);        bottomliney = nn(n2:n3-1,3);
    keypointsx  = xlist(mbest(i,1:3));  keypointsy  = ylist(mbest(i,1:3));
    boxx = [x1 x2 x3 x4 x1];            boxy = [y1 y2 y3 y4 y1];
    disp(sprintf('Showing point %g of %g',i,ntriplets))
    figure(1)
    clf, hold on
    for j=1:nblocks
      plot([dn(j,2),dn(j,4),dn(j,6),dn(j,8),dn(j,2)], ...
           [dn(j,3),dn(j,5),dn(j,7),dn(j,9),dn(j,3)],'b-')
    end
    plot(toplinex,topliney,'y-',bottomlinex,bottomliney,'y-', ...
      xlist,ylist,'wo',keypointsx,keypointsy,'wx',boxx,boxy,'g-');
    hold off
    axis([-.3 .1 -.2 .2])
    axis('square')
    title(sprintf('Score = %g',mbest(i,8)))

    % draw distribution for near_center_point
    figure(2)
    subplot(221)
    tx=linspace(0,5*patchwidth,100);
    ty=tx.^anc.*exp(-bnc.*tx);
    % draws it with x scale in patchwidths
    plot(tx/patchwidth,ty,'y-',distnc/patchwidth,mbest(i,4),'ro');
    set(gca,'xtick',[0 1 2 3 4 5])
    title('Nearness to patch')

    % draw distribution for distance_apart
    subplot(222)
    tx=linspace(0,5*patchwidth,100);
    ty=tx.^ada.*exp(-bda.*tx);
    % draws it with x scale in patchwidths
    plot(tx/patchwidth,ty,'y-',distda/patchwidth,mbest(i,5),'ro');
    set(gca,'xtick',[0 1 2 3 4 5])
    title('Distance from each other')

    % draw graph with edge point
    subplot(223)
    tx=linspace(0,1,100);
    ty=tx.^EDGEG;
    plot(tx,ty,'y-',ftedge,mbest(i,6),'ro');
    title('Closest point to edge')

    % draw graph with angle point
    subplot(224)
    tx=linspace(0,1,100);
    ty=tx.^ANGLEG;
    plot(tx,ty,'y-',ftangle,mbest(i,7),'ro');
    title('evenly spaced angles')
    pause
  end
end

% return the best points
[dummy,tindex] = max(mbest(:,8));
ntriplet = mbest(tindex,1:3);

if DEBUG~=0 & DEBUG<=3
    % draw the overall stent picture with best triplets highlighted
    n1 = nn(1,1);                       n2 = nn(1,2);
    toplinex    = nn(n1:n2-1,2);        topliney    = nn(n1:n2-1,3);
    bottomlinex = nn(n2:n3-1,2);        bottomliney = nn(n2:n3-1,3);
    keypointsx  = xlist(ntriplet);      keypointsy  = ylist(ntriplet);
    boxx = [x1 x2 x3 x4 x1];            boxy = [y1 y2 y3 y4 y1];
```

```
    figure(1)
    hold off
    cla
    title('')
    hold on
    for j=1:nblocks
      plot([dn(j,2),dn(j,4),dn(j,6),dn(j,8),dn(j,2)], ...
          [dn(j,3),dn(j,5),dn(j,7),dn(j,9),dn(j,3)],'b-')
    end
    plot(toplinex,toplineY,'y-',bottomlinex,bottomliney,'y-', ...
     xlist,ylist,'wo',keypointsx,keypointsy,'wx',boxx,boxy,'g-');
    axis([-.3 .1 -.2 .2])
    axis('square')
    hold off
end
```

function shoriz = findstrh(khoriz,na,nb)

```
% FINDSTRH finds the strain between two key normalized points
%           shoriz = findstrh(khoriz,na,nb)
%
%           khoriz is in the form of [index1, index2]
%           index is an index into dn.
%           See fit_hypm for description of form of na,nb.
%
%           James C. Squire   August 1997
%  modified October 1998 to work under assumption of zero torsion
%  modified September 1999 to change uniaxial strain definition
%    to tensor definition

% initialize variables
n3a = na(1,3);                  n3b = nb(1,3);
p2a  = na(3,1);                 p2b  = nb(3,1);
qa  = sqrt(na(3,2));              qb  = sqrt(nb(3,2));


% Cartesian coordinates for points pairs 1,2 of before a and after b   horiz: x  vert: y  out of
page: z
% start point triad is A,B,C; end triad is a,b,c

hxa1 = na(n3a+khoriz(1)-1,2);  hya1 = na(n3a+khoriz(1)-1,3);  hza1 =
zcalc(hxa1,hya1,p2a,qa);
hxa2 = na(n3a+khoriz(2)-1,2);  hya2 = na(n3a+khoriz(2)-1,3);  hza2 =
zcalc(hxa2,hya2,p2a,qa);
hxb1 = nb(n3b+khoriz(1)-1,2);  hyb1 = nb(n3b+khoriz(1)-1,3);  hzb1 =
zcalc(hxb1,hyb1,p2b,qb);
hxb2 = nb(n3b+khoriz(2)-1,2);  hyb2 = nb(n3b+khoriz(2)-1,3);  hzb2 =
zcalc(hxb2,hyb2,p2b,qb);


% distances between points 1,2
horiza = abs(hxa1-hxa2);
horizb = abs(hxb1-hxb2);

% compute strain

shoriz = (horizb-horiza)/horiza * (horiza+horizb)/(2*horiza);
```

function strain_tensor = findstrt(ntriplet,nb,na)

```
% FINDSTRT finds the strain tensor around three points
%           strain_tensor = findstrt(ntriplet,n1,n2)
%
%           ntriplet is in the form of [index1 index2 index3] into n1,n2
%           strain_tensor is in the form of [e_thetatheta e_zz e_ztheta]
%           See fit_hypm for description of form of na,nb.
%
%           James C. Squire   August 1997

DEBUG = 3;  % set to 9999 for no debugging

% initialize variables
n3a = na(1,3);                  n3b = nb(1,3);
p2a  = na(3,1);                 p2b  = nb(3,1);
qa  = sqrt(na(3,2));             qb  = sqrt(nb(3,2));

% Cartesian coordinates for points A,B,C,a,b,c   horiz: x  vert: y  out of page: z
% start point triad is A,B,C; end triad is a,b,c
xA = na(n3a+ntriplet(1)-1,2);  yA = na(n3a+ntriplet(1)-1,3);  zA = zcalc(xA,yA,p2a,qa);
xB = na(n3a+ntriplet(2)-1,2);  yB = na(n3a+ntriplet(2)-1,3);  zB = zcalc(xB,yB,p2a,qa);
xC = na(n3a+ntriplet(3)-1,2);  yC = na(n3a+ntriplet(3)-1,3);  zC = zcalc(xC,yC,p2a,qa);
xa = nb(n3b+ntriplet(1)-1,2);  ya = nb(n3b+ntriplet(1)-1,3);  za = zcalc(xa,ya,p2b,qb);
xb = nb(n3b+ntriplet(2)-1,2);  yb = nb(n3b+ntriplet(2)-1,3);  zb = zcalc(xb,yb,p2b,qb);
xc = nb(n3b+ntriplet(3)-1,2);  yc = nb(n3b+ntriplet(3)-1,3);  zc = zcalc(xc,yc,p2b,qb);
if DEBUG<=1
  disp('         x        y        z')
  disp(sprintf('A   %7.3g   %7.3g   %7.3g',xA,yA,zA))
  disp(sprintf('B   %7.3g   %7.3g   %7.3g',xB,yB,zB))
  disp(sprintf('C   %7.3g   %7.3g   %7.3g',xC,yC,zC))
  disp(sprintf('a   %7.3g   %7.3g   %7.3g',xa,ya,za))
  disp(sprintf('b   %7.3g   %7.3g   %7.3g',xb,yb,zb))
  disp(sprintf('c   %7.3g   %7.3g   %7.3g',xc,yc,zc))
end

% Convert to cylindrical coords and store in matricies A,B,C,a,b,c
% each point of form [r theta z]
% z is measured along the stent axis (x value in screen coords), ie
% horiz: z    around axis: theta     distance from axis: r

A(1) = norm([yA zA]);   A(2) = atan2(yA,zA);   A(3) = xA;
B(1) = norm([yB zB]);   B(2) = atan2(yB,zB);   B(3) = xB;
C(1) = norm([yC zC]);   C(2) = atan2(yC,zC);   C(3) = xC;
a(1) = norm([ya za]);   a(2) = atan2(ya,za);   a(3) = xa;
b(1) = norm([yb zb]);   b(2) = atan2(yb,zb);   b(3) = xb;
c(1) = norm([yc zc]);   c(2) = atan2(yc,zc);   c(3) = xc;
if DEBUG<=1
  disp(' ')
  disp('         r        t        z')
  disp(sprintf('A   %7.3g   %7.3g   %7.3g',A(1),A(2),A(3)))
  disp(sprintf('B   %7.3g   %7.3g   %7.3g',B(1),B(2),B(3)))
  disp(sprintf('C   %7.3g   %7.3g   %7.3g',C(1),C(2),C(3)))
  disp(sprintf('a   %7.3g   %7.3g   %7.3g',a(1),a(2),a(3)))
  disp(sprintf('b   %7.3g   %7.3g   %7.3g',b(1),b(2),b(3)))
  disp(sprintf('c   %7.3g   %7.3g   %7.3g',c(1),c(2),c(3)))
end


% Compute strain

r=mean([a(1) b(1) c(1)]);
R=mean([A(1) B(1) C(1)]);
an=R*(B(2)-A(2));  bn=R*(C(2)-A(2));  cn=B(3)-A(3);  dn=C(3)-A(3);
am=r*(b(2)-a(2));  bm=r*(c(2)-a(2));  cm=b(3)-a(3);  dm=c(3)-a(3);

de = am*dm-bm*cm;
F=[an*dm-bn*cm bn*am-an*bm; cn*dm-dn*cm dn*am-cn*bm]/de;
```

```
E = .5*(F'*F-eye(2));

if DEBUG<=2
  disp(' ')
  disp('F:')
  disp(F)
  disp(' ')
  disp('Euler:')
  disp(E)
end

strain_tensor = [E(1,1) E(2,2) mean([E(1,2) E(2,1)])];
```

function strainv = findstnv(index,d1,d2)

```
% FINDSTNV finds vertical strain about index point index
% strainv = findstnv(index,d1,d2)
%
%           index is an index into dn
%           See out_dat for description of form of dn.
%
%           James C. Squire   August 1997
%  modified September 1998 to change uniaxial strain definition
%    to tensor definition

% initialize variables

nvert  = d1(size(d1,1),2);
nhoriz = d1(size(d1,1),3);
ibot   = ceil(index/nvert)*nvert;
itop   = ibot-nvert+1;

length1 = mean(d1(itop,[3,5])) - mean(d1(ibot,[7,9]));
length2 = mean(d2(itop,[3,5])) - mean(d2(ibot,[7,9]));

strainv = (length2-length1)/length1 * (length1+length2)/(2*length1);
```

function err = fit_hyp(lambda)

```
%FIT_HYP Used by fit_hypm
%           FIT_HYP(lambda) returns the error between the data and the
%           values computed by the current function of lambda.
%           FITFUN assumes a function of the form
%
%             y =  -e-bx (+/-) sqrt((e+bx)^2-4c(ax^2+dx-1)^2)
%           ------------------------------------------
%                       2c
%
%           with 0 linear parameters and 5 nonlinear parameters
%           accounting for translational(2), rotational(1), and shape(2) DOF
%
%           James C. Squire   July 1997

global Data Plothandle

n1 = Data(1,1); n2 = Data(1,2); n3 = Data(1,3);
xt  = Data(n1:n2-1,2);
yt  = Data(n1:n2-1,3);
xb = Data(n2:n3-1,2);
yb = Data(n2:n3-1,3);
```

```
zt = zeros(size(xt));
for j = 1:length(xt)
  ftemp = sqrt((lambda(5)+lambda(2)*xt(j))^2-
4*lambda(3)*(lambda(1)*xt(j)^2+lambda(4)*xt(j)-1));
  zt(j) = (-lambda(5) - lambda(2)*xt(j) + ftemp) / (2*lambda(3));
end

zb = zeros(size(xb));
for j = 1:length(xb)
  ftemp = sqrt((lambda(5)+lambda(2)*xb(j))^2-
4*lambda(3)*(lambda(1)*xb(j)^2+lambda(4)*xb(j)-1));
  zb(j) = (-lambda(5) - lambda(2)*xb(j) - ftemp) / (2*lambda(3));
end

set(Plothandle(1),'ydata',zt)
set(Plothandle(2),'ydata',zb)
drawnow
err = norm([zt;zb]-[yt;yb]);
```

function nn=fit_hypm(data2, auto, lambda)

```
%FIT_HYPM fits a hyperbolic model to stent data.
%           nn=fit_hypm(rn, auto, lambda)
%
%           See get_data for form of rn.
%
%           It returns nn =
%           [n1  n2  n3]  n1=start row of top envelope, n2 for bottom, n3 for key points
%           [sin(theta) cos(theta) theta]
%           [p^2       q^2       0]
%           [h         k         0]
%           [hn        kn        0]
%           [-2        x1        y1]  -2 means start of top envelope
%           [-1        x1        y1]  -1 means start of bottom envelope
%           [1         x1        y1]  key point number 1
%
%           If lambda = [a,b,c,d,e] is supplied, it works in debug mode.
%      If auto is supplied, it does not pause while showing its work
%
%           fit_hypm fits the data to the following equation
%
%             y =  -e-bx (+/-) sqrt((e+bx)^2-4c(ax^2+dx-1)^2)
%            ------------------------------------------
%                        2c
%
%           It uses fit_hyp as a helper function
%
%      Fits to (y-k)^2/q^2 - (x-h)^2/p^2 = 1
%      Returns the actual derotated hyperboloid
%           James C. Squire   July 1997
%           Modified August 1998

global Data
global Plothandle

% Setup data structures
Data = data2;
figure(1)
clf
hold on
n1 = Data(1,1);
n2 = Data(1,2);
n3 = Data(1,3);
```

```
xt  = Data(n1:n2-1,2);
yt  = Data(n1:n2-1,3);
xb = Data(n2:n3-1,2);
yb = Data(n2:n3-1,3);
xp = Data(n3:length(Data),2);
yp = Data(n3:length(Data),3);

% Initialize first guess by taking exact soln to 5 well-thought-out sampled points
if nargin < 3

  tl=0; tr=0; br=0; bl=0; %these refer to if a corner is taken
  [minxt,indminxt]=min(xt);
  [minxb,indminxb]=min(xb);
  [maxxt,indmaxxt]=max(xt);
  [maxxb,indmaxxb]=max(xb);
  [minyb,indminyb]=min(yb);

  % x1 must be the zero x point; store position in x1p
  if minxt==0 % it's in the top
    y1=yt(indminxt);
    tl=1;
  elseif minxb==0
    y1=yb(indminxb);
    bl=1;
  else
    error('Error: r data not normalized properly')
  end
  x1=0; % by definition

  % put the zero y point (or closest if already point1) into point2.
  if xb(indminyb)==0  % uh,oh: point(0,0) exists
    disp('Sorry: point 0,0 exists.  You must manually enter start point, or redigitize')
    error('Probability of this happening = machine precision ~= 10^-16')
  end
  x2=xb(indminyb);
  if indminyb==1
    bl=1;
  elseif indminyb==length(yb)
    br=1;
  end
  y2=0; % by definition

  % fill in point3 trying clockwise from tl (either tl or tr)
  if tl==0
    x3=minxt;
    y3=yt(indminxt);
    tl=1;
  elseif tr==0
    x3=maxxt;
    y3=yt(indmaxxt);
    tr=1;
  else error('Error in assigning point 3')
  end

  % fill in point4 trying tr,br,bl
  if tr==0
    x4=maxxt;
    y4=yt(indmaxxt);
    tr=1;
  elseif br==0
    x4=maxxb;
    y4=yb(indmaxxb);
    br=1;
  elseif bl==0
    x4=minxb;
    y4=yb(indminxb);
```

```
    bl=1;
  else error('Error in assigning point 4')
  end

  % fill in point5 trying br,bl,middle
  if br==0
    x5=maxxb;
    y5=yb(indmaxxb);
    br=1;
  elseif bl==0
    x5=minxb;
    y5=yb(indminxb);
    bl=1;
  else % top middle
    lastind = round(length(xt)/2);
    x5=xt(lastind);
    y5=yt(lastind);
  end
  % Solution to exact fit over these 5 points (thanks, Mathematica!)
  e=-((-(x2*x3*x5*y1^2*(x2^2*y3*y4*(-(x4*y3) + x3*y4) + ...
y1^2*(-(x2^2*x3*y3) + x3*x4^2*y3 + x2^2*x4*y4 - x3^2*x4*y4))* ...
 (x2*y3 - x5*y3 - x2*y5 + x3*y5)) + ...
x2*x3*x4*y1^2*(x2*y3 - x4*y3 - x2*y4 + x3*y4)* ...
(x2^2*y3*y5*(-(x5*y3) + x3*y5) +  ...
y1^2*(-(x2^2*x3*y3) + x3*x5^2*y3 + x2^2*x5*y5 - x3^2*x5*y5)))/ ...
(x2^3*x3*x4*y1^3*y3*(x2*y3 - x4*y3 - x2*y4 + x3*y4)*y5* ...
(x3*y1 - x5*y1 + x5*y3 - x3*y5) +  ...
x2^3*x3*x5*y1^3*y3*y4*(x3*y1 - x4*y1 + x4*y3 - x3*y4)* ...
(-(x2*y3) + x5*y3 + x2*y5 - x3*y5)));
  c=-((-1 + e*y1)/y1^2);
  d=-((x2^2*(1 - e*y1)*y3*y4*(-(x4*y3) + x3*y4) + ...
y1^2*(x3*x4^2*y3 - x3^2*x4*y4 + ...
x2^2*(-(x3*y3) + x4*y4 + e*x3*y3*y4 - e*x4*y3*y4)))/ ...
(x2*x3*x4*y1^2*(x2*y3 - x4*y3 - x2*y4 + x3*y4)));
  a=(1 - d*x2)/x2^2;
  b=-((-1 + d*x3 + a*x3^2 + e*y3 + c*y3^2)/(x3*y3));
  lambda = [a b c d e];
end

end
if nargin==1
  auto = 1;
end

plot(xt,yt,'ro',xb,yb,'ro','EraseMode','none')
title('Model Stent Envelope')
if ~auto, pause, end    % Strike any key to continue.

Plothandle = plot(xt,yt,'y-',xb,yb,'y-','EraseMode','xor');

trace = 0;
tol = .0005;  % usu. .00005
options=foptions;
options(1)=trace;
options(2)=tol;
options(14)=3000;
lambda = fmins('fit_hyp',lambda,options);
if ~auto, pause, end

hold off
echo off
disp('Ax^2+Bxy+Cy^2+Dx+Ey')
disp(sprintf('%g %g %g %g %g',lambda(1),lambda(2),lambda(3),lambda(4),lambda(5)))

if lambda(2) == 0, lambda(2) = eps; end
ft = sqrt(lambda(1)^2+lambda(2)^2-2*lambda(1)*lambda(3)+lambda(3)^2);
```

```
mt1 = (-lambda(1)+lambda(3)+ft)/lambda(2);
mt2 = (-lambda(1)+lambda(3)-ft)/lambda(2);
if abs(mt1) < pi & abs(mt2) < pi
  if mt1 > 0 & mt2 > 0
    mt = min(mt1, mt2);
  else
    mt = max(mt1, mt2);
  end
else
  if abs(mt1) < abs(mt2)
    mt = mt1;
  else
    mt = mt2;
  end
end
theta = atan(mt);
l = sin(theta);
m = cos(theta);
a = lambda(1)*m^2+lambda(2)*l*m+lambda(3)*l^2;
c = lambda(1)*l^2-lambda(2)*l*m+lambda(3)*m^2;
d = lambda(4)*m+lambda(5)*l;
e = -lambda(4)*l+lambda(5)*m;

h = -d/(2*a);
k = -e/(2*c);
p2 = (-4-d^2/a-e^2/c)/(4*a);
q2 = (4*a*c+c*d^2+a*e^2)/(4*a*c^2);
disp(sprintf('theta = %g degrees', theta/pi*180))

figure(1)
clf
plot(xt, yt, 'ro', xb, yb, 'ro', xp, yp, 'yo')

% Rotation
xr1 =  xt * m + yt * l;
yr1 = -xt * l + yt * m;
xr2 =  xb * m + yb * l;
yr2 = -xb * l + yb * m;
xr3 =  xp * m + yp * l;
yr3 = -xp * l + yp * m;
figure(2)
plot(xr1, yr1, 'ro', xr2, yr2, 'ro', xr3, yr3, 'yo')

% Translation
xt1 = xr1 - h;
yt1 = yr1 - k;
xt2 = xr2 - h;
yt2 = yr2 - k;
xt3 = xr3 - h;
yt3 = yr3 - k;
figure(3)
xtt=linspace(min([xt1;xt2]),max([xt1;xt2]),100); ytt = sqrt(q2)*sqrt(1+(xtt/sqrt(p2)).^2);
ytb=-ytt;
plot(xt1, yt1, 'ro', xt2, yt2, 'ro', xt3, yt3, 'yo',xtt,ytt,'g.',xtt,ytb,'g.')

% Final normalization
% note: this does not change the data; it is only to make irregular horn-shaped
%       stents appear centered (when they should actually be out to one side)
hn = mean([min(xt3),max(xt3)]);
kn = mean([min(yt3),max(yt3)]);
xn1 = xt1 - hn;
yn1 = yt1 - kn;
xn2 = xt2 - hn;
yn2 = yt2 - kn;
xn3 = xt3 - hn;
yn3 = yt3 - kn;
```

```
% This determines the r^2 value of the fit
ytcalc = zeros(size(xt));
for j = 1:length(xt)
   ftemp = sqrt((lambda(5)+lambda(2)*xt(j))^2-
4*lambda(3)*(lambda(1)*xt(j)^2+lambda(4)*xt(j)-1));
   ytcalc(j) = (-lambda(5) - lambda(2)*xt(j) + ftemp) / (2*lambda(3));
end

ybcalc = zeros(size(xb));
for j = 1:length(xb)
   ftemp = sqrt((lambda(5)+lambda(2)*xb(j))^2-
4*lambda(3)*(lambda(1)*xb(j)^2+lambda(4)*xb(j)-1));
   ybcalc(j) = (-lambda(5) - lambda(2)*xb(j) - ftemp) / (2*lambda(3));
end

ytrue = [yt;yb];
ycalc = [ytcalc;ybcalc];
r = corrcoef(ytrue,ycalc); r = r(1,2);
disp(sprintf('The r^2 value is: %g',r^2))

% output results
nn = [6                    n2+4  n3+4; ...
     l                   m     theta; ...
     p2                   q2    0; ...
     h                   k     0; ...
     hn                   kn    0; ...
     -2*ones(length(xn1),1)  xt1   yt1; ...
     -ones(length(xn2),1)    xt2   yt2; ...
     [1:length(xn3)]'        xt3   yt3];
```

```
function [x,y] = getlin(fig,s)
%GETLIN Track mouse movement with rubberbanded line.
%           [X,Y] = GETLINE(FIG) tracks the movement of a mouse in
%           the figure FIG.
 %          Clay M. Thompson 1-28-93
%           Modified July 1997 James C. Squire

global Pt1 Pt2 hline fig ax

if nargin<1, fig = gcf; end

if nargin==2, % Process call-backs
  if strcmp(s,'motion'),
    if length(hline)>0,
      Pt2 = get(ax,'CurrentPoint'); Pt2 = Pt2(1,1:2);
      set(hline,'Xdata',[Pt1(1) Pt2(1)],'Ydata',[Pt1(2) Pt2(2)])
    end
  else
    error('Invalid call-back');
  end
  return
end

figure(fig), ax = gca;
c = [1 0 1];

% Create an invisible line to preallocate the xor line color.
handles = line(min(get(ax,'xlim'))*ones(1,2),min(get(ax,'ylim'))*ones(1,2),...
            'eraseMode','xor','linestyle','-','Color',c,'visible','off');

if any(get(ax,'view')~=[0 90]), error('GETLINE works only on 2-D plots'); end
curse = get(gcf,'pointer');
```

```
set(gcf,'pointer','crosshair');

btndown = get(gcf,'windowbuttondownfcn');
btnup = get(gcf,'windowbuttonupfcn');
btnmotion = get(gcf,'windowbuttonmotionfcn');
set(gcf,'windowbuttondownfcn','','windowbuttonupfcn','')

Pts = []; handles = []; done = 0; first = 1;
while ~done
  done = waitforbuttonpress;
  if gcf==fig,
    axes(ax) % Protect against user clicking in another axis
    Pt1 = get(ax,'CurrentPoint');
    Pt1 = Pt1(1,1:2);
    Pts = [Pts;Pt1];
    if ~strcmp(get(fig,'selectiontype'),'normal'),
      done = 1;
      hline = [];
    else
      hline = line(Pt1(1)*ones(1,2),Pt1(2)*ones(1,2),'eraseMode','xor', ...
              'linestyle','-','Color',c);
      if first,
        set(fig,'WindowButtonMotionFcn','getline(gcf,"motion")')
        first = 0;
      end
      handles = [handles hline];
    end
    drawnow
  end
end
delete(handles)
set(fig,'pointer',curse);
clear global Pt1 Pt2 hline fig ax
set(gcf,'windowbuttondownfcn',btndown,'windowbuttonupfcn',btnup, ...
        'windowbuttonmotionfcn',btnmotion)
if nargout < 2, x = Pts; return, end
if ~isempty(Pts), x = Pts(:,1); y = Pts(:,2); else x = []; y = []; end

function [rn,scale]=get_dat(x,map,scale)
%GET_DAT Gets edge modelling data from an image.
%             [rn,scale] = get_dat(x,map,scale)
%             Returns a matrix of input points centered
%             Input first top half, then bottom half, then the key data points
%  If scale is provided as input, does not ask for user to provide reference
%  If scale is returned, may use this in next get_dat to eliminate ref errors.
%             Returns
%             [2   4   6]   2 is index of up upper stent envelope, 6 is index of data points
%             [-2  x1  y1]  -2 also signifies upper envelope
%             [-2  x2  y2]
%             [-1  x1  y1]  -1 is lower stent envelope
%             [-1  x2  y2]
%             [1   x1  y1]  these are point numbers
%             [2   x2  y2]
%
%             James C. Squire   July 1997
%       Modified September 1998 to include reference distance

imshow(x,map)

[txx,tyy] = getlin;
nx = length(txx);
disp(setstr(7));
disp(sprintf('%g points collected',nx))

[bxx,byy] = getlin;
nt = length(bxx);
```

```
disp(setstr(7));
disp(sprintf('%g points collected',nt))

[pxx,pyy] = getpts;
np = length(pxx);
disp(setstr(7));
disp(sprintf('%g points collected',np-1))

if nargin==2
  disp('draw line over reference length')
  [refx,refy]=getlin
  ll = norm([diff(refx),diff(refy)]);
  disp(sprintf('Line length is %g pixels',ll));
  scale = input('Enter length of line in mm -> ')/ll;
end

% Scale in real units and translate so just touching Quadrant 1 boundary
in = [-2*ones(nx,1);  -ones(nt,1);  [1:np]' ];
tyy=-tyy; byy=-byy; pyy=-pyy; % flip up/down: screen coords vs. matrix coords
xoffset = min([txx;bxx])*scale;
yoffset = min([tyy;byy])*scale;
xx = [txx; bxx; pxx]*scale - xoffset;
yy = [tyy; byy; pyy]*scale - yoffset;

% Store them
n1 = 2;
n2 = nx + n1;
n3 = nt + n2;
rn = [n1 n2 n3;  in xx yy];
rn(length(rn),:) = [];  % throw out the last row given by the right button click
hold off


function dn=out_dat(nvert,nhoriz,nn)

%OUT_DAT calculates a list of quadrilateral patches to form a hyperboloid projection
%     dn=out_dat(nvert,nhoriz,nn)
%
%     See fit_hypm for form of nn.
%     nvert, nhoriz describe the number of vertical and horizontal patches.
%
%     It returns dn =
%     [1  x11  y11  x12  y12  x13  y13  x14  y14 ett ezz ezt d(ett)/dt d(ezz)/dt d(ezt)/dt]
%     [2  x21  y21  x22  y22  x23  y23  x24  y24 ett ezz ezt d(ett)/dt d(ezz)/dt d(ezt)/dt]
%     [n+1 nvert nhoriz 0  0    0    0    0    0        0              0]
%     vertices are labelled 1 2 in each patch j
%                           3 4
%
%
%     James C. Squire   August 1997
%     modified August 1998

DEBUG = 0;

p2 = nn(3,1);
q = sqrt(nn(3,2));
xpoints = nn(nn(1,3):size(nn,1),2);
ypoints = nn(nn(1,3):size(nn,1),3);
xmin = min(xpoints);
xmax = max(xpoints);
Npatch = nvert*nhoriz;
clf
% axis([-1 1 -1 1])
dn = zeros(Npatch+1,15);
dn(:,1) = [1:Npatch+1]';
```

```
for j=1:Npatch

  jrow = nvert/2 - rem(j-1,nvert);
  jcol = ceil(j/nvert);

  if rem(j-1,nvert) < nvert/2
    half = 't'; trow = jrow;
  elseif rem(j-1,nvert) >= nvert/2
    half = 'b'; trow = 1 - jrow;
  else disp('Trouble in out_dat point 1')
  end

  x1 = xmin + (xmax-xmin)/nhoriz*(jcol-1);
  x2 = xmin + (xmax-xmin)/nhoriz*jcol;
  x3 = x2;
  x4 = x1;
  yt1 = q*sqrt(1+(x1^2/p2))*sin(pi*trow/nvert);
  yt2 = q*sqrt(1+(x2^2/p2))*sin(pi*trow/nvert);
  yt3 = q*sqrt(1+(x3^2/p2))*sin(pi*(trow-1)/nvert);
  yt4 = q*sqrt(1+(x4^2/p2))*sin(pi*(trow-1)/nvert);

  if half == 't'
    y1 =  yt1;  y2 = yt2;  y3 = yt3;  y4 = yt4;
  elseif half == 'b'
    y1 = -yt1; y2 = -yt2; y3 = -yt3; y4 = -yt4;
  end

  dn(j,2) = x1; dn(j,3) = y1; dn(j,4) = x2; dn(j,5) = y2;
  dn(j,6) = x3; dn(j,7) = y3; dn(j,8) = x4; dn(j,9) = y4;

  patch([x1,x2,x3,x4],[y1,y2,y3,y4],(1-yt1/.8)*128)
end

dn(Npatch+1, 2) = nvert;
dn(Npatch+1, 3) = nhoriz;

if DEBUG
  hold on
  plot(xpoints,ypoints,'wo')
  while 1
    [xx,yy] = getlin;
    zz=zcalc(xx,yy,p2,q,DEBUG);
    dx = diff(xx)
    dy = diff(yy)
    dz = diff(zz)
    ds = norm([dx dy dz]);
    disp(sprintf('x1 = %g   y1 = %g  z1 = %g',xx(1),yy(1),zz(1)))
    disp(sprintf('x2 = %g   y2 = %g  z2 = %g',xx(2),yy(2),zz(2)))
    disp(sprintf('dx = %g   dy = %g  dz = %g',dx,dy,dz))
    disp(sprintf('Total distance separation is %g',ds))
    if (input('Again? ','s')) == 'n',break,end
  end
  hold off
end


function show(filename,skip,action)
%SHOW   Displays results of stent data
%          function show(filename,skip)
%          filename holds data in variables d0,d2,d4,d6, etc.
%          skip is the jump between variable names (eg 2 above)

%          James Squire
%          September 1997

% Information regarding the movie play status will be held in
```

```
% the axis user data according to the following table:
play= 1;
stop=-1;

if nargin==2,
   action='initialize';
else
  action = 'display';
end

if strcmp(action,'initialize'),

   figNumber=figure( ...
      'Name','Endovascular Stent Strain', ...
      'NumberTitle','off', ...
            'Visible','off', ...
            'BackingStore','off', ...
            'Position', get(0,'screensize'));
            %'Colormap','hsv

   axes( ...
      'Units','normalized', ...
      'Position',[0.05 0.05 0.82 0.90], ...
      'Visible','on', ...
            'NextPlot','replace');

   axis([-1 1 -1 1]);
   set(gca,'userdata',0)

   %====================================
   % Information for all buttons
   %labelColor=[0.8 0.8 0.8];
   yInitPos=0.90;
   xPos=0.912;
   btnWid=0.079;
   btnHt=0.06;
   % Spacing between the button and the next command's label
   spacing=0.05;

   %====================================
   % The Console frame
   frmBorder=0.01;
   yPos=0;
   frmPos=[xPos-frmBorder yPos btnWid+2*frmBorder 1];
   h=uicontrol( ...
      'Style','frame', ...
      'Units','normalized', ...
      'Position',frmPos);
            %'BackgroundColor',[0.5 0.5 0.5]

   %====================================
   % The Tensor Component popup button
   btnNumber=1;
   yPos=0.95-(btnNumber-1)*(btnHt+spacing);
   textStr='Component';
   popupStr=reshape(' Axial     Circumfr. Torsion   All       None     ',10,5)';

   % Generic button information
   btnPos1=[xPos yPos-spacing+btnHt/1.5 btnWid btnHt/2];
   btnPos2=[xPos yPos-spacing btnWid btnHt/2];
   popupHndlc=uicontrol( ...
      'Style','text', ...
      'Units','normalized', ...
      'Position',btnPos1, ...
      'String',textStr);
   btnPos=[xPos yPos-spacing btnWid btnHt/2];
```

```
popupHndlc=uicontrol( ...
   'Style','popup', ...
   'Units','normalized', ...
   'Position',btnPos2, ...
   'String',popupStr);

%====================================
% The Differential popup button
btnNumber=2;
yPos=0.95-(btnNumber-1)*(btnHt+spacing);
textStr='Differential?';
popupStr=reshape(' No  Yes',4,2)';

% Generic button information
btnPos1=[xPos yPos-spacing+btnHt/1.5 btnWid btnHt/2];
btnPos2=[xPos yPos-spacing btnWid btnHt/2];
popupHndld=uicontrol( ...
   'Style','text', ...
   'Units','normalized', ...
   'Position',btnPos1, ...
   'String',textStr);
btnPos=[xPos yPos-spacing btnWid btnHt/2];
popupHndld=uicontrol( ...
   'Style','popup', ...
   'Units','normalized', ...
   'Position',btnPos2, ...
   'String',popupStr);

%====================================
% The Frame popup button
btnNumber=3;
yPos=0.95-(btnNumber-1)*(btnHt+spacing);
textStr='Frame';
eval(['load ' filename]);
num_data_sets = 0;
while exist(sprintf('d%g',num_data_sets))
  num_data_sets = num_data_sets + skip;
end
num_data_sets = num_data_sets - skip;

popupStr=[];
for i=0:skip:num_data_sets
  popupStr=[popupStr;sprintf('%3g',i)];
end

% Generic button information
btnPos1=[xPos yPos-spacing+btnHt/1.5 btnWid btnHt/2];
btnPos2=[xPos yPos-spacing btnWid btnHt/2];
popupHndlf=uicontrol( ...
   'Style','text', ...
   'Units','normalized', ...
   'Position',btnPos1, ...
   'String',textStr);
btnPos=[xPos yPos-spacing btnWid btnHt/2];
popupHndlf=uicontrol( ...
   'Style','popup', ...
   'Units','normalized', ...
   'Position',btnPos2, ...
   'String',popupStr);

%====================================
% The Movie popup button
btnNumber=4;
yPos=0.95-(btnNumber-1)*(btnHt+spacing);
textStr='Movie?';
popupStr=reshape(' No  Yes',4,2)';
```

```
% Generic button information
btnPos1=[xPos yPos-spacing+btnHt/1.5 btnWid btnHt/2];
btnPos2=[xPos yPos-spacing btnWid btnHt/2];
popupHndlm=uicontrol( ...
   'Style','text', ...
   'Units','normalized', ...
   'Position',btnPos1, ...
   'String',textStr);
btnPos=[xPos yPos-spacing btnWid btnHt/2];
popupHndlm=uicontrol( ...
   'Style','popup', ...
   'Units','normalized', ...
   'Position',btnPos2, ...
   'String',popupStr);

%====================================
% The Display button
btnNumber=5;
yPos=0.95-(btnNumber-1)*(btnHt+spacing);
labelStr='Display';
cmdStr='display';
callbackStr=['show('" filename "',' num2str(skip) ',"display")'];

% Generic button information
btnPos=[xPos yPos-spacing btnWid btnHt];
startHndl=uicontrol( ...
   'Style','pushbutton', ...
   'Units','normalized', ...
   'Position',btnPos, ...
   'String',labelStr, ...
   'Interruptible','yes', ...
   'Callback',callbackStr);

%====================================
% The Interrupt button
btnNumber=6;
yPos=0.95-(btnNumber-1)*(btnHt+spacing);
labelStr='Interrupt';
% Setting userdata to -1 (=interrupt) will stop the movie.
callbackStr='set(gca,"Userdata",-1)';

% Generic button information
btnPos=[xPos yPos-spacing btnWid btnHt];
stopHndl=uicontrol( ...
   'Style','pushbutton', ...
   'Units','normalized', ...
   'Position',btnPos, ...
   'Enable','off', ...
   'String',labelStr, ...
   'Callback',callbackStr);

%====================================
% The Close button
labelStr='Close';
callbackStr='close(gcf)';
closeHndl=uicontrol( ...
   'Style','push', ...
   'Units','normalized', ...
   'Position',[xPos 0.05 btnWid 0.10], ...
   'String',labelStr, ...
   'Callback',callbackStr);

% Uncover the figure

hndlCB = 0; % Since no colorbar yet
```

```
   axispos = get(gca,'position');
   hndlList=[startHndl stopHndl closeHndl popupHndlc popupHndld popupHndlf
popupHndlm hndlCB axispos];
   set(figNumber,'Visible','on', ...
               'UserData',hndlList);
   figure(figNumber);

elseif strcmp(action,'display'),
   axHndl=gca;
   figNumber=gcf;
   hndlList=get(figNumber,'UserData');
   startHndl=hndlList(1);
   stopHndl=hndlList(2);
   closeHndl=hndlList(3);
   popupHndlc=hndlList(4);
   popupHndld=hndlList(5);
   popupHndlf=hndlList(6);
   popupHndlm=hndlList(7);
   hndlCB = hndlList(8);

   % ====== Display data
   component    = get(popupHndlc,'Value');
   differential = get(popupHndld,'Value');
   frame        = get(popupHndlf,'Value');
   movie        = get(popupHndlm,'Value');

   if component <= 3 & movie == 1
     show1(filename,skip)
   elseif component <= 3 & movie ==2
     show2(filename,skip)
   elseif component == 4 & movie == 1
     show3(filename,skip)
   elseif component == 4 & movie == 2
     show3(filename,skip)
   elseif component == 5 & movie == 1
     show5(filename,skip)
   elseif component == 5 & movie == 2
     show6(filename,skip)
   else
     error('internal error-invalid component/movie in show.m')
   end

end;    % if strcmp(action, ...


function show1(filename,skip)

% initialize graphics
hndlList=get(gcf,'UserData');

startHndl=hndlList(1);
stopHndl=hndlList(2);
closeHndl=hndlList(3);
popupHndlc=hndlList(4);
popupHndld=hndlList(5);
popupHndlf=hndlList(6);
popupHndlm=hndlList(7);
hndlCB = hndlList(8);
axispos = hndlList(9:12);

component    = get(popupHndlc,'Value');
differential = get(popupHndld,'Value');
frame        = get(popupHndlf,'Value');

set([startHndl closeHndl ],'Enable','off');
set(stopHndl,'Enable','on');
```

```
% initalize data
load(filename)
dn = eval(['d' num2str((frame-1)*skip)]);


nvert  = dn(size(dn,1),2);
nhoriz = dn(size(dn,1),3);
nblocks = nvert*nhoriz;
if component == 1 & differential == 1 % axial
   y = dn(1:nblocks,11);
elseif component == 1 & differential == 2 % axial difference
   y = dn(1:nblocks,14);
elseif component == 2 & differential == 1 % circum.
   y = dn(1:nblocks,10);
elseif component == 2 & differential == 2 % circum.  difference
   y = dn(1:nblocks,13);
elseif component == 3 & differential == 1 % torsion
   y = dn(1:nblocks,12);
elseif component == 3 & differential == 2 % torsion difference
   y = dn(1:nblocks,15);
else
   error('Error in show1.m; incorrectly called')
end

cla
set(gca,'position',axispos)
axis('auto')
axis('equal')
view(0,90)
grid off
colormap(jet(200));
if hndlCB~=0         % colorbar present
   close(hndlCB);
   hndlCB=0;
end

xmin = dn(1,2);
xmax = dn(nblocks,8);
nsub = mean([xmin xmax]);

hold on
for j=1:nblocks
   fill([dn(j,2),dn(j,4),dn(j,6),dn(j,8)]-nsub,[dn(j,3),dn(j,5),dn(j,7),dn(j,9)],y(j))
end
hold off
cmin = min(y);
cmax = max(y);
if cmin < 0 & cmax < 0
   cmax = 0;
elseif cmin > 0 & cmax > 0
   cmin = 0;
elseif cmin==0 & cmax == 0
   cmax = cmax + eps;
end
caxis([cmin cmax])

hndlList(8)=colorbar('v');
set(gcf,'userdata',hndlList);

set([startHndl closeHndl],'Enable','on');
set(stopHndl,'Enable','off');

end
```

```
function show2(filename,skip)

% initialize graphics
hndlMainWin = gca;
hndlList=get(gcf,'UserData');

startHndl=hndlList(1);
stopHndl=hndlList(2);
closeHndl=hndlList(3);
popupHndlc=hndlList(4);
popupHndld=hndlList(5);
popupHndlf=hndlList(6);
popupHndlm=hndlList(7);
hndlCB = hndlList(8);
axispos = hndlList(9:12);

component    = get(popupHndlc,'Value');
differential = get(popupHndld,'Value');

set([startHndl closeHndl ],'Enable','off');
set(stopHndl,'Enable','on');

% initalize data
load(filename)
num_data_sets = 0;
while exist(sprintf('d%g',num_data_sets))
  num_data_sets = num_data_sets + skip;
end
num_data_sets = num_data_sets/skip;
if component == 1 & differential == 1 % axial
  keycol=11;
elseif component == 1 & differential == 2 % axial difference
  keycol=14;
elseif component == 2 & differential == 1 % circum.
  keycol=10;
elseif component == 2 & differential == 2 % circum.  difference
  keycol=13;
elseif component == 3 & differential == 1 % torsion
  keycol=12;
elseif component == 3 & differential == 2 % torsion difference
  keycol=15;
else
  error('Error in show1.m; incorrectly called')
end

% find the caxis,x,range (so colorbar and scale do not change);
% y is set to make it square with x (y always smaller for thin stent)
minc =  99999;
maxc = -99999;
widest = 0;
for i=0:skip:(num_data_sets-1)*skip;
  dn = eval(['d' num2str(i)]);
  nblocks = size(dn,1)-1;
  if min(dn(1:nblocks,keycol)) < minc
    minc = min(dn(1:nblocks,keycol));
  end
  if max(dn(1:nblocks,keycol)) > maxc
    maxc = max(dn(1:nblocks,keycol));
  end
  if (dn(nblocks,8) - dn(1,2)) > widest
    widest = dn(nblocks,8) - dn(1,2);
  end
end
if minc < 0 & maxc < 0
  maxc = 0;
elseif minc > 0 & maxc > 0
```

```
  minc = 0;
elseif minc==0 & maxc == 0
  maxc = maxc + eps;
end
caxis([minc maxc])
axlim = widest/2;

% do the drawing
first = 1;
for i=0:skip:(num_data_sets-1)*skip
  dn = eval(['d' num2str(i)]);
  view(0,90)
  grid off
  colormap(jet(200));
  hndlList=get(gcf,'UserData');
  hndlCB = hndlList(8);
  cla
  set(gca,'xlim',[-axlim axlim]);
  set(gca,'ylim',[-axlim axlim]);
  axispos = hndlList(9:12);
  if hndlCB~=0          % colorbar present
    close(hndlCB);
    hndlCB=0;
    set(gca,'position',axispos)
  end
  xmin = dn(1,2);
  xmax = dn(nblocks,8);
  nsub = mean([xmin xmax]);

  hold on
  caxis([minc maxc])
  for j=1:nblocks
    fill([dn(j,2),dn(j,4),dn(j,6),dn(j,8)]-nsub,[dn(j,3),dn(j,5),dn(j,7),dn(j,9)],dn(j,keycol))
  end
  hold off
  hndlList(8)=colorbar('v');
  set(gcf,'userdata',hndlList);

  if first
    m = moviein(num_data_sets);
    first = 0;
  end
  axes(hndlMainWin)
  m(:,i/skip+1) = getframe;
  if get(gca,'userdata')==-1
    break
  end
end

if get(gca,'userdata')==0
  movie(m,15,2.5);
else
  set(gca,'userdata',0)
end
caxis('auto')

show1(filename,skip);
```

function show3(filename,skip)

```
% initialize graphics
hndlList=get(gcf,'UserData');

startHndl=hndlList(1);
stopHndl=hndlList(2);
```

```
closeHndl=hndlList(3);
popupHndlc=hndlList(4);
popupHndld=hndlList(5);
popupHndlf=hndlList(6);
popupHndlm=hndlList(7);
hndlCB = hndlList(8);
axispos = hndlList(9:12);

differential = get(popupHndld,'Value');
frame        = get(popupHndlf,'Value');

%set([startHndl closeHndl ],'Enable','off');
set(stopHndl,'Enable','on');

% initalize data
load(filename)
dn = eval(['d' num2str((frame-1)*skip)]);

nvert  = dn(size(dn,1),2);
nhoriz = dn(size(dn,1),3);
nblocks = nvert*nhoriz;
data = zeros(nhoriz,3);   % data of form [circum axial torsion]
if differential == 1 % regular
  for i=1:nhoriz
    data(i,:) = mean(dn((i-1)*nvert+1:i*nvert,10:12));
  end
elseif differential == 2
  for i=1:nhoriz
    data(i,:) = mean(dn((i-1)*nvert+1:i*nvert,13:15));
  end
end
xmin = dn(1,2);
xmax = dn(nblocks,8);
xlim = (xmax-xmin)/2;
datax = linspace(-xlim,xlim,nhoriz);

if hndlCB~=0         % colorbar present
  close(hndlCB);
  hndlList(8)=0;
end
cla
set(gca,'position',axispos)
axis('normal')
axis('auto')
view(0,90)
hold on

plot(datax,data)
grid on
hndlList(8) = legend('Circumf.','Axial','Torsion',-1);
set(gcf,'userdata',hndlList);

set(startHndl,closeHndl,'Enable','on');
set(stopHndl,'Enable','off');

end
```

function show5(filename,skip)

```
% initialize graphics
hndlList=get(gcf,'UserData');
startHndl=hndlList(1);
stopHndl=hndlList(2);
closeHndl=hndlList(3);
popupHndlf=hndlList(6);
```

```
hndlCB = hndlList(8);
axispos = hndlList(9:12);
frame       = get(popupHndlf,'Value');

set([startHndl closeHndl ],'Enable','off');
set(stopHndl,'Enable','on');

% initalize data
load(filename)
dn = eval(['d' num2str((frame-1)*skip)]);
d0 = eval('d0');
nvert  = dn(size(dn,1),2);
nhoriz = dn(size(dn,1),3);
nblocks = nvert*nhoriz;

cla
set(gca,'position',axispos)
if hndlCB~=0          % colorbar present; get rid of it
  close(hndlCB);
  hndlList(8) = 0;
  set(gcf,'userdata',hndlList);
end
set(gca,'xlimmode','auto')
set(gca,'aspectratio',[NaN NaN])
grid on
hold on

xnmin = dn(1,2);              xnmax = dn(nblocks,8);
x0min = d0(1,2);              x0max = d0(nblocks,8);
xnscale = xnmax-xnmin;
x0scale = x0max-x0min;
ynlist = zeros(nhoriz+1,1);
y0list = zeros(nhoriz+1,1);
for i=0:nhoriz-1
  ynlist(i+1)=dn(i*nvert+1,3);
  y0list(i+1)=d0(i*nvert+1,3);
end
ynlist(nhoriz+1) = dn(nblocks-nvert+1,5);
y0list(nhoriz+1) = d0(nblocks-nvert+1,5);

[z0,y0,x0] = cylinder(y0list,25);
x0 = x0*x0scale;  x0 = x0-x0scale/2;
surfl(x0',y0',z0')

[zn,yn,xn] = cylinder(ynlist,25);
xn(:,18:19) = NaN*zeros(nhoriz+1,2);
xn = xn*xnscale;  xn = xn-xnscale/2;
hndlSurf=surfl(xn',yn',zn');
set(hndlSurf,'edgecolor','none')
set(hndlSurf,'facecolor','interp')

view(340,30)
colormap(bone(200))
axlim = diff(get(gca,'xlim'))/2;
set(gca,'ylim',[-axlim axlim]);
set(gca,'zlim',[-axlim axlim]);
hold off

set([startHndl closeHndl],'Enable','on');
set(stopHndl,'Enable','off');

end
```

function show6(filename,skip)

```
% initialize graphics
hndlList=get(gcf,'UserData');
startHndl=hndlList(1);
stopHndl=hndlList(2);
closeHndl=hndlList(3);
hndlCB = hndlList(8);
axispos = hndlList(9:12);

set([startHndl closeHndl ],'Enable','off');
set(stopHndl,'Enable','on');

% initalize data
load(filename)
num_data_sets = 0;
while exist(sprintf('d%g',num_data_sets))
  num_data_sets = num_data_sets + skip;
end
num_data_sets = num_data_sets/skip;


% find the movie's x axis limits range (so axes do not change);
widest = 0;
for i=0:skip:(num_data_sets-1)*skip;
  dn = eval(['d' num2str(i)]);
  nvert  = dn(size(dn,1),2);
  nhoriz = dn(size(dn,1),3);
  nblocks = nvert*nhoriz;
  if (dn(nblocks,8) - dn(1,2)) > widest
    widest = dn(nblocks,8) - dn(1,2);
  end
end
axlim = widest/2;


% do the drawing
first = 1;
for i=0:skip:(num_data_sets-1)*skip
  dn = eval(['d' num2str(i)]);
  d0 = eval('d0');
  cla
  set(gca,'position',axispos)
  if hndlCB~=0          % colorbar present; get rid of it
    close(hndlCB);
    hndlCB = 0;
    hndlList(8) = 0;
    set(gcf,'userdata',hndlList);
  end
  axis('auto')
  hold on

  xnmin = dn(1,2);              xnmax = dn(nblocks,8);
  x0min = d0(1,2);              x0max = d0(nblocks,8);
  xnscale = xnmax-xnmin;
  x0scale = x0max-x0min;
  ynlist = zeros(nhoriz+1,1);
  y0list = zeros(nhoriz+1,1);
  for j=0:nhoriz-1
    ynlist(j+1)=dn(j*nvert+1,3);
    y0list(j+1)=d0(j*nvert+1,3);
  end
  ynlist(nhoriz+1) = dn(nblocks-nvert+1,5);
  y0list(nhoriz+1) = d0(nblocks-nvert+1,5);
  y0list=y0list-100*eps;  % so when both are shown together...

  [z0,y0,x0] = cylinder(y0list,25);
  x0 = x0*x0scale;  x0 = x0-x0scale/2;
```

```
  surfl(x0',y0',z0')

  [zn,yn,xn] = cylinder(ynlist,25);
  xn(:,18:19) = NaN*zeros(nhoriz+1,2);
  xn = xn*xnscale;  xn = xn-xnscale/2;
  hndlSurf=surfl(xn',yn',zn');
  set(hndlSurf,'edgecolor','none')
  set(hndlSurf,'facecolor','interp')

  view(340,30)
  colormap(bone(200))
  set(gca,'xlim',[-axlim axlim]);
  set(gca,'ylim',[-axlim axlim]);
  set(gca,'zlim',[-axlim axlim]);
  grid('on')
  hold off

  if first
    m = moviein(num_data_sets);
    first = 0;
  end
  if get(gca,'userdata')==-1
    break
  end
  m(:,i/skip+1) = getframe;

end
if get(gca,'userdata')==0
  movie(m,20,1.5);
else
  set(gca,'userdata',0)
end

show5(filename,skip)


function zlist=zcalc(xlist,ylist,p2,q,debug)

%ZCALC  finds the z value of a hyperbola (part of thesis2)
%            zlist=zcalc(xlist,p,q,debug)
%
%      set debug~0 for diagnostic information
%            See get_data for form of rn.
%            This assumes a hyperbola of form (y/q)^2 - (x/p)^2 = 1
%
%
%            James C. Squire   August 1997

debug=1;
rlist = sqrt(q^2*(1+(xlist.^2/p2)));
zlist = sqrt(rlist.^2 - ylist.^2);
tindex = find(imag(zlist));
if debug
  for j=1:length(tindex)
    disp(' ')
    disp(sprintf('Warning: point #%g passed to zcalc outside model',tindex(j)))
  end
end
zlist(tindex) = zeros(size(tindex));
```

APPENDEX B Evan's blue staining protocol

Materials

- Animals
- Standard surgical pack plus arteriotomy scissors, stent insertion kit
- Endoinflator
- Stents mounted on balloon catheters
- 5% Evan's blue, 5 ml per rabbit, e.g.
    - 50 ml lactated Ringer's
    - 2.5 g Evan's blue in crystalline form
    - stir 15 minutes at 50°C
    - filter 0.5 μm under vacuum
- 4% paraformaldehyde in individual transport bottles
- Lactated Ringer's solution for perfusion

Staining Procedure

Note: No control necessary (area distal to stent is built-in control)

- Expand stent without predilating
- Wait 30 minutes
- Perfuse w/ 5% Evan's Blue (binds to albumin & stains basement membrane) at 5ml for 4 kg rabbit
- Wait 45 minutes (shorter than 30 stain is inadequate, longer than 60 stain begins to diffuse into all tissue)
- Pressure perfuse animal w/ 2 liters lactated Ringer's (animal will die during this)
- Fix *in situ* by perfusing with fixative (4% paraformaldehyde, not MFK)
- Excise artery with long distal tail to identify and transport to histological area. Do not wait over 12 hours to image since Evan's Blue is slightly soluble in water.

Imaging procedure

- Open artery longitudinally using iris scissors while holding artery at point away from stented region
- Remove stent and pin onto paraffin block
- Image without cover slip (must use a low-power microscope with long field of focus to do this. Slight folds in tissue prevent standard microscope from focusing over entire field.
- Throw the sample away. *Do not try mount*. The dehydrating process prior to mounting will substantially alter the deposition of Evan's Blue.

APPENDEX C Intrastrut strain analysis code

The code used to determine the intrastrut strain is listed below. The code is written in Matlab 5.3 programming language by Mathworks.

C.1 Analysis procedures summary

The procedures are listed below in the order in which they are presented in this thesis.

Show2D determines the surface strain in the simplified flat model of the stent.

Show3D does the same as the above for the more complex three-dimensional model.

xyz_pos is called by the above main functions to solve the membrane equation.

Solve_stent is a wrapper function and calls the component functions below to determine the three-dimensional location of the membrane-modeled artery, stent, and balloon.

Get2DBoundary defines the intrastrut boundary of a given stent geometry when the stent is "unrolled" onto a planar surface.

Wrap takes the planar boundaries computed above and wraps them onto a cylinder in three dimensional space.

Widen takes the inner strut boundary and the thickness of the strut and returns the outside boundary of the strut

STStraightBoundaries determines the vertex locations of a straight-edged slotted tube stent in three dimensional space.

FillMatrixBorder creates a matrix describing strut locations and artery placement given the vectors describing the strut boundaries.

SolveMatrixInterior solves the membrane equations.

CreateArteryMesh creates a series of matricies that can be used with the built-in function surf to view the artery surface in three dimensions.

CreateBalloonMesh creates a series of matricies that can be used with the built-in function surf to view the balloon surface in three dimensions.

C.2 Intrastrut strain code

```
function Show2D
% SHOW2D Determines xyz strains in tissue by a flat slotted tube stent
%
% Nov 95   James C. Squire
% updated January 2000

% [R0 R1 Width0 Width1 Len0 Len1]  = [0.9 1.5 0.9896 1.6493 2.9872 2.68]
for ST

% input data
disp(' ')
disp(' ')
disp('^ direction of blood flow ^')
disp(' ')
disp('         a')
disp(' ')
disp('    b        b"')
disp(' ')
disp('         a"')
disp(' ')

elem    = 15;
Nl      = 1000;  % large to approximate flat surface
sthick  = .1;    % strut thickness
iRadius = 0.9;
fRadius = 1.5;
iheight = 2.25;
iwidth  = .9425;
fheight = 1.87;
fwidth  = 1.57;

% calculate

itemp1 = iRadius/cos(pi/(2*Nl));
itemp2 = itemp1/cos(pi/Nl);
idepth = -itemp1/itemp2*(itemp2-itemp1); % depth should be negative (down)
ftemp1 = fRadius/cos(pi/(2*Nl));
ftemp2 = ftemp1/cos(pi/Nl);
fdepth = -ftemp1/ftemp2*(ftemp2-ftemp1);
[xi,yi,zi]=xyz_pos(elem,iwidth,iheight,idepth,iRadius);
[xf,yf,zf]=xyz_pos(elem,fwidth,fheight,fdepth,fRadius);
[n1,n2]=xyz_str(elem,xi,yi,zi,xf,yf,zf);
nt = sqrt(n1.^2+n2.^2);

% balloon
legdrop = sthick/cos(pi/(2*Nl));
xbi=ones(elem,1)*linspace(-iwidth,iwidth,elem);
xbf=ones(elem,1)*linspace(-fwidth,fwidth,elem);
ybi=linspace(-iheight,iheight,elem)'*ones(1,elem);
ybf=linspace(-fheight,fheight,elem)'*ones(1,elem);
% balloon is cylinder x^2 + (z-k)^2 = R^2
ballzi = -iRadius/cos(pi/(2*Nl)) + sqrt(iRadius^2 - xbi.^2); % global balloon
height over
ballzf = -fRadius/cos(pi/(2*Nl)) + sqrt(fRadius^2 - xbf.^2); %   rectangular
matrix
```

```
ballzis = -iRadius/cos(pi/(2*Nl)) + sqrt(iRadius^2 - xi.^2); % global balloon
height over
ballzfs = -fRadius/cos(pi/(2*Nl)) + sqrt(fRadius^2 - xf.^2); %   stent cell matrix
balldi = zi-legdrop-ballzis;        % distance from balloon to artery
balldf = zf-legdrop-ballzfs;
%disp(sprintf('legdrop: %g',legdrop))
%disp(sprintf('offset: %g',-iRadius/cos(pi/(2*Nl))))

% display
a1=min(min(n1));
b1=max(max(n1));
a2=min(min(n2));
b2=max(max(n2));
n2=(n2-(a2+b2)/2)*((b1-a1)/(b2-a2));
n2disp=n2+(a2+b2)/2;
n2calc=n2*.82+(a1+b1)/2;

figure(1)
surf(yi,xi,zi,n1)
view(2)
axis('equal')
%str1='\fontname{Arial}\fontsize{18}\epsilon_{\theta\theta}\fontsize{14} strain
component';
%title(str1)
%xlabel('\fontsize{12}\bfcircumferential distance (mm)')
%ylabel('\fontsize{12}\bfaxial distance(mm)')
if max(max(n1))-min(min(n1)) < 0.000001
  caxis([0 1])
end
colormap(jet(255))
h=colorbar;
%set(h,'position',[0.8321    0.1690    0.0571    0.7024])
set(gcf,'renderer','painters')

figure(2)
surf(yi,xi,zi,n1)
view(2)
axis('equal')
str1='\fontname{Arial}\fontsize{18}\epsilon_{\theta\theta}\fontsize{14} strain
component';
%title(str1)
%xlabel('\fontsize{12}\bfcircumferential distance (mm)')
%ylabel('\fontsize{12}\bfaxial distance(mm)')
if max(max(n1))-min(min(n1)) < 0.000001
  caxis([0 1])
end
%colormap(jet(255))
%h=colorbar;
%set(h,'position',[0.8321    0.1690    0.0571    0.7024])
set(gcf,'renderer','painters')

figure(3)
surf(yi,xi,zi,n2disp)
view(2)
axis('equal')
%str1='\fontname{Arial}\fontsize{18}\epsilon_{zz}\fontsize{14} strain
component';
%title(str1)
%xlabel('\fontsize{12}\bfcircumferential distance (mm)')
```

```
%ylabel('\fontsize{12}\bfaxial distance(mm)')
if max(max(n2disp))-min(min(n2disp)) < 0.000001
  caxis([-0.25 0.25])
end
axis('off')
%colormap(jet(255))
%h=colorbar;
%set(h,'position',[0.8321    0.1690    0.0571    0.7024])
set(gcf,'renderer','painters')

%figure(3)
%n3=sqrt(n1.^2+n2calc.^2);
%surf(xi,yi,zi,n3)
%view(2)
%axis('equal')
%if max(max(n3))-min(min(n3)) < 0.000001
%   caxis([0 1])
%end
%colorbar
```

function Show3D

```
% SHOW2D Determines xyz strains in tissue by a flat slotted tube stent
%
% Nov 95   James C. Squire
% updated January 2000

% [R0 R1 Width0 Width1 Len0 Len1]  = [0.9 1.5 0.9896 1.6493 2.9872 2.68]
for ST

% input data
disp(' ')
disp(' ')
disp('^ direction of blood flow ^')
disp(' ')
disp('         a')
disp(' ')
disp('    b        b"')
disp(' ')
disp('         a"')
disp(' ')

elem    = 15;
Nl      = 6;  % large to approximate flat surface
sthick  = .1;    % strut thickness
iRadius = 0.9;
fRadius = 1.5;
iheight = 2.25;
iwidth  = .9425;
fheight = 1.87;
fwidth  = 1.57;

% calculate

itemp1 = iRadius/cos(pi/(2*Nl));
itemp2 = itemp1/cos(pi/Nl);
idepth = -itemp1/itemp2*(itemp2-itemp1); % depth should be negative (down)
ftemp1 = fRadius/cos(pi/(2*Nl));
ftemp2 = ftemp1/cos(pi/Nl);
```

```
fdepth = -ftemp1/ftemp2*(ftemp2-ftemp1);
[xi,yi,zi]=xyz_pos(elem,iwidth,iheight,idepth,iRadius);
[xf,yf,zf]=xyz_pos(elem,fwidth,fheight,fdepth,fRadius);
[n1,n2]=xyz_str(elem,xi,yi,zi,xf,yf,zf);
nt = sqrt(n1.^2+n2.^2);

% balloon
legdrop = sthick/cos(pi/(2*Nl));
xbi=ones(elem,1)*linspace(-iwidth,iwidth,elem);
xbf=ones(elem,1)*linspace(-fwidth,fwidth,elem);
ybi=linspace(-iheight,iheight,elem)'*ones(1,elem);
ybf=linspace(-fheight,fheight,elem)'*ones(1,elem);
% balloon is cylinder x^2 + (z-k)^2 = R^2
ballzi = -iRadius/cos(pi/(2*Nl)) + sqrt(iRadius^2 - xbi.^2); % global balloon
height over
ballzf = -fRadius/cos(pi/(2*Nl)) + sqrt(fRadius^2 - xbf.^2); %   rectangular
matrix
ballzis = -iRadius/cos(pi/(2*Nl)) + sqrt(iRadius^2 - xi.^2); % global balloon
height over
ballzfs = -fRadius/cos(pi/(2*Nl)) + sqrt(fRadius^2 - xf.^2); %   stent cell matrix
balldi = zi-legdrop-ballzis;        % distance from balloon to artery
balldf = zf-legdrop-ballzfs;
%disp(sprintf('legdrop: %g',legdrop))
%disp(sprintf('offset: %g',-iRadius/cos(pi/(2*Nl))))

% display
a1=min(min(n1));
b1=max(max(n1));
a2=min(min(n2));
b2=max(max(n2));
n2=(n2-(a2+b2)/2)*((b1-a1)/(b2-a2));
n2disp=n2+(a2+b2)/2;
n2calc=n2*.82+(a1+b1)/2;

% remap
n1=remap(n1);
n2calc=remap(n2calc);
n2disp=remap(n2disp);
n3=sqrt(n2calc.^2+n1.^2);


figure(1)
surf(yi,xi,zi,n1)
view(2)
axis('equal')
%str1='\fontname{Arial}\fontsize{18}\epsilon_{\theta\theta}\fontsize{14} strain
component';
%title(str1)
%xlabel('\fontsize{12}\bfcircumferential distance (mm)')
%ylabel('\fontsize{12}\bfaxial distance(mm)')
if max(max(n1))-min(min(n1)) < 0.000001
  caxis([0 1])
end
axis('off')
colormap(jet(255))
%h=colorbar;
%set(h,'position',[0.8321    0.1690    0.0571    0.7024])
set(gcf,'renderer','painters')
```

```
figure(2)
surf(yi,xi,zi,n2disp)
view(2)
axis('equal')
str1='\fontname{Arial}\fontsize{18}\epsilon_{\theta\theta}\fontsize{14} strain
component';
%title(str1)
%xlabel('\fontsize{12}\bfcircumferential distance (mm)')
%ylabel('\fontsize{12}\bfaxial distance(mm)')
if max(max(n1))-min(min(n1)) < 0.000001
  caxis([0 1])
end
axis('off')
colormap(jet(255))
%h=colorbar;
%set(h,'position',[0.8321    0.1690    0.0571    0.7024])
set(gcf,'renderer','painters')

figure(3)
surf(yi,xi,zi,n3)
view(2)
axis('equal')
%str1='\fontname{Arial}\fontsize{18}\epsilon_{zz}\fontsize{14} strain
component';
%title(str1)
%xlabel('\fontsize{12}\bfcircumferential distance (mm)')
%ylabel('\fontsize{12}\bfaxial distance(mm)')
if max(max(n2disp))-min(min(n2disp)) < 0.000001
  caxis([-0.25 0.25])
end
axis('off')
colormap(jet(255))
%h=colorbar;
%set(h,'position',[0.8321    0.1690    0.0571    0.7024])
set(gcf,'renderer','painters')


function nout=remap(n3);
xmin=min(min(n3));xmax=max(max(n3));p=[xmin 1;xmax 1]\[xmax;xmin];
nout=polyval(p,n3);


function [x,y,z]=xyz_pos(elem,xi,yi,zi,R,DEBUG)
% XYZ_POS Determines xyz position along a stent leg
% [x,y,z]=xyz_pos(elem,xi,yi,zi,R,DEBUG)
% xi is initial width, yi is initial length, zi are initial heights of corners
% R is the radius
% debug is optional
%
% Feb 97   James C. Squire

half = (elem-1)/2 +1;
if fix(half)-half, error('elements must be odd'), end
if nargin==1, DEBUG=0;end
if nargin==2, DEBUG=xi;end
if nargin<=2, xi=1; yi = .5; zi = -.2; R = 4; end
if nargin>2&nargin<6, DEBUG=0; end
% break into matricies of points
x = zeros(elem);
```

```
y = zeros(elem);
z = NaN*ones(elem)*zi/2;
for i=1:elem
  x(i,:) = linspace(-xi*(i-1)/(elem-1),xi-xi*(i-1)/(elem-1),elem);
  y(i,:) = linspace(yi*(i-elem)/(1-elem),yi*(i-elem)/(1-elem)-yi,elem);
end

% determine z at boundaries
%bline = sqrt(R^2-linspace(0,zi,elem).^2) - R;  % curving line around balloon
bline=linspace(0,zi,elem);
z(1,:) = bline;
z(:,elem) = fliplr(bline)';
z(elem,:) = fliplr(bline);
z(:,1) = bline';


% determine interior z points
z=SolveMatrixInterior(z);
```

function [mAx,mAy,mAz,mBx,mBy,mBz,mSx,mSy,mSz]=SolveStent(Type,N2,draw)

```
% SOLVESTENT calculates the arterial position over a stent
% [mx,my,mz]=SolveStent(Type,N2,Draw)
% Type may be 'simple','complex','STstraight','STcurved','ML'.
% N2 is number of columns of result (ie width in x or circumferential direction)
% Draw=1 means entire system is drawn height-referenced, or 2 in natural color
% Draw=[balloon,struts,artery] draws it in height-referenced color if 1, natural
color if 2
%
% [mx,my,mz,sx,sz,sz,bx,by,bz]=SolveStent[...] returns meshes for the struts
and balloon also
% M=SolveStent(...) returns the arterial matrix, viewable with pcolor2(M).  This
is in
% the 2D local coordinate system.
%
% Jim Squire, January 2000

zoffset=0.01;  % small offset to raise stent boundaries to cover jagged artery
edges

if nargin<1, Type='stcurved'; end
if nargin<2, N2=50; end
if nargin<3, draw=[3 3 3]; end       % default is to draw
if length(draw)==1
  if draw==1
    draw=[1 1 1];
  elseif draw==2
    draw=[2 2 2];
  else
    draw=[0 0 0];
  end
end

Expand=1.5*N2; % how many points in each line segment
switch lower(Type)
case {'s','si','sim','simp','simpl','simple'}
  Type='simple';
  N2min=6;
```

```
  Expand = N2*2;
        [b1x_2D,b1y_2D,b2x_2D,b2y_2D,Radius,Rings,Len,W,T]=Get2DBo
undary(Type,Expand);
        [b1x,b1y,b1z,b2x,b2y,b2z,b3x,b3y,b3z,b4x,b4y,b4z]=Wrap(b1x_2D,b
1y_2D,b2x_2D,b2y_2D,Radius,T);
case {'c','co','com','comp','compl','complex'}
  Type='complex';
  N2min=8;
  Expand=N2;

[b1x_2D,b1y_2D,b2x_2D,b2y_2D,Radius,Rings,Len,W,T]=Get2DBoundary(Ty
pe,Expand);

[b1x,b1y,b1z,b2x,b2y,b2z,b3x,b3y,b3z,b4x,b4y,b4z]=Wrap(b1x_2D,b1y_2D,b2
x_2D,b2y_2D,Radius,T);
case {'st','sts','ststr','straight','ststraight'}
  Type='ststraight';
  N2min=3;
  Expand=round(N2*2);
        [b1x_2D,b1y_2D,b2x_2D,b2y_2D,Radius,Rings,Len,W,T]=Get2DBo
undary(Type,round(Expand/2));
        [b1x,b1y,b1z,b2x,b2y,b2z,b3x,b3y,b3z,b4x,b4y,b4z]=STStraightBoun
daries(Radius,Rings,Len,W,T,round(Expand/2));
case {'a','av','ave','aves','as'}
  Type='ave';
  N2min=3;
  Expand=round(N2*2);
        [b1x_2D,b1y_2D,b2x_2D,b2y_2D,Radius,Rings,Len,W,T]=Get2DBo
undary(Type,round(Expand/2));
        [b1x,b1y,b1z,b2x,b2y,b2z,b3x,b3y,b3z,b4x,b4y,b4z]=STStraightBoun
daries(Radius,Rings,Len,W,T,round(Expand/2));
case {'ac','avc','avec'}
  Type='avec';
  N2min=3;
  Expand=N2;
        [b1x_2D,b1y_2D,b2x_2D,b2y_2D,Radius,Rings,Len,W,T]=Get2DBo
undary(Type,Expand);

        [b1x,b1y,b1z,b2x,b2y,b2z,b3x,b3y,b3z,b4x,b4y,b4z]=Wrap(b1x_2D,b
1y_2D,b2x_2D,b2y_2D,Radius,T);
case {'n','ni','nir'}
  Type='nir';
  N2min=10;
  Expand=round(N2*1.2);

[b1x_2D,b1y_2D,b2x_2D,b2y_2D,Radius,Rings,Len,W,T]=Get2DBoundary(Ty
pe,Expand);

[b1x,b1y,b1z,b2x,b2y,b2z,b3x,b3y,b3z,b4x,b4y,b4z]=Wrap(b1x_2D,b1y_2D,b2
x_2D,b2y_2D,Radius,T);
case {'stc','curved','stcurved'}
  Type='stcurved';
  N2min=3;
  Expand=N2;
        [b1x_2D,b1y_2D,b2x_2D,b2y_2D,Radius,Rings,Len,W,T]=Get2DBo
undary(Type,Expand);

        [b1x,b1y,b1z,b2x,b2y,b2z,b3x,b3y,b3z,b4x,b4y,b4z]=Wrap(b1x_2D,b
1y_2D,b2x_2D,b2y_2D,Radius,T);
```

```
case {'ml','mlc','mlcurved','cr'}
  Type='mlcurved';
  N2min=14;
  Expand=round(N2/2);
          [b1x_2D,b1y_2D,b2x_2D,b2y_2D,Radius,Rings,Len,W,T]=Get2DBo
undary(Type,Expand);

          [b1x,b1y,b1z,b2x,b2y,b2z,b3x,b3y,b3z,b4x,b4y,b4z]=Wrap(b1x_2D,b
1y_2D,b2x_2D,b2y_2D,Radius,T);
otherwise
  error(sprintf('Stent type %s not recognized in SolveStent',Type))
end
if (N2<N2min)
  error(sprintf('Stent type %s requires a minimum N2 of %g to
solve',Type,N2min))
end

% c2x, r2y determines (x,y) coordinates from (row,col) locations
%[M,c2x,r2y]=FillMatrixBorder(b1x_2D,b1y_2D,b1z,N2);
[M,c2x,r2y]=FillMatrixBorder(b1x,b1y,b1z,N2);

% Solve for the artery position using the Laplacian condition over the interior
M=SolveMatrixInterior(M);

% create the artery mesh
[mAx,mAy,mAz]=CreateArteryMesh(M,c2x,r2y);

% create the stent mesh
mSx = [b1x; b2x; b3x; b4x; b1x];
mSy = [b1y; b2y; b3y; b4y; b1y];
mSz = [b1z; b2z; b3z; b4z; b1z]+zoffset;  % offset to hide artery edge and avoid
interference w/ balloon
% special case: straight slotted tube.  Simplify the stent mesh
switch Type
case 'ststraight'

[x1,y1,z1,x2,y2,z2,x3,y3,z3,x4,y4,z4]=STStraightBoundaries(Radius,Rings,Len,
W,T,2);
          mSx = [x1; x2; x3; x4; x1];
          mSy = [y1; y2; y3; y4; y1];
  mSz = [z1; z2; z3; z4; z1]+zoffset;
case 'nir'
  mSz = mSz-zoffset+zoffset/20;
end

% create the balloon mesh
[mBx,mBy,mBz]=CreateBalloonMesh(Type,Radius,Rings,Len);

if nargout==1
  mAx = M; % return the artery 2D matrix
end

% Two color codes.  1 is height-referenced, 2 is natural color-referenced
if any(draw)
  cmin = inf;
  cmax =-inf;
  if draw(1)  % Balloon
    if draw(1)~=3
      tmin = min(min(mBz)); tmax = max(max(mBz));
```

```
            if tmin<cmin, cmin=tmin; end
        if tmax>cmax, cmax=tmax; end
    end
end
if draw(2)  % Stent
    if draw(2)~=3
        tmin = min(min(mSz)); tmax = max(max(mSz));
            if tmin<cmin, cmin=tmin; end
        if tmax>cmax, cmax=tmax; end
    end
end
if draw(3)  % Artery
    tmin = min(min(mAz)); tmax = max(max(mAz));
    if tmin<cmin, cmin=tmin; end
    if tmax>cmax, cmax=tmax; end
end
map=jet(255);
map(1,:)=[.5 .5 .5];
colormap(map);
t = (cmax-cmin)/(255-2);
gray = cmin-t;
blue = cmin+t;
red = cmin+(cmax-cmin)*.9;
cmin  = cmin-t;
caxis([cmin cmax]);
switch draw(1)  % Balloon
            case 1, surf(mBx,mBy,mBz,mBz); hold on
            case {2,3}, surf(mBx,mBy,mBz,blue*ones(size(mBz))); hold on
end
switch draw(2)  % Stent
            case 1, surf(mSx,mSy,mSz,mSz); hold on
            case {2,3}, surf(mSx,mSy,mSz,gray*ones(size(mSz))); hold on
end
switch draw(3)  % Artery
            case {1,3}, surf(mAx,mAy,mAz,mAz,'facecolor','interp'); hold on
            case 2, surf(mAx,mAy,mAz,red*ones(size(mAz))); hold on
end

% zoom out to hold both plots, then lock zoom again
set(gca,'xlimmode','auto','ylimmode','auto','zlimmode','auto')

switch Type  % ideal views
case 'ststraight'
    sx(-2,2)
    sz(1,2)
    sy
    view(-52,0)
case 'ave'
case 'stcurved'
    sx(-2,2)
    sz(1,2)
    sy
    view(-52,0)
case 'mlcurved'
    axis('normal')
    sz(.5,1.5)
    view(133,50)
case 'nir'
    axis('normal')
```

```
    view(-108,38)
        end


  %set(gca,'xlimmode','manual','ylimmode','manual','zlimmode','manual')

  colormap(map)
  %caxis([cmin cmax])
  %colorbar
  hold off
  figure(gcf)
  %set(gcf,'renderer','painters')
end
% alternate plot: gray stent, blue balloon, color coded artery
  % make the plot have black edges but interp inside
  %a=get(gca,'children');
  %for i=1:length(a)
  %   set(a(i),'facecolor','interp')
  %   set(a(i),'edgecolor','k')
  %end
```

function [b1x_2D,b1y_2D,b2x_2D,b2y_2D,Radius,Rings,Len,W,T]=Get2DBoundary (Type,Expand)

```
% Get2DBoundary(Type,Expand) returns evenly-spaced 2D boundary verticies
%
[b1x_2D,b1y_2D,b2x_2D,b2y_2D,Radius,Rings,Len,W,T]=Get2DBoundary(Ty
pe,Expand)
% No points are doubled, and the ends are not joined
%
% James Squire January 2000

DEBUG=0;
Radius=1.5;  % 3mm diameter balloon
switch lower(Type)
case {'s','simple'}
  % definitions
  Rings = 4;  % there are four repeating elements like this around the stent
  Len = 4;    % the length of the cell along the axis of the balloon
  W=0.5;      % strut width
  T=0.5;      % strut thickness
  % interior shape.  Must be specified counterclockwise
  [uBorderx2,uBordery2]=ExpandArc(1,0,-1000,0,1,-1,0,1000,Expand);
  [uBorderx1,uBordery1]=ExpandLine([-1 1],[0 0],Expand);
  b1x_2D = [uBorderx1 uBorderx2(2:end-1)]; % get rid of doubled points
  b1y_2D = [uBordery1 uBordery2(2:end-1)];
        % center
        b1x_2D=b1x_2D-mean(b1x_2D);
        b1y_2D=b1y_2D-mean(b1y_2D);
        % exterior shape
  [b2x_2D, b2y_2D] = Widen(b1x_2D,b1y_2D, W);
case{'c','complex'}
  % definitions
  Rings = 2;
  Len=4;
  W=.5;
  T=.5;
  % 2D shape
```

```
  [uBorderx1,uBordery1]=ExpandLine([3 3 0 -3 -3],[1 -1 -2 -1 1],Expand);
        [uBorderx2,uBordery2]=ExpandArc(-3,1,1000,-2,2,-1,1,-
1000,Expand);
        [uBorderx3,uBordery3]=ExpandArc(-1,1,-1000,0,0,1,1,1000,Expand);
  [uBorderx4,uBordery4]=ExpandArc(1,1,1000,2,2,3,1,-1000,Expand);
        b1x_2D = [uBorderx1(1:end-1) uBorderx2(1:end-1) uBorderx3(1:end-
1) uBorderx4(1:end-1)];
  b1y_2D = [uBordery1(1:end-1) uBordery2(1:end-1) uBordery3(1:end-1)
uBordery4(1:end-1)];
  % flip to make counterclockwise
  b1x_2D = fliplr(b1x_2D);
  b1y_2D = fliplr(b1y_2D);
        % center
        b1x_2D=b1x_2D-mean(b1x_2D);
        b1y_2D=b1y_2D-mean(b1y_2D);
        % exterior shape
  [b2x_2D, b2y_2D] = Widen(b1x_2D,b1y_2D, W);
case{'sts','ststraight'}
  % definitions in mm
  Rings=6;
  Len=1.9;
  T=.015; % radial strut thickness
  W=.1; % strut in-plane width
  % 2D shape
  [b1x_2D,b1y_2D]=ExpandLine([0 -pi*Radius/Rings 0 pi*Radius/Rings
0],[Len/2 0 -Len/2 0 Len/2],Expand);
  b1x_2D(end)=[];
  b1y_2D(end)=[];
  % center
  b1x_2D = b1x_2D-mean(b1x_2D);
  b1y_2D = b1y_2D-mean(b1y_2D);
        % exterior shape
  [b2x_2D, b2y_2D] = Widen(b1x_2D,b1y_2D, W);
case{'ave'}
  % definitions in mm
  Rings=4;
  Len=2.68;
  T=.05; % radial strut thickness
  W=.1; % strut in-plane width
  % 2D shape
  [b1x_2D,b1y_2D]=ExpandLine([0 -pi*Radius/Rings 0 pi*Radius/Rings
0],[Len/2 0 -Len/2 0 Len/2],Expand);
  b1x_2D(end)=[];
  b1y_2D(end)=[];
  % center
  b1x_2D = b1x_2D-mean(b1x_2D);
  b1y_2D = b1y_2D-mean(b1y_2D);
        % exterior shape
  [b2x_2D, b2y_2D] = Widen(b1x_2D,b1y_2D, W);
case{'avec'}
  % definitions in mm
  Rings=4;
  Len=2.68;
  T=.1; % radial strut thickness
  W=.1; % strut in-plane width
  % 2D shape
  [b1x_2D,b1y_2D]=ExpandLine([0 -pi*Radius/Rings 0 pi*Radius/Rings
0],[Len/2 0 -Len/2 0 Len/2],Expand);
  b1x_2D(end)=[];
```

```
    b1y_2D(end)=[];
    % center
    b1x_2D = b1x_2D-mean(b1x_2D);
    b1y_2D = b1y_2D-mean(b1y_2D);
            % exterior shape
    [b2x_2D, b2y_2D] = Widen(b1x_2D,b1y_2D, W);
  case{'stcurved'}
    % definitions in mm
    Rings=6;
    Len=1.9;
    T=.04; % radial strut thickness
    W=.1; % strut in-plane width
    % 2D shape
    [b1x_2D,b1y_2D]=ExpandLine([0 -pi*Radius/Rings 0 pi*Radius/Rings
  0],[Len/2 0 -Len/2 0 Len/2],Expand);
    b1x_2D(end)=[];
    b1y_2D(end)=[];
    % center
    b1x_2D = b1x_2D-mean(b1x_2D);
    b1y_2D = b1y_2D-mean(b1y_2D);
            % exterior shape
    [b2x_2D, b2y_2D] = Widen(b1x_2D,b1y_2D, W);
  case {'nir'}
    % definitions in mm
    Rings=7;
    Len=1.05;
    T=0.017;
    W=0.035;
    % 2D shape
    [uBorderx1,uBordery1]=ExpandArc(0,2.7,0,2,0,-3.7,Expand);
    [uBorderx2,uBordery2]=ExpandLine([2 6.75 2],[0 3.25 7.5],Expand);
    [uBorderx3,uBordery3]=ExpandArc(2,7.5,-2.75,0,10.5,0,Expand);
    b1x_2D = [uBorderx1(1:end-1) uBorderx2(1:end-1) uBorderx3(1:end-1)];
    b1y_2D = [uBordery1(1:end-1) uBordery2(1:end-1) uBordery3(1:end-1)];
    b1x_2D = [b1x_2D -b1x_2D(end-1:-1:2)]; % reflect around x axis
    b1y_2D = [b1y_2D  b1y_2D(end-1:-1:2)];
    b1x_2D = b1x_2D * 0.1;                                    % scale to get in mm
    b1y_2D = b1y_2D * 0.1;
    % center
    b1x_2D = b1x_2D-mean(b1x_2D);
    b1y_2D = b1y_2D-mean(b1y_2D);
    % reflect to get counterclockwise
    b1x_2D = fliplr(b1x_2D);
    b1y_2D = fliplr(b1y_2D);
    % rotate 90 degrees
    t = b1x_2D;
    b1x_2D = b1y_2D;
    b1y_2D = t;
            % exterior shape
    [b2x_2D, b2y_2D] = Widen(b1x_2D,b1y_2D, W);
  case{'ml','mlcurved'}
    % definitions in mm
    Rings=3;
    Len=1.65;
    T=.024; % radial strut thickness
    W=0.1; % strut in-plane width
    % 2D shape
    [uBorderx1,uBordery1]=ExpandArc(0,4.6,-1,.4,4.4,.8,4.6,1,Expand);
    [uBorderx2,uBordery2]=ExpandLine([.8 2.5],[4.6 7.5],Expand);
```

```
  [uBorderx3,uBordery3]=ExpandArc(2.5,7.5,1.7,3.9,8.5,5.3,7.5,-1.8,Expand);
  [uBorderx4,uBordery4]=ExpandLine([5.3 7.8 7.8],[7.5 4.4 0],Expand);
  [uBorderx5,uBordery5]=ExpandArc(7.8,0,0,7,.5,-1.4,Expand);
  [uBorderx6,uBordery6]=ExpandLine([7 5.7],[.5 2.3],Expand);
  [uBorderx7,uBordery7]=ExpandArc(5.7,2.3,-1.4,3.9,4,2.1,2.3,1.4,Expand);
  [uBorderx8,uBordery8]=ExpandLine([2.1 .8],[2.3 .5],Expand);
  [uBorderx9,uBordery9]=ExpandArc(.8,.5,1.4,0,0,0,Expand);
  b1x_2D = [uBorderx1(1:end-1) uBorderx2(1:end-1) uBorderx3(1:end-1)
uBorderx4(1:end-1) uBorderx5(1:end-1) uBorderx6(1:end-1) uBorderx7(1:end-
1) uBorderx8(1:end-1) uBorderx9(1:end-1)];
  b1y_2D = [uBordery1(1:end-1) uBordery2(1:end-1) uBordery3(1:end-1)
uBordery4(1:end-1) uBordery5(1:end-1) uBordery6(1:end-1) uBordery7(1:end-
1) uBordery8(1:end-1) uBordery9(1:end-1)];
  b1x_2D = [b1x_2D -b1x_2D(end-1:-1:2)]; % reflect around x axis
  b1y_2D = [b1y_2D  b1y_2D(end-1:-1:2)];
  b1x_2D = b1x_2D * 0.195;                                    % scale to
get in mm
  b1y_2D = b1y_2D * 0.195;
  % center
  b1x_2D = b1x_2D-mean(b1x_2D);
  b1y_2D = b1y_2D-mean(b1y_2D);
  % reflect to get counterclockwise
  b1x_2D = fliplr(b1x_2D);
  b1y_2D = fliplr(b1y_2D);
        % exterior shape
  [b2x_2D, b2y_2D] = Widen(b1x_2D,b1y_2D, W);
otherwise
  error(sprintf('Stent type %s not recognized in SolveStent',Type))
end

% close up the curves
b1x_2D(end+1)=b1x_2D(1);
b1y_2D(end+1)=b1y_2D(1);
b2x_2D(end+1)=b2x_2D(1);
b2y_2D(end+1)=b2y_2D(1);


if DEBUG

plot(b1x_2D,b1y_2D,'b',b2x_2D,b2y_2D,'g',b1x_2D,b1y_2D,'b.',b2x_2D,b2y_2
D,'g.')
  axis('equal')
  figure(gcf)
end


function
[b1x,b1y,b1z,b2x,b2y,b2z,b3x,b3y,b3z,b4x,b4y,b4z]=Wrap(b1x_2D,b1y_2D,b2x
_2D,b2y_2D,Radius,T);
% Wrap wraps 2 different 1D manifolds in 2D space around a cylinder in 3D
space
%
[b1x,b1y,b1z,b2x,b2y,b2z,b3x,b3y,b3z,b4x,b4y,b4z]=Wrap(b1x_2D,b1y_2D,b2
x_2D,b2y_2D,Radius,T);

DEBUG=0;

k=1/(Radius+T);
```

```
b1x = (Radius+T) * sin(k*b1x_2D);
b1y = b1y_2D;
b1z = (Radius+T) * cos(k*b1x_2D);

b2x = (Radius+T) * sin(k*b2x_2D);
b2y = b2y_2D;
b2z = (Radius+T) * cos(k*b2x_2D);

b3x = Radius * sin(k*b2x_2D);
b3y = b2y_2D;
b3z = Radius * cos(k*b2x_2D);

b4x = Radius * sin(k*b1x_2D);
b4y = b1y_2D;
b4z = Radius * cos(k*b1x_2D);

if DEBUG
  figure(1)
  plot(b1x_2D,b1y_2D,b2x_2D,b2y_2D)
  axis('equal')
  selflabel
  figure(2)
  plot3(b1x,b1y,b1z,b2x,b2y,b2z,b3x,b3y,b3z,b4x,b4y,b4z)
  axis('equal')
  figure(2)
  selflabel
end
```

function [xp,yp]=Widen(x,y,W)

```
% WIDEN traces an outer boundary around a closed curve traced
counterclockwise
% [xp,yp]=Widen(x,y,W) returns an outer boundary W units out from x,y
% no x,y points may be doubled, including the endpoints

DEBUG=0;
if length(x)~=length(y), error('x,y arguments to Widen must be equal
length'),end
if length(x)<3, error('x,y arguments to Widen must have at least 3 points'),end
if min(size(x))~=1, error('x,y arguments to Widen must be vectors, not
matricies'), end

if size(x,2)~=1 % Fill data in [x y] column vector data0
  Trans=1;
  x=x';
  y=y';
else
  Trans=0;
end
data0=[x y];
datam=[data0(end,:); data0(1:end-1,:)];
datap=[data0(2:end,:); data0(1,:)];

Rm=data0-datam;
Rp=data0-datap;

% check to see if any points are repeated
TOL=1e-10;
t=find(abs(Rm(:,1))+abs(Rm(:,2))<TOL);
```

```
if any(t)
  error(sprintf('Error: point at indicies %g and %g are repeated in Widen',t(1)-
1,t(1)))
end

% find theta of widened point (could be at + or - theta)
thetam=atan2(Rm(:,2),Rm(:,1));
thetap=atan2(Rp(:,2),Rp(:,1));
thetaN=mean([thetam thetap]')';

% find magnitude of the vector reaching to the new points
thetaR=thetap+pi/2;
i=find(abs(thetaR-thetaN)>pi/2);
thetaR(i)=thetap(i)-pi/2;
rN=W./cos(thetaR-thetaN);

% create two possible vectors
xp1=x+rN.*cos(thetaN); yp1=y+rN.*sin(thetaN);
xp2=x-rN.*cos(thetaN); yp2=y-rN.*sin(thetaN);

% choose the correct side
thetaL=thetap+pi/2; % points outside a ccw curve
xL=x+cos(thetaL).*rN;
yL=y+sin(thetaL).*rN;
d=(xL-xp1).^2 + (yL-yp1).^2 - (xL-xp2).^2 - (yL-yp2).^2;
i1=d<0;
i2=d>=0;
xp(i1)=xp1(i1);
yp(i1)=yp1(i1);
xp(i2)=xp2(i2);
yp(i2)=yp2(i2);

if DEBUG
  plot(x,y,'b.',x,y,'b-',xp,yp,'g.',xp,yp,'g',xp1,yp1,'m.',xp2,yp2,'c.',xL,yL,'rx')
axis('equal')
figure(gcf)

        axis('equal')
        figure(gcf)
end
```

function [b1x,b1y,b1z,b2x,b2y,b2z,b3x,b3y,b3z,b4x,b4y,b4z]=STStraightBoudaries(Radius,Rings,Len,W,T,Expand)

```
% STStraightBoundaries returns the 3D boundaries for a straight-style slotted
tube stent
%
[b1x,b1y,b1z,b2x,b2y,b2z,b3x,b3y,b3z,b4x,b4y,b4z]=STStraightBoudaries(Radi
us,Rings,Len,W,T,Expand)
% bnx, where n refers to arterial (inside top)=1, outside top=2, outside
bottom=3, inside bottom=4

DEBUG=0;

theta0 = pi/(2*Rings);
z1=(Radius+T)/cos(theta0);
z1p=Radius/cos(theta0);
z2=z1*cos(2*theta0);
```

```
z2p=z1p*cos(2*theta0);

x2=2*(Radius+T)*sin(theta0);
x2p=2*Radius*sin(theta0);

wid=4*z1*sin(theta0);
theta2=atan(Len/wid);
f=W/cos(theta2);    % f=W/cos(theta2)*1.1;
g=T/cos(theta2);
d=W/sin(theta2);

theta5=atan((z2-z1)/(Len/2));
m=g*cos(theta5);

p1=d*cos(theta0);
p2=d*sin(theta0);

P11=[0 Len/2 z1];
P12=[0 Len/2+f z1];
P13=[0 Len/2+f-m z1p];
P14=[0 Len/2-m z1p];

P21=[x2 0 z2];
P22=[x2+p1 0 z2-p2];
P23=[x2p+p1 0 z2p-p2];
P24=[x2p 0 z2p];

%theta3=atan((z1-z2)/x2);   % alternate method
%x3=d*cos(theta3);
%y3=d*sin(theta3);

%P22=[x2+x3 0 z2-y3];
%P23=[x2p+x3 0 z2p-y3];


b1x=[    0  -P21(1)       0  P21(1)     0];
b1y=[P11(2)       0  -P11(2)       0  P11(2)];
b1z=[P11(3)   P21(3)   P11(3)  P21(3)  P11(3)];

b2x=[    0  -P22(1)       0   P22(1)     0];
b2y=[P12(2)       0  -P12(2)       0  P12(2)];
b2z=[P12(3)   P22(3)   P12(3)  P22(3)  P12(3)];

b3x=[    0  -P23(1)       0   P23(1)     0];
b3y=[P13(2)       0  -P13(2)       0  P13(2)];
b3z=[P13(3)   P23(3)   P13(3)  P23(3)  P13(3)];

b4x=[    0  -P24(1)       0   P24(1)     0];
b4y=[P14(2)       0  -P14(2)       0  P14(2)];
b4z=[P14(3)   P24(3)   P14(3)  P24(3)  P14(3)];

[b1x,b1y,b1z] = ExpandLine(b1x,b1y,b1z,Expand);
[b2x,b2y,b2z] = ExpandLine(b2x,b2y,b2z,Expand);
[b3x,b3y,b3z] = ExpandLine(b3x,b3y,b3z,Expand);
[b4x,b4y,b4z] = ExpandLine(b4x,b4y,b4z,Expand);

if DEBUG
  % draw the stent
  x = [b1x; b2x; b3x; b4x; b1x];
```

```
  y = [b1y; b2y; b3y; b4y; b1y];
  z = [b1z; b2z; b3z; b4z; b1z];
  surf(x,y,z,z)
  axis('equal')
  hold on
  % draw the balloon
  n=50; % segments in theta theta direction
  m=20; % segments in axial direction
  cr=Radius*ones(m,1);
  m = length(cr);
  theta = linspace(-pi/Rings,pi/Rings,n+1)*1.1+pi/2;
  sintheta = sin(theta); sintheta(n+1) = sintheta(1);
  cx = cr * cos(theta);
  cy = cr * sintheta;
  cz = (0:m-1)'/(m-1) * ones(1,n+1);
  cz=cz-.5; cz=cz*1.2*Len;
  mesh(cx,cz,cy);
  hold off
  set(gca,'xlimmode','auto','ylimmode','auto','zlimmode','auto')
  figure(gcf)
  % make the plot have black edges but interp inside
  %a=get(gca,'children');
  %for i=1:length(a)
  %   set(a(i),'facecolor','interp')
  %   set(a(i),'edgecolor','k')
  %end
end


function [M,c2x,r2y]=FillMatrixBorder(b1x_2D,b1y_2D,b1z,N2)
% FillMatrix border fills the border region of a matrix M with z boundary
heights
% [M,px,py]=FillMatrixBorder(b1x_2D,b1y_2D,b1z,N2)
% M has N2 cols and as many rows as needed to keep proportion
% M exists in the local coordinate system of x,y, therefore a remapping to
% an absolute frame of reference is needed.  This is done with c2x, r2y such that
% the true 3D location of point
M(row,col)={polyval(c2x,col),polyval(r2y,row),M(row,col)}
%
% James Squire
% January 2000

DEBUG=0;

if length(b1x_2D)~=length(b1y_2D)
  error('length of x_2D and y_2D are not equal in FillMatrixBorder')
end
if length(b1x_2D) ~= length(b1z)
  error('length of 2D borders and 3D heights are not equal in FillMatrixBorder')
end

% Turn into column vectors
b1x_2D = b1x_2D(:);
b1y_2D = b1y_2D(:);
b1z = b1z(:);

% Scale the numbers in x and y into matrix rows and columns
x1 = min(b1x_2D); x2 = max(b1x_2D);
y1 = min(b1y_2D); y2 = max(b1y_2D);
```

```
N1 = (y2-y1)/(x2-x1)*N2;
y2r = [y2 1;y1 1]\[1;N1];
x2c = [x2 1;x1 1]\[N2;1];
bc = round(polyval(x2c,b1x_2D));
br = round(polyval(y2r,b1y_2D));

% Fill matrix M with zvalue to indicate a border, NaN otherwise
M = NaN*ones(round(N1),N2);
for i=1:length(bc)
  [t1,t2]=size(M);
  M(br(i),bc(i))=b1z(i); % indexing changes x,y to row,col
end

% Create the scaling factors to go from (row,col) to (x,y)
c2x = [1 1;N2 1]\[x1;x2];
r2y = [1 1;N1 1]\[y2;y1];

if DEBUG
  figure(1)
  plot3(b1x_2D,b1y_2D,b1z,'b',b1x_2D,b1y_2D,b1z,'b.')
  axis('equal'), selflabel
  figure(2)
  pcolor2(M)
end


function Mfinal=SolveMatrixInterior(M)
% SolveMatrixInterior solves the Laplacian (soap bubble) over matrix Mi
% M2=SolveMatrixInterior(M1)
% M1 is NaN everywhere but along a single 8-connected closed loop
% where numbers indicate height
% M2 returns M1 everywhere but on the interior of this loop, where it contains
% the Laplacian solution of the border

DEBUG=0;

if DEBUG
  M=[NaN NaN NaN 7 8;NaN 2 3 NaN 3;6 NaN NaN NaN 2;NaN 2 NaN 2
NaN;NaN NaN 6 NaN NaN];
end

% create masks Minside.  Note Moutside = ~Minside-Mt (except for sizes)
Mt = NaN*ones(size(M)+2);
Mt(2:end-1,2:end-1)=M;
Mt(~isnan(Mt))=1;
Mt(isnan(Mt))=0;
Mf=double(bwfill(Mt,1,1,8));
Minside=~Mf;
Minside=Minside(2:end-1,2:end-1);

% nunber inside border
i=find(Minside);
Minside(i)=[1:length(i)]';
D=delsq(Minside);
if length(i)==0
  error('M not 8 connected in SolveMatrixInterior.  Increase Expand in
SolveStent')
end
```

```
% create the RHS: the laplacian = 0 if not touching a boundary,
% o.w. sum of boundary points
N=max(max(Minside)); % number of interior points
rhs=zeros(N,1);
for i=1:N
  [r,c]=find(Minside==i);
  t=[M(r+1,c) M(r-1,c) M(r,c+1) M(r,c-1)];
  rhs(i) = sum(t(~isnan(t)));
end
u = D\rhs;  % these are the individual points

% format result
U = Minside;
U(Minside>0) = full(u(Minside(Minside>0)));  % these are the interior points
Mfinal=NaN*ones(size(M));
Mfinal(~isnan(M))=M(~isnan(M)); % fill with NaN on outside, o/w
boundary+interior
Mfinal(Minside>0) = full(u(Minside(Minside>0)));

% display result
if DEBUG
  %clabel(contour(U));
  %prism
  %axis('square'), axis('ij')
end
```

function [mAx,mAy,mAz]=CreateArteryMesh(M,c2x,r2y)

```
% CreateArteryMesh returns a 3D meshable x,y,z given a 2D matrix M and
scales
% [mAx,mAy,mAz]=CreateArteryMesh(M,c2x,r2y)
% the true 3D location of point
M(row,col)={polyval(c2x,col),polyval(r2y,row),M(row,col)}
%
% James Squire, January 2000

[N1,N2]=size(M);
mAx=ones(N1,1)*[1:N2];
mAx=polyval(c2x,mAx);
mAx(isnan(M))=NaN;

mAy=[1:N1]'*ones(1,N2);
mAy=polyval(r2y,mAy);
mAy(isnan(M))=NaN;

mAz=M;
```

function [mBx,mBy,mBz]=CreateBalloonMesh(Type,Radius,Rings,Len)

```
% CreateBalloonMesh returns a 3D meshable x,y,z under a stent
% [mBx,mBy,mBz]=CreateBalloonMesh(Type,Radius,Rings,Len)
%
% James Squire, January 2000

n=50;                       % segments in theta theta direction
m=20;                       % segments in axial direction
overtheta=0.1; % 10% more curvature in theta direction than required by stent
overy=0.2;                  % 20% more extension in axial direction than
required by stent
```

```
cr=Radius*ones(m,1);
mintheta = -pi/Rings*(1+overtheta)+pi/2;
maxtheta = pi/Rings*(1+overtheta)+pi/2;
switch Type
case 'nir'
  mintheta=mintheta; % minus lengthens in direction of the head
  maxtheta=maxtheta-.1; % plus lengthens in direction of the tail
end
theta = linspace(mintheta,maxtheta,n+1);

sintheta = sin(theta); %sintheta(n+1) = sintheta(1);
mBx = cr * cos(theta);
mBz = cr * sintheta;

mBy = (0:m-1)'/(m-1) * ones(1,n+1);
mBy=mBy-.5; mBy=mBy*(1+overy)*Len;

switch Type
case 'mlcurved'
  mBy=mBy+0.15;
case 'nir'
  mBy=mBy*1.2;
end
```

References

1. Cheng G.C., Libby P., Grodzinsky A.J., and Lee R., "Induction of DNA synthesis by a single transient mechanical stimulus of human vascular smooth muscle cells: Role of fibroblast growth factor-2," *Circ.*, vol. 93, pp. 99-105, 1996.

2. Sumpio B.E., Barnes A.J., Buckley M. and Johnson G. Jr., "Alterations in aortic endothelial cell morphology and cytoskelatal protein synthesis during cyclic tensional deformation," *J. Vasc. Surgery*, vol. 7, pp. 130-8, 1988.

3. Reidy M.A., "Factors controlling smooth muscle cell proliferation," *Arch. Pathol. Lab. Med.*, vol. 116, pp. 1276-1280, 1992.

4. Schwartz R.S., Huber K.C., and Murphy J.G., "Restenosis and the proportional neointimal response to coronary artery injury: results in porcine model," *JACC*, vol. 19, pp. 267-274, 1992.

5. Ross R., "The pathogenesis of atherosclerosis – an update," *NEJM*, vol. 314, pp. 488-500, 1986.

6. American Heart Association, "Heart and Stroke Facts: 1998 Statistical Supplement," p. 3, 1998.

7. Wilson R., "Simple device to prop clogged arteries open changes coronary care", *Wall Street Journal*, Oct. 23, pp. 1-2, 1995.

8. Lemaitre D.T., Barber A. P., Mullen M.G., "Interventional Cardiology," *The Cowen Report*, March 6, pp. 1-32, 1996.

9. Scimed, *Stent Handbook*, Boston Scientific, 1995.

10. van der Giessen W.J., Slager C.J., Gussenhoven E.J., van Beusekom H.M., Huijts R.A., Schuurbiers J.C., Wilson R.A., Serruys P.W., and Verdouw P.D., "Mechanical features and in

vivo imaging of a polymer stent," *Int. J. Card. Imaging*, vol. 9, pp. 219-26, 1993.

11. Tanguay J.F., Zidar J.P., Phillips 3rd H.R., and Stack R.S. "Current status of biodegradable stents," *Cardiol. Clin.*, vol. 12, pp. 699-713, 1994.

12. Agrawal C.M., and Clark H.G., "Deformation characteristics of a bioabsorbable intravascular stent," *Invest. Radiol.*, vol. 27, pp. 1020-4, 1992.

13. Schomig A., Kastrati A., Mudra H., Blasini R., Schuhlen H., Klauss V., Richardt G., and Neumann F.J., "Four-year experience with Palmaz-Schatz stenting in coronary angioplasty complicated by dissection with threatened or present vessel closure," *Circ.*, vol. 90, pp. 2716-24, 1994.

14. Wolfe M.W., Roubin G.S., Schweiger M., et al., "Length of hospital stay and complications after percutaneous transluminal coronary angioplasty: clinical and procedural predictors," *Circ.*, vol. 92, pp. 311-9, 1995.

15. Rogers C., Parikh S., Seifert P., and Edelman E. R., "Endogenous Cell Seeding; Remnant Endothelium After Stenting Enhances Vascular Repair," *Circ.*, vol. 94, pp. 2909-14, 1996.

16. Squire J.C., Rogers C., and Edelman E. R., "Stent Geometry Influences Later Restenosis," *Circ.,* vol. 94, pp. I-259, 1996.

17. Peacock J., Hawkins S., Jones T., and Lutz R., "Flow instabilities induced by coronary artery stents: assessment with an in vitro pulse duplicator," *J. Biomech*, vol. 28, pp. 892-9, 1995.

18. Huang H., Modi V.J., and Seymour B.R., "Fluid mechanics of stenosed arteries," *Intl. J. Engineering Science*, vol. 33, pp. 67-76, 1995.

19. Bittl J., "Advances in Coronary Angioplasty," *NEJM*, vol. 335, pp. 1290-1302, 1996.

20. Parikh S., Rogers C., and Edelman E. R., "Endovascular Stents: Experimental Data," *Endoluminal Stenting*, by Sigwart U., W. B. Saunders, London, p. 6, 1996.

21. Sigwart U., Puel J., Mirkovich V., Joffre F., and Kappenberger L., "Intravascular stents to prevent occlusion and restenosis after transluminal angioplasty," *NEJM*, vol. 316, pp. 701-706, 1987.

22. Keren G., “Compensatory enlargement, remodeling, and restenosis,” *Analytical and Quantitative Cardiology*, Plenum Press, NY, pp. 187-195, 1997.

23. Wilson E., Sudhir K., and Ives H.E., “Mechanical strain of rat vascular smooth muscle cells is sensed by specific extracellular matrix/integrin interactions,” *J. Clin Invest.*, vol. 96, pp. 2364-72, 1995.

24. Chen G., Briggs W., Gerson D., Libby P., Grodzinsky A., Gray M., and Lee R., “Mechanical strain tightly controls fibroblast growth factor-2 release from cultured human vascular smooth muscle cells,” *Circ. Res.*, vol. 80, pp. 28-36, 1997.

25. Buck R., “Behavior of vascular smooth muscle cells during repeated stretching of the substratum in vitro,” *Atherosclerosis*, vol. 46, pp. 217-223, 1983.

26. Gimbrone M. Jr., Nagel T., and Topper J. N., “Biomechanical activation: an emerging paradigm in endothelial adhesion biology,” *J. Clin. Invest.*, vol. 99, pp. 1809-1813, 1997.

27. Murphy J.G., Schwartz R.S., Edwards W.D., Camrud A.R. Vlietstra R.E., and Holmes D.R.J., “Percutaneous polymeric stents in porcine coronary arteries,” *Circ.*, vol. 86, pp. 1596-604, 1992.

28. van der Giessen W.J., Lincoff M., Schwartz R.S., *et al.*, “Marked inflammatory sequelae to implantation of biodegradable and nonbiodegradable polymers in porcine coronary arteries,” *Circ.*, vol. 94, pp. 1690-7, 1996.

29. Fung Y.C., Liu S.Q., and Zhou J.B., “Remodeling of the constitutive equation while a blood vessel remodels itself under stress,” *J. Biomech. Eng.*, vol. 115, pp. 453-459, 1993.

30. Rachev A., Stergiopulos N., and Meister J., “A model for geometric and mechanical adaptation of arteries to sustained hypertension,” *J. Biomech. Eng.*, vol 120, pp. 9-17, 1998.

31. Lieber B.B., Stancampiano A.P., and Wakhloo A.K., “Alteration of hemodynamics in aneurysm models by stenting: influence of stent porosity”, *Annals of Biomed. Eng.*, vol. 25, pp. 460-9, 1997.

32. Garassic J., Squire J.C., Edelman E.R., Rogers C., “Stent and Artery Geometry Determine Intimal Thickening Independent of Arterial Injury,” *Circ*., vol. 96, pp. I-402, 1997.

33. Chiu J.J., Wang D.L., Chien S., Skalak R., and Usami S., "Effects of Disturbed Flow on Endothelial Cells," *J. Biomech. Eng.*, vol 120, pp. 2-8, 1998.

34. Rogers C., Parikh S., Seifert P., and Edelman E., "Endogenous Cell Reseeding," *Circ*., vol. 94, pp. 2909-14, 1996.

35. Edelman E.R., and Rogers C., "Hoop Dreams: Stents Without Restenosis", *Circ*., vol. 94, pp. 1199-1202, 1996.

36. Rogers C., and Edelman E.R., "Endovascular Stent Design Dictates Experimental Restenosis and Thrombosis", *Circ*., vol. 91, pp. 2995-3001, 1995.

37. Nelder J.A., and Meade R., "A Simplex Method for Function Minimisation", *Computer J.*, vol 7, pp. 308-313, 1965.

38. McCulloch A.D., Smaill B.H., and Hunter P.J., "Left Ventricular Epicardia Deformation in Isolated Arrested Dog Heart", *Am. Physiol. Society*, vol 252, pp. H233-H241, 1987.

39. Fung Y.C., *Foundations of Solid Mechanics*, Prentice-Hall, Englewood Cliffs, NJ, 1965.

40. Hoffman A.H., and Grigg P, "A Method for Measuring Strains in Soft Tissues", *J. Biomech.*, vol. 17, pp. 795-800, 1984.

41. Humphrey J.D., Vito R.P., and Vawter D.L., "Quantification of Strains in Biaxially Tested Soft Tissues", *J. Biomech.*, vol. 20, pp. 59-65, 1987.

42. Fung Y.C., and Liu S.Q., "Changes of Zero Stress State of Rat Pulmonary Arteries in Hypoxic Hypertension", *J. Appl. Physiol.*, vol. 70, pp. 2455-2470, 1991.

43. Waldman L.K., Fung Y.C., and Covell J.W., "Transmural Myocardial Deformation in the Canine Left Ventricle: Normal *In vivo* Three-Dimensional Finite Strains", *Cir. Res.*, vol. 57, pp. 152-163, 1985.

44. Skovoroda A.R., Emelianov S.Y., Lubinski M.A., Sarvazyan A.P., and O'Donnell, M., "Theoretical Analysis and Verification of Ultrasound Displacement and Strain Imaging", *IEEE Trans. on Ultrasonics, Ferroelectrics, and Frequency Control*, vol. 41, pp. 302-313, 1994.

45. Yin F.C.P., Tompkins W.R., Peterson K.L., and Intaglietta M., "A Video Dimension Analyzer", *IEEE Trans. Biomed. Eng.*, vol. 19, pp. 376-381, 1972.

46. Drace J.E., and Pelc N.J., "Elastic Deformation in Tendons and Myotendinous Tissue: Measurement by Phase-Contrast MR Imaging", *Radiology*, vol. 191, pp. 835-839, 1994.

47. Weizsacker H.W. "Isotropy and Anisotropy of the Arterial Wall", *J. Biomechanics*, vol. 21, pp. 477-487, 1988.

48. Yu Q., Zhou J., and Fung Y.C., "Neutral Axis Location in Bending and the Young's Modulus of Different Layers of Arterial Wall", *Am. J. Physiol*., vol. 265, pp. H52-H60, 1993.

49. Vito R.P., Whang M.C., Glagov S., and Aoki T., "The Distribution of Strains and Stresses in the Arterial Cross Section", *1991 Advances in Bioengineering Conference*, ASME, Atlanta, Georgia, Dec. 1-6, 1991.

50. Barbee K.A., Macarak E.J., and Thibault L.E., "Strain Measurements in Cultured Vascular Smooth Muscle Cells Subjected to Mechanical Deformation", *Ann. of Biomed. Eng.*, vol. 22, pp. 14-22, 1994.

51. Hsu F.P.K., Schwab C., Rigamonti D., and Humphrey J.D., "Identification of Response Functions from Axisymmetric Membrane Inflation Tests: Implications for Biomechanics", *International J. of Solids and Structures*, vol. 31, pp. 17-26, 1994.

52. Califf R., Fortin D., Frid D., Bengtson J., et al., "Restenosis after coronary angioplasty: a review," *J. Am. Coll. Cardiol.*, vol 18, pp. 234-42, 1991.

53. Tominaga R., Harasaki H., Sutton C., et al., "Effects of stent design and serum cholesterol level on the restenosis rate in atherosclerotic rabbits", *Am Heart J.*, vol. 126, pp. 1049-58, 1993.

54. Karas SP, Gravanis MB, Santoian EC, et al., "Coronary intimal proliferation after balloon injury and stenting in swine: an animal model of restenosis", *J. Am. Coll. Cardiol.*, vol. 20, pp. 467-74, 1992.

55. Buntin CM, Silver FH, "Non invasive assessment of mechanical properties of peripheral arteries", *Ann. Biomed. Eng.*, vol. 18, pp. 549-66, 1990.

56. Serruys P.W., Keane D., Ozaki Y., deFeyter P., Rujgrok P., DiMario P., Giessen W., "New strategy of deployment of the Less Shortening Wallstent (LSS) for the treatment of long lesions and the reconstruction of coronary arteries", *Eur. Heart J.*, vol. 25, pp. 223-29, 1995.

57. Rosner B., *Fundamentals of Biostatistics 5th ed.*, Duxbury Press, Pacific Grove, pp. 518-520, 2000.

58. Clowes A.W., Clowes M.M., "Kinetics of cell proliferation after arterial injury, I: smooth muscle cell growth in the absence of endothelium", *Lab Invest*., vol. 49, pp. 327-335, 1983.

59. Kanda K., Matsuda T., "Behavior of arterial wall cells cultured on periodically stretched substrates", *Cell Transplantation*, vol. 6, pp. 475-84, 1993.

60. Nerem R.M., "Hemodynamics of the vascular endothelium", *J. Biomech Eng.*, vol. 48, pp. 115-22, 1993.

61. Rachev A., Stergiopulos N., Meister J., "A model for geometric and mechanical adaptation of arteries to sustained hypertension", *J. of Biomech. Eng.*, vol. 120, pp. 2-17, 1998.

62. Fung Y.C., Biomechanics: mechanical properties of living tissues, Springer-Verlag, New York, pp. 321-327, 1993.

63. Feynman R, Leighton R., Sands M.L., "Electrostatic Analogs", The Feynman Lectures on Physics, vol. II, Addison-Wesley, Reading, pp. 12.5-12.7, 1965.

64. Xu X., Collins M.W., "Fluid dynamics in stents", *Endoluminal Stenting*, The University Press, Cambridge, pp. 52-59, 1996.

65. Rogers C., Tseng D.Y., Squire J.C., Edelman E.R., "Balloon-artery interactions during stent placement. A finite element analysis approach to pressure, compliance, and stent design as contributors to vascular injury", Circ. Res., vol. 84., pp. 378-83, 1999.